

Copyright
by
Tyler Holt Summers
2010

The Dissertation Committee for Tyler Holt Summers
certifies that this is the approved version of the following dissertation:

**Cooperative Shape and Orientation Control of
Autonomous Vehicle Formations**

Committee:

Maruthi R. Akella, Supervisor

Brian D.O. Anderson, Supervisor

Changbin Yu

E. Glenn Lightsey

David G. Hull

Belinda G. Marchand

Robert H. Bishop

**Cooperative Shape and Orientation Control of
Autonomous Vehicle Formations**

by

Tyler Holt Summers, B.S., M.S.

DISSERTATION

Presented to the Faculty of the Graduate School of
The University of Texas at Austin
in Partial Fulfillment
of the Requirements
for the Degree of

DOCTOR OF PHILOSOPHY

THE UNIVERSITY OF TEXAS AT AUSTIN

December 2010

To my family.

Acknowledgments

It is a pleasure to thank the many people who supported me during the past five plus years as I worked toward my doctorate. If I have made any progress, both intellectually and personally, I have certainly not done it alone, and I am deeply grateful for the help of my family, friends, colleagues, teachers, and mentors along the journey.

First, I would like to thank my supervisors, Professor Maruthi R. Akella and Professor Brian D.O. Anderson. They exposed me to a wide range of research interests, guided my own research, and helped me to develop my own engineering worldview and formulate new challenges. Their wisdom, leadership, and technical brilliance have been an inspiration.

I am grateful for my collaborators, Dr Brad Yu, Professor Soura Dasgupta, Apurva Chunodkar, and Dr Mark Mears, and my committee members Professors E. Glenn Lightsey, Belinda G. Marchand, David G. Hull, and Robert H. Bishop, who shared their time, effort, and expertise with me. I would also like to thank my friends, colleagues, and fellow students Lachlan Blackhall, Kyle DeMars, Travis Mercker, Srikant Sukumar, Apurva Chunodkar, Iman Shames, Dr Stuart Stanton, Srinivas Sridharan, Dr Karl Obermeyer, Dr Adrian Bishop, Dirk van der Walle, and others who helped me preserve my sanity and keep a balanced perspective during this long and sometimes

grueling process.

Finally, I would like to express my deep gratitude to all my family, in particular to mom, dad, Stephanie, and Cameron, for their unconditional love and support. I simply would not be where I am today without them.

Cooperative Shape and Orientation Control of Autonomous Vehicle Formations

Publication No. _____

Tyler Holt Summers, Ph.D.

The University of Texas at Austin, 2010

Supervisors: Maruthi R. Akella
Brian D.O. Anderson

This dissertation solves variations of three mathematical problems for autonomous vehicle formations: (1) formation shape control in the plane, (2) robust information architecture design, and (3) formation attitude synchronization. An autonomous vehicle formation is a collection of vehicles, each with computation, communication, sensing, and control capabilities, that cooperate to achieve a common objective. Accelerating advancements are making possible a range of science and engineering applications, such as satellite formations for deep-space imaging, teams of unmanned aircraft for military reconnaissance and surveillance missions, and submarine swarms for oceanic exploration. The ubiquitous potential of these applications is driving theoretical work on autonomous vehicle formations across a range of disciplines.

A major theoretical question in the field of control theory, and the main focus of this dissertation, is how the properties of the information architecture

(i.e. a mapping of the information flow amongst the agents), relate to the stability properties of the desired shape and orientation under certain control laws. A secondary focus is how to design the information flow so that loss of an agent does not destroy the formation's ability to maintain a desired shape. As a motivating example, a solution to a coordinated standoff tracking problem is presented to demonstrate how an *instance* of a class of information architectures, which are called persistent and related to rigid graph theory, can be used to achieve a formation objective in a practical scenario involving a team of unmanned aircraft. A generalized formation shape control problem is then solved for a *class* of persistent architectures. This solution gives only local stability results; global stability is analyzed for a four-agent formation and several open problems are identified. The problem of agent loss is addressed by performing a self-repair operation in the event of agent loss and separately by designing robustness into the information architecture a priori. Finally, a rigid body attitude synchronization problem with communication time delays is solved for a class of information architectures based on spectral graph theory.

Table of Contents

Acknowledgments	v
Abstract	vii
List of Figures	xiii
Chapter 1. Introduction	1
1.1 Motivation	1
1.2 Literature Review	4
1.2.1 Formation Shape Control	4
1.2.2 Robust Information Architecture Design	9
1.2.3 Rigid Body Attitude Synchronization	12
1.3 Dissertation Outline	14
1.4 Statement of Contributions	16
Chapter 2. Background: Rigid Graph Theory	23
2.1 Graph Theory Preliminaries	24
2.2 Rigid and Persistent Formations	25
2.2.1 Rigidity	25
2.2.2 Persistence	30
2.2.3 Minimally Persistent Formations	32
2.3 Global Rigidity	37
2.4 Conclusion	38
Chapter 3. Coordinated Standoff Tracking: Control Laws and Information Architectures	39
3.1 Introduction	39
3.2 The Coordinated Standoff Tracking Problem	42
3.2.1 Lyapunov Guidance Vector Field Construction	43

3.2.2	Heading Convergence	47
3.2.2.1	Heading Feedback	48
3.2.2.2	Initial Loiter Circle	53
3.3	Moving Target Tracking with Wind	61
3.3.1	Variable Airspeed Controller with Adaptive Wind/Target Motion Estimates	61
3.3.2	Stability Analysis	64
3.3.3	Kinematic Constraints	66
3.4	Stationary Target Tracking: Multiple Vehicle Spacing	70
3.5	Simulations	75
3.6	Conclusions	78

**Chapter 4. Control of Minimally Persistent Leader-Remote-Follower
and Coleader Formations in the Plane 82**

4.1	Introduction	82
4.2	Center Manifold Theory	84
4.3	Center Manifold Result for a System with an Equilibrium Manifold	87
4.4	Equations of Motion	92
4.4.1	Nonlinear Equations of Motion	93
4.4.2	Linearized Equations	95
4.4.3	A Reduced-Order System for LRF Formations	97
4.4.4	Full-Order System for Coleader Formations	99
4.5	Choosing Gains and the Principal Minor Condition	100
4.5.1	LRF Formations	101
4.5.2	Coleader Formations	103
4.6	Simulations	112
4.6.1	LRF Formations	112
4.6.2	Coleader Formations	112
4.7	Concluding Remarks	120

Chapter 5. Formation Shape Control: Global Asymptotic Stability of a Four-Agent Formation	122
5.1 Introduction	122
5.2 Equations of Motion and Examples	124
5.2.1 Equations of Motion	124
5.2.2 Krick Example	127
5.3 Rectangular Formations	128
5.4 Computing a Desired Equilibrium Shape from an Incorrect Equilibrium Shape	131
5.5 Concluding Remarks	134
Chapter 6. Addressing Agent Loss in Vehicle Formations and Sensor Networks	136
6.1 Introduction	136
6.2 The Self-Repair Approach	138
6.2.1 The Closing Ranks Problem	138
6.2.2 Decentralized Rigidity Recovery	142
6.2.3 Decentralized Global Rigidity Recovery	146
6.3 Implementation	147
6.4 Redundant Information Architectures	150
6.4.1 Redundant Rigidity Concepts	152
6.4.2 Strongly Minimal 2-Vertex-Rigidity	153
6.4.3 Weakly Minimal 2-Vertex-Rigidity	157
6.5 Strongly Minimal 2-Vertex-Global-Rigidity	162
6.6 Concluding Remarks	166
Chapter 7. Rigid Body Attitude Synchronization with Communication Time Delays	168
7.1 Introduction	168
7.2 Problem Statement and Graph Theory Preliminaries	171
7.2.1 Rigid Body Attitude Synchronization	171
7.2.2 Spectral Graph Theory Preliminaries	172
7.3 Consensus of Second-Order Systems with Communication Time Delays	177

7.3.1	Delay-independent stability	178
7.3.2	Characterization of the Consensus Position	182
7.4	Feedback linearization and linear closed loop dynamics	186
7.5	Simulations	187
7.6	Conclusions	191
Chapter 8.	Conclusion	192
8.1	Summary	192
8.2	Future Research Directions for Control of Autonomous Vehicle Formations	193
8.2.1	Formation Shape Control	193
8.2.2	Robust Information Architecture Design	197
8.2.3	Rigid Body Attitude Synchronization	198
8.3	Conclusion	198
Bibliography		200
Vita		212

List of Figures

2.1	Illustration of a (a) non-rigid, (b) minimally rigid, and (c) non-minimally rigid formation.	27
2.2	Representation of (a) vertex addition operation (b) edge splitting operation.	28
2.3	Constraint consistent and non-constraint consistent graphs with the same underlying undirected graph.	32
2.4	Examples of LFF and LRF formations with four agents: (a) in LFF formations the one-DOF agent is connected to the leader, and (b) in LRF formations the one-DOF agent is not connected to the leader.	34
2.5	Examples of coleader formations with connected coleaders: (a) cyclic coleaders, (b) inline coleaders, (c) v-coleaders. Examples of coleader formations with non-connected coleaders: (d) one-two coleaders, (e) distributed coleaders. Each coleader has only one interagent distance to maintain and so has only one outgoing arrow.	34
3.1	Lyapunov guidance field trajectory with heading initially aligned with the field.	46
3.2	Heading Error Quadrants	50
3.3	Trajectory using heading feedback with initial heading in quadrant III and small feedback gain.	54
3.4	Trajectory using initial left-turn loiter circle to converge exactly to the desired heading. The dashed line represents the guidance trajectory if the vehicle's initial heading was aligned with the guidance field.	58
3.5	Trajectory using initial right-turn loiter circle to converge exactly to the desired heading.	59
3.6	Trajectory using initial left-turn loiter circle with quadrant IV heading to avoid penetrating the standoff radius. The trajectory get close to, but does penetrate, the standoff radius. However, there are certain initial conditions from which it is impossible to avoid penetrating the standoff radius without violating the heading rate constraint.	60

3.7	Four UAVs engaging a stationary target in local coordinates.	76
3.8	Airspeed commands for spacing.	77
3.9	Relative spacing errors for four UAVs engaging a stationary target.	77
3.10	Two UAVs engaging a moving target in inertial coordinates (m).	79
3.11	Two UAVs engaging a moving target in local target frame coordinates (m).	79
3.12	Airspeed commands for spacing and maintaining circular orbit around a moving target.	80
3.13	Relative spacing error for two UAVs engaging a moving target.	80
4.1	Coleader formation with only one coleader having its outgoing edge to the set of ordinary followers V' . There may be other edges from V' to the coleaders.	106
4.2	Coleader formation with two coleaders having outgoing edges to the set of ordinary followers V' . There may be other edges from V' to the coleaders.	108
4.3	LRF formation in unstable agent positions for identity gain.	113
4.4	Agent trajectories in the plane: circles represent the initial desired formation shape, triangles represent the perturbed agent positions, and X's represent the final agents positions under the formation shape maintenance control laws. The desired shape has been restored. The leader does not move.	113
4.5	The interagent distance errors, defined as $e_{ij} = p_i - p_j - d_{ij}$, all converge to zero, thus recovering the desired formation shape.	114
4.6	Coleader formation in the plane in unstable agent positions for identity gain.	115
4.7	Agent trajectories in the plane: circles represent the initial desired formation shape, triangles represent the perturbed agent positions, and X's represent the final agents positions under the formation shape maintenance control laws. The desired shape has been restored, though the final formation is translated and rotated from the original unperturbed formation.	116
4.8	The interagent distance errors all converge to zero, thus recovering the desired formation shape. That e_{24} , which does not correspond to an edge of the formation graph, goes to zero is due to the underlying rigidity and the convergence of the other e_{ij} to zero.	117

4.9	Agent trajectories after a larger perturbations: the desired shape has been restored, though the final formation is translated and rotated from the original unperturbed formation. The circles, triangles and X's are as for Figure 7.	117
4.10	The interagent distance errors all converge to zero, thus recovering the desired formation shape.	118
4.11	Agent trajectories in the plane after large perturbations: the formation converges to an equivalent, but not congruent, shape.	118
4.12	All interagent distance errors except one converge to zero.	119
4.13	Agent trajectories in the plane after larger perturbations: instability.	119
4.14	The interagent distance errors all blow up.	120
5.1	A desired formation configuration and its reflection in the plane both satisfy the same prescribed interagent distance constraints.	125
5.2	The desired formation is rectangular and there are two possible "twisted rectangles" that are incorrect equilibrium shapes. Note that each formation has two different pairs of agents on the diagonals of the rectangle: (a) 13 and 24, (b) 12 and 34, and (c) 14 and 23.	130
6.1	Illustration of Closing Ranks: (a) original rigid formation (b) a vertex and incident edges are removed (c) the minimum number of new edges are added to regain rigidity. It is sufficient to add edges to neighbours of the lost vertex.	139
6.2	Edge splitting creates edge dependency between the highlighted vertices. Repeatedly applying edge splitting increases the size of the dependent subgraph.	141
6.3	Illustration of the Double Patch: The two highlighted vertices serve as coordinators to which every other vertex is connected.	143
6.4	Utilizing existing cover edges with the Double Patch: (a) the lost vertex has degree 6, (b) edges exist among neighbours of the lost vertex, (c) coordinators for the Double Patch are chosen to utilize these existing edges, and 4 <i>new</i> edges are added - a minimal cover.	144
6.5	Single Patch Counterexample. The two dependent edges cause the single patch to fail.	145
6.6	Illustration of the Wheel Patch: the highlighted vertex serves as the coordinator and connects to every other vertex in the cycle.	148
6.7	Double Patch: (a) rigid formation with agent IDs, (b) agent 0 fails, neighbours recognize the loss, (c) coordinators 1 and 2 are chosen via minimum agent ID and links established.	150

6.8	Wheel Patch: (a) globally rigid formation with agent IDs, (b) agent 0 fails, neighbours recognize the loss, (c) coordinator 1 is chosen via minimum agent ID, cycle formed via agent ID ordering, and links established.	151
6.9	Examples of the two possible partitions of the edge set for strongly minimal 2-vertex-rigid graphs: (a) the degree three vertices are adjacent, and (b) the degree three vertices are non-adjacent.	156
6.10	Example of a weakly minimal 2-vertex-rigid graph. The graph has an excess of three, but removing any edge destroys 2-vertex-rigidity. Thus, this graph cannot be obtained by adding an edge to a graph described by Theorem 6.4.3.	158
6.11	Smallest example of a weakly minimal 2-vertex-rigid graph in the class defined by the Servatius example.	159
6.12	Representation of the <i>X-replacement</i> operation.	160
6.13	A new class of weakly minimal 2-vertex-rigidity: (a) a weakly minimal 2-vertex-rigid graph with excess three, (b) adding a degree 3 vertex to create a weakly minimal 2-vertex-rigid graph with excess four. By successively adding a degree 3 vertex to either end, one can obtain weakly minimal 2-vertex-rigid graphs with arbitrarily large excess.	161
6.14	Example of a strongly minimal 2-vertex-globally-rigid graph described in Theorem 6.5.3.	166
7.1	Leaderless directed communication architecture.	187
7.2	Leader-follower directed communication architecture. Agent 1 is the leader.	188
7.3	Leader-follower directed communication architecture, $\alpha = 1$, $\beta = 2$, $\tau = 6.91$	189
7.4	Leaderless directed communication architecture, $\alpha = 1$, $\beta = 1.2$, $\tau = 4$	190
7.5	Leaderless directed communication architecture, $\alpha = 1$, $\beta = 1.2$, $\tau = 6.91$	190

Chapter 1

Introduction

1.1 Motivation

An autonomous vehicle formation is a collection of vehicles, each with computation, communication, sensing, and control capabilities, that cooperate to achieve a common objective. Accelerating advancements are making possible a range of science and engineering applications, such as satellite formations for deep-space imaging, teams of unmanned aircraft for military reconnaissance and surveillance missions, and submarine swarms for oceanic exploration. The ubiquitous potential of these applications is driving theoretical work on autonomous vehicle formations across a range of disciplines. In the field of control theory, a major research topic is how to cooperatively control the individual vehicles, or agents, so that the formation accomplishes a global objective or exhibits a cohesive behavior.

Autonomous vehicle formations can deliver a number of practical advantages over a single autonomous vehicle. First, organizing vehicles into formations can significantly improve sensing capability, e.g resolution and sensitivity in space-based interferometry [39, 42]. A team of vehicles can also search or monitor a large area faster and more effectively than any single ve-

hicle could. Second, formations offer new sensing capabilities that are unable to be achieved with a single vehicle. For example, determining the spatial position of a target through three-dimensional distance-based localization requires four distinct relative distance measurements from sensors with known positions to instantaneously localize the target. Third, formations allow for robustness to failure of a single agent, or a small number of agents. This modularity of autonomous vehicle formations also allows for easily adding or subtracting agents from the formation. Lastly, cooperative formations of simple, inexpensive agents may provide significant cost advantages over a single complex agent. Other advantages of organizing and controlling vehicles in formations to undertake designated technical tasks might include reducing drag and improving the range and fuel efficiency of aircraft, and many more are still to be apprehended.

Sensing capability can be improved by precisely maintaining the formation in a prescribed shape and orientation.¹ To do this, each vehicle must acquire information about the relative position and orientation of other vehi-

¹To illustrate with an example, a team of satellites flying in a precisely controlled formation can synthesize a space-based interferometer that could offer several orders of magnitude improvement over the resolution of monolithic satellites [70], a technological leap akin to that from Galileo's telescope to the Hubble Space Telescope. Space-based interferometry with satellite formations has been studied in several recent projects including NASA's Terrestrial Planet Finder [42] and the European Space Agency's Darwin [39] to search for and characterize extrasolar Earth-like planets. Each satellite collects light from distant sources and sends the beam to be combined by a separate satellite. The interference pattern between beams from various satellites provides information about the properties of the light source. The resolution can be improved by using many satellites and by having large satellite separations, but precision formation shape and orientation control are crucial [74].

cles in the formation and use this information to control its own position and orientation. A major theoretical question, and the main focus of this dissertation, is how the properties of the information architecture (i.e. a mapping of the information flow amongst the agents), relate to the stability properties of the desired shape and orientation under certain control laws. A secondary focus is how to design the information flow so that loss of an agent does not destroy the formation's ability to maintain a desired shape. The information architecture must be *designed* to preserve certain properties in the event of agent failure.

Formation shape control, orientation control, and information architecture design problems can be formulated into analogous mathematical problems. Vehicle motion can be modeled by a set of ordinary differential equations, and the information architecture can be modeled by a graph. This dissertation solves variations of three mathematical problems for autonomous vehicle formations: (1) formation shape control in the plane, (2) robust information architecture design, and (3) formation attitude synchronization. The next section elaborates on these research challenges and locates the work of this dissertation within the field through a literature review of work on these problems. The final section of this chapter presents a dissertation outline and details the original contributions of this work.

1.2 Literature Review

1.2.1 Formation Shape Control

The challenge of the formation shape control problem is to design motion control laws for each agent, given certain relative position information, so that the formation converges to a *prescribed* formation shape.² An overarching requirement for large formations is that implementation of the design be decentralized. Having a single centralized agent that handles the control, communication, sensing, and computation tasks for the whole formation would be computationally prohibitive and makes the formation much more vulnerable to unanticipated catastrophic failure. Instead, each agent is typically assumed to have access to relative position information from a limited set of other agents in the formation. The formation shape control problem involves determining what relative position information is required and how this information should be used in the control law.

This problem has received significant attention in literature across a range of engineering disciplines. In the control theory literature, a major point of divergence is whether the *controlled* variables are chosen as a set of relative positions or a set of interagent distances. When relative positions are chosen, the formation shape maintenance problem can be formulated as a *consensus problem* [23, 54, 59, 60]. A consensus problem is to design decentralized control

²This contrasts with another related formation control problem called *flocking*, in which the objectives are for agents to move in a common direction, avoid collisions, and stay close to one another, though not necessarily maintain a *prescribed* shape; see [45, 53, 71, 72].

laws to drive a team of agents toward agreement upon certain quantities of interest, such as position or velocity. For example, in a *rendezvous problem*, the control laws drive the agents to a common position.³ Constant offset position vectors can be introduced into these control laws to produce any desired formation shape [23]. In consensus problems, the stability of the formation shape can be related to the spectral properties of the information architecture *graph Laplacian matrix*.

When interagent distances are chosen as the controlled variables, then the stability of the formation shape is instead related to the *graph rigidity* [73] of the information architecture, and the *rigidity matrix* plays a crucial role in the stability analysis [1, 12, 14, 21, 38, 55, 83]. An advantage of this approach is that each agent can locally operate in an arbitrary coordinate basis. By contrast, controlling relative positions and using a consensus algorithm assumes agents to have knowledge of a global coordinate basis. Another advantage of this approach is that a single agent or small subset of agents can be given responsibility for the orientation of the whole formation, thus making a rotation of the whole formation relatively easy. Rotating the whole formation is not as straightforward with a consensus approach.

Graph rigidity has a long history in combinatorial theory [34, 40, 73]. It has been recently introduced in [7, 21, 55] as a means for describing the information architecture required to maintain formation shape. The information

³Other cooperative control tasks that can be cast as consensus problems include flocking and cyclic pursuit, where a group of agents follow one another in a cyclic pattern [46, 48].

architecture is modeled with a graph $G(V, E)$, where V is a set of vertices representing agents and $E \subseteq V \times V$ is a set of edges representing information flow amongst the agents. In the formation shape control problem, the edge set E represents the set of inter-agent distances to be actively held constant via control of individual vehicle motion. If a suitably large and well-chosen set of inter-agent distances is held constant, then all remaining inter-agent distances will be constant as a consequence, and the formation shape will be maintained. Graph rigidity theory addresses the nontrivial question of identifying which inter-agent distances should be actively controlled to maintain a desired formation shape. Although an easy answer is to control *every* possible inter-agent distance, this is not a decentralized approach. It also requires controlling $O(n^2)$ distances, where n is the number of agents, when it is only necessary to control $O(n)$ distances. Another answer is to only control distances within a prescribed sensing and communication range of each agent. However, this approach in general does not guarantee rigidity, and determining the minimum sufficient sensing radius for each agent to guarantee rigidity for an arbitrary configuration of agents is a nontrivial open problem. Typically, it is assumed that a designer specifies the interagent distances to actively control and that the involved agents are within sensing and communication range of each other.

A further divergence in the literature for rigidity-based formation control is whether the information architecture is directed or undirected. In an undirected formation, the task of controlling a particular interagent distance is shared by the involved agents. Undirected formations with gradient-based

control laws are studied in [38]. In a directed formation, the task of controlling a particular interagent distance is given to only one of the involved agents. This has the advantage of halving the number of links in the information architecture. Directed formations are studied in [1, 7, 12, 14, 83].

The concept of rigidity for directed graphs is not a simple transposition of rigidity for undirected graphs, so these concepts are distinguished by the use of the term *persistence* for directed graphs [33]. Persistence includes the concept of rigidity, but also requires a further condition called *constraint consistence*, which precludes certain directed information flow patterns [84]. In directed formations, it becomes possible to have cycles in the information architecture. Acyclic formations allow for a triangular decomposition that makes the stability analysis much easier to deal with [12], while cyclic formations may require more complex control laws to achieve stability. A persistent formation with the smallest number of links in the information architecture is referred to as a *minimally persistent formation*. This type of formation falls into three categories: Leader-First-Follower (LFF), Leader-Remote-Follower (LRF) and Coleader. Acyclic LFF formations are studied in [12], however, LFF does not always imply an acyclic formation. In [83], Yu et al consider minimally persistent LFF formations in the plane *with cycles*. They apply decentralized nonlinear control laws to restore formation shape in the presence of small distortions from the desired shape. They show that choosing locally stabilizing control gains is possible if a certain submatrix of the *rigidity matrix* has all leading principal minors nonzero and prove that all minimally

persistent LFF formations generically obey this principal minor condition.

To fully characterize the stabilizability of minimally persistent formations, formation shape control problems for LRF and Coleader also need to be solved. The method used to prove local stabilizability for LFF formations does not directly apply to LRF and Coleader formations. How to deal with LRF and Coleader formations is summarized in the next section and is the subject of Chapter 4.

Most of the work on rigidity-based formations shape control shows *local* stability or stabilizability of the desired shape, with a few exceptions. Almost⁴ global stability is demonstrated for a directed, cyclic, three-agent formation in [1] and for a directed, acyclic three-agent formation in [13, 14]. It is noted in [19] that these results extend easily to the undirected three-agent case. In [12], almost⁵ global stability is demonstrated for directed, acyclic, n -agent formations. In [38], Krick et al study an undirected n -agent rigidity-based formation control problem. They prove for undirected rigid formations that the desired formation shape is *locally* asymptotically stable under a gradient control law if the information architecture is rigid. The global stability properties of the desired shape remain a challenging open problem for undirected formations with more than three agents. There are a number of technical difficulties, including the effect of non-minimal rigidity and the existence of

⁴The formations converge to a desired triangular shape from any *non-collinear* initial configuration, so what is demonstrated is actually *almost* global stability since the set of collinear configurations is thin (Lebesgue measure zero).

⁵Again, convergence is shown from all initial configurations outside of a thin set.

incorrect equilibrium formation shapes, that make these formations difficult to analyze. Characterizing global stability for a four-agent formation as a special case is an essential step to solving the problem for larger formations. Chapter 5 considers the global stability of an undirected, four-agent formation and shows that a class of rectangular incorrect equilibrium formation shapes, previously thought to be attractive, are unstable saddle points.

All formation shape control results in this dissertation are restricted to motion in the plane. This restriction is mainly due to the fact that rigid graph theory is incomplete in higher dimensions, as discussed in the following chapter. Although there are partial results for higher dimensions, a full characterization of graph rigidity remains a significant open problem.

1.2.2 Robust Information Architecture Design

Formations require the *design* of information architectures that allow robustness to agent loss. This loss could occur in a number of ways: from enemy attack or jamming; from random mechanical or electrical failure; or from intentionally deploying an agent for a separate task. Large-scale formations may be composed of relatively inexpensive agents that are prone to such failures. Loss of an agent can prevent the successful performance of fundamental tasks. This dissertation focuses on preserving a formation’s ability for formation shape control.

The loss of an agent can be addressed via two separate approaches. The first is to perform a “self-repair” operation on the information architecture in

the event of agent loss to recover rigidity or global rigidity⁶. The second is to introduce robustness into the information architecture *a priori* so that agent loss does not destroy rigidity or global rigidity. The “self-repair” approach is *reactive* in that the formation reacts to an agent loss event. The robustness approach is *proactive* in that redundancy is built into the formation in anticipation of an agent loss event.

The “self-repair” approach is an instance of the *closing ranks problem*, described below. For large-scale formations that do not support centralized computation, communication, and sensing, the repair must be made in a decentralized way. The term “decentralized” is used in this context to encompass two properties: (1) the formation makes a *local repair* involving only neighbors of a lost agent, and (2) the neighbors perform the repair using only *local*

⁶Closely related to the concept of rigidity is *global rigidity* (the precise distinction is covered in the next chapter), which is important for the separate task of sensor network self-localization [5, 18, 56] and also has applications in robot pose estimation [76]. Many applications for sensor networks require knowledge of agent positions in order to detect and record events and for geographic routing. The global rigidity property pertains to a set of vertices having a *unique* configuration in Euclidean space. The self-localization task is to uniquely determine positions of each agent from knowledge of a partial set of inter-agent distances and knowledge of the positions in a global coordinate basis of several agents (“anchors”). The information architecture is modeled as a graph $G(V, E)$ where the vertex set V represents the agents and the edge set E represents the set of known inter-agent distances. If a suitably large and well-chosen set of inter-agent distances is known, then the remaining inter-agent distances may be *uniquely* determined. Further, if the positions of three non-collinear agents are known, then all other agent positions may be uniquely determined [5]. Noise in known distances causes nontrivial problems in self-localization, but global rigidity remains a central idea [18]. Both rigidity and global rigidity are important properties of information architectures for autonomous vehicle formations and sensor networks because of the crucial role they play in formation shape control and self-localization. Although these are two rather different tasks, they are related by the concept of rigidity, and they both serve as a motivating basis for our discussion of robust information architectures.

information (independent of formation size).

The *closing ranks problem* is to recover rigidity by determining new sensing/communication links in the event of agent loss. Closing ranks does not necessarily result in motion of the agents; it is a sensing/communication deficiency that is repaired, which means that a set of edges is added to the graph. In [20], Eren et al present a systematic method to solve the closing ranks problem with local repair. This result draws from a graph theoretic theorem given by Tay and Whiteley in [73], which proves that rigidity can be recovered when a vertex is removed from a rigid graph by adding edges only between neighbors of the lost vertex. In terms of formation shape maintenance, this is equivalent to assigning further agent pairs between which the distance should be preserved.

Although the method in [20] determines a minimal local repair, in terms of adding the least number of links to restore rigidity, it cannot always be implemented using only local information. The effect of adding a particular link may depend on the information architecture in a non-local way. How the closing ranks problem can be solved in a decentralized way is the subject of Chapter 6.

The robustness approach is related to the concept of *redundant rigidity*. A redundantly rigid graph has the property that rigidity is preserved after removing any single vertex. This concept is analyzed by Servatius in [67] and the recent work by Yu and Anderson in [82]. Chapter 6 also builds on this preliminary work by solving an open problem introduced by Servatius

in [67] and further investigating the structure of redundantly rigid graphs, and providing new results for redundantly globally rigid graphs.

1.2.3 Rigid Body Attitude Synchronization

The rigid body attitude synchronization problem is to design torque control laws to asymptotically synchronize the orientation of a team of rigid bodies. There is an extensive body of literature on consensus/synchronization problems that utilize *spectral graph theory* rather than rigid graph theory; for recent surveys see e.g. [54, 60]. In these problems, a team of cooperating agents exchange certain local information, through either communication or sensing, in order to achieve the synchronization. A key feature of these results is that the structure of the communication architecture can be related to the stability and performance of the synchronization via spectral graph theory; the eigenvalues of the graph Laplacian govern both stability and speed of convergence.

Recently, focus has turned to consensus problems with double integrator agent dynamics [57, 58, 80]. Double integrators are a more suitable model for mechanical systems than single integrators as mechanical systems are generally controlled through acceleration, not velocity. More recently, communication time delays have been considered in consensus problems with double integrators [51, 68, 85]. In [85], simple necessary and sufficient conditions for second-order consensus of both position and velocity are given for a directed communication architecture and homogeneous delay, but with self-

delay⁷. Consensus is achieved if and only if the time delay is less than a specified value. In [68], sufficient stability conditions based on linear matrix inequalities (LMI) are given for second-order consensus with directed graphs and homogeneous delay (no self-delay); however, the analysis is restricted to graphs in which the degree matrix can be written as a scalar multiple of the identity matrix. In [51] sufficient conditions are stated in terms of control gains for second-order consensus with heterogeneous delays; however, the results are restricted to undirected graphs. Consensus problems for higher order agent dynamics are considered in [44, 52]. In [44] sufficient stability conditions for consensus in terms of the individual agent's closed loop frequency response are provided for directed graphs with heterogeneous delays. In [52], somewhat more complicated set-valued necessary and sufficient conditions for higher-order consensus (of position and higher-order derivatives) are given for an undirected communication architecture and heterogeneous time delays. However, these results do not readily provide explicit conditions on control gain parameters that guarantee stability. New consensus results are needed for double integrator agents in a directed communication architecture with homogenous delay (without self-delay).

Satellite formations have received significant attention in the literature due to potential applications such as space interferometry. Rigid body attitude synchronization is an important problem for these applications, and extending

⁷Self-delay means that the value of an agent's own state has an associated delay in its control law. This may occur if there is a computational processing delay.

the linear consensus results to this problem with nonlinear dynamics and time delays is a significant challenge, which is taken up in Chapter 7. Several papers consider leader-follower communication architectures in which each follower simply tracks the attitude of a designated leader, or other architectures in which there is a common external reference attitude known to all agents [43, 77]. However, directed graphs that represent leader-follower architectures can take on more general forms, and situations in which there is no designated leader and no common external reference attitude may be of interest [57, 63]. Synchronization of rigid body attitudes without a leader or common external reference may also provide practical benefits and are also more challenging theoretically. When only the relative, not absolute, orientations of the rigid bodies are of interest (e.g. for autonomous on-orbit assembly), the formation attitude is not constrained to a designated leader or reference, which gives an extra degree of freedom that may reduce costs [63].

Chapter 7 solves a rigid body attitude synchronization problem with communication time delays for leader-follower and leaderless communication architectures.

1.3 Dissertation Outline

The rest of the dissertation is organized as follows:

Chapter 2 is a background chapter that overviews of graph rigidity theory as used in Chapters 3-6. Graphs can be used as basic models for information flow in autonomous vehicle formations. Graph rigidity theory is

non-standard in the control theory literature but provides important information architecture properties in the formation shape control problem when the controlled variables are interagent distances.

To introduce the rigidity-based formation shape control problems in Chapters 4 and 5, Chapter 3 demonstrates how directed persistent information architectures can be used to achieve a formation objective in a practical scenario involving a team of unmanned aircraft, called the *coordinated standoff tracking problem*. Control laws are designed for a team of unmanned aircraft to fly a circular orbit around a target with prescribed inter-vehicle angular spacing. To achieve the angular spacing, the vehicles sense or communicate certain relative position information according to a graph. The control objective suggests an information architecture that is equivalent to an *instance* of a persistent graph. This finding motivates the study of more general *classes* of graphical information architectures.

Chapter 4 solves a formation shape control problem for a *class* of directed persistent information architectures. It builds on work undertaken for minimally persistent leader-first-follower formations and completes the characterization of the stabilizability of minimally persistent architectures by solving the problem for minimally persistent LRF and Coleader formations.

The stability results in Chapter 4 are local, so that converging to the desired shape is not guaranteed for all initial positions. Chapter 5 turns to the question of *global* stability of an undirected four-agent formation in the plane. The analysis is restricted to the undirected four-agent case because this

still remains an interesting and challenging open problem and because this will be an important special case that may shed light on the problem for larger formations and directed formations.

Chapter 6 returns to another motivation for autonomous vehicle formations and addresses the problem of agent loss by performing a self-repair operation in the event of agent loss and separately by designing robustness into the information architecture. The architectures in this chapter are all undirected.

Chapters 3-6 are concerned with formation shape control problems in which each agent can be modeled as a point; Chapter 7 is concerned with an attitude synchronization problem in which each agent is modeled as a rigid body and the communicated signals have a time delay. This chapter relates the stability of the formation around a configuration with synchronized attitude to the spectral graph properties of the information architecture.

Chapter 8 summarizes the key results of the dissertation and identifies several possible directions for future research.

1.4 Statement of Contributions

This section summarizes the original contributions of this dissertation. The relevant publications for each contribution are indicated.

1. We solve a *coordinated standoff tracking problem* using a Lyapunov guidance vector field approach recently introduced by Frew, Lawrence, and

Morris in [24] to achieve the desired circular trajectory. The contributions involve both single vehicle path planning and multiple vehicle coordination. For single vehicle path planning, we complete a proof of heading convergence using feedback, which has thus far not been fully addressed in the literature, and also offer a novel approach for heading convergence that does not require continuous feedback in the ideal case (no wind, stationary target), taking advantage of an analytical solution for the guidance field. Further, we use a variable airspeed controller to maintain the circular trajectory despite unknown, constant-velocity wind and target motion. Adaptive estimates of the unknown wind and target motion are introduced to ensure stability of the circular trajectory. A novel feature of our results is rigorous satisfaction of vehicle specific kinematic constraints on heading rates and airspeed variations. For multiple vehicle coordination, we again use a variable airspeed controller to achieve the prescribed angular spacing. We demonstrate that a persistent information architecture can be used to achieve the formation objective, and we implement decentralized control laws based on this architecture.

- T.H. Summers, M.R. Akella, and M.J. Mears, Coordinated Standoff Tracking of Moving Targets: Control Laws and Information Architectures, *AIAA Journal of Guidance, Navigation, and Control*, Vol. 32, No. 1, pp. 56-82, 2009.
- T.H. Summers, M.R. Akella, and M.J. Mears, Coordinated Stand-

off Tracking of Moving Targets, *AIAA Guidance, Navigation, and Control Conference*, August 19- 21 2008, Honolulu, HI, USA.

2. We solve an n -agent formation shape maintenance problem in the plane for two classes of directed, cyclic information architectures associated with *minimally persistent* formations: *leader-remote-follower* and *coleader*. We propose a decentralized control law using relative position measurements to control certain interagent distances. The resulting nonlinear closed-loop system has a manifold of equilibria, which implies that the linearized system is nonhyperbolic. We apply center manifold theory to show local exponential stability of the desired formation shape. The result circumvents the non-compactness of the equilibrium manifold. Choosing stabilizing gains is possible if a certain submatrix of the rigidity matrix has all leading principal minors nonzero, and we show that this condition holds for all minimally persistent leader-remote-follower and coleader formations with generic agent positions.

- T.H. Summers, C. Yu, B.D.O. Anderson, and S. Dasgupta, Control of leader- remote-follower and coleader formations in the plane, submitted to *IEEE Transactions on Automatic Control*.
- T.H. Summers, C. Yu, B.D.O. Anderson, and S. Dasgupta, Control of coleader formations in the plane, *IEEE Conference on Decision and Control*, December 16-18 2009, Shanghai, China.
- T.H. Summers, C. Yu, B.D.O. Anderson, and S. Dasgupta, Control

of leader- remote-follower formations in the plane, *European Control Conference*, August 23-26, 2009, Budapest, Hungary.

3. We study global stability of a four agent formation in the plane, motivated by an example from Krick et al in [38]. The control laws are bidirectional, gradient-based interagent distance and are designed so that the agents cooperatively and autonomously achieve a specified desired formation shape. When every interagent distance is actively controlled (i.e. the information architecture is a complete graph), there may exist equilibrium formation shapes with incorrect interagent distances. We show that a class of rectangular incorrect equilibrium shapes identified in [38], which was previously thought to be stable, is actually locally unstable and provide a way to compute a desired equilibrium shape from a supposed incorrect equilibrium shape.

- T.H. Summers, C. Yu, B.D.O. Anderson, and S. Dasgupta, Formation shape control: Complete graph with four agents, *IEEE Conference on Decision and Control*, December 16-18 2009, Shanghai, China.

4. We address the problem of agent loss in vehicle formations and sensor networks via two separate approaches: (1) perform a “self-repair” operation in the event of agent loss to recover desirable information architecture properties, or (2) introduce robustness into the information architecture a priori such that agent loss does not destroy desirable prop-

erties. We focus on two properties of the graph called rigidity and global rigidity, which are required for formation shape maintenance and sensor network self-localization, respectively. For the self-repair approach, we show that while previous results permit local repair involving only neighbors of the lost agent, the repair cannot always be implemented using only local information. We present new results that make the local repair using only local information. We describe implementation and illustrate with algorithms and examples. For the robustness approach, we investigate the structure of graphs with the property that rigidity or global rigidity is preserved after removing any single vertex (we call the property *2-vertex-rigidity* or *2-vertex-global-rigidity*, respectively). Information architectures with such properties would allow formation shape maintenance or self-localization to be performed even in the event of agent failure. We review a characterization of a class of *2-vertex-rigidity* and develop a separate class. We also characterize of a class of *2-vertex-global-rigidity*.

- T.H. Summers, C. Yu, and B.D.O. Anderson, Addressing Agent Failure in Vehicle Formations and Sensor Networks, *International Journal of Robust and Nonlinear Control*, Vol. 19, No. 15, pp. 1673-1696, 2009.
- T.H. Summers, C. Yu, and B.D.O. Anderson, Robustness to Agent Loss in Vehicle Formations and Sensor Networks, *IEEE Conference on Decision and Control*, December 9-11 2008, Cancun, Mexico.

- T.H. Summers, C. Yu, and B.D.O. Anderson, Decentralized Closing Ranks in Vehicle Formations and Sensor Networks, *Mediterranean Conference and Control and Automation*, June 25-27 2008, Ajaccio, Corsica, France.

5. We design torque control laws that asymptotically synchronize the attitude of a team of rigid bodies subject to constant, unknown communication time delays, but without self-delays. Directed communication graphs that contain a spanning tree, which encompass both leader-follower and leaderless architectures are considered. A feedback linearization result involving the modified Rodrigues parameter (MRP) representation of attitude kinematics is employed to prescribe control torques that reduce the attitude dynamics to blocks of double integrator agents; the remainder of the control effort is prescribed to achieve attitude pointing to a consensus. Necessary and sufficient delay-independent stability conditions for the resulting closed-loop system are obtained. For leader-follower architectures, the desired consensus orientation is prescribed; for leaderless architectures, an analytical expression for the consensus attitude in terms of the initial conditions, control gains, and communication delay is derived.

- A. Chunodkar, T.H. Summers⁸, and M.R. Akella, Rigid body attitude synchronization with unknown communication time delays,

⁸A. Chunodkar and T.H. Summers each contributed equally to this work.

submitted to *Systems & Control Letters*.

- T.H. Summers, A. Chunodkar and M.R. Akella, Rigid body attitude synchronization with unknown communication time delays, *AAS/AIAA Space Flight Mechanics Meeting*, 14-17 February 2010, San Diego, CA, USA.

Chapter 2

Background: Rigid Graph Theory

Rigid graph theory has a long history in combinatorial mathematics [3, 27, 34, 40, 73], tracing back to a conjecture by Euler in 1766 [22] and a result by Cauchy in 1813 [16] on the rigidity of triangulated polyhedral surfaces. It has since been applied in a range of other fields including the molecular structures of proteins [36] and non-crystalline solids (e.g. glass) [75], and has recently been applied to model information architectures in autonomous vehicle formations [7, 21, 55]. Persistence theory, which is rigid graph theory generalized to directed graphs, has been developed only within the last few years to model one-way information flow in formation shape control problems [31–33, 81, 84]. Persistence in the plane is developed in [33] and extended to higher dimensions in [84]. The aim of this chapter is to provide a summary overview of rigidity and persistence theory in the plane as used in subsequent chapters on the formation shape control problem.

This chapter also briefly reviews global rigidity theory in the plane. Global rigidity is related to rigidity and is important in sensor network self-localization problems [5]. The robust information architecture design problems in this dissertation are developed to recover or preserve both rigidity and global

rigidity in the event of agent loss.

2.1 Graph Theory Preliminaries

An *undirected graph* $G(V, E)$ is a set $V = \{1, \dots, n\}$ of vertices and a set $E \subseteq V \times V$ of unordered pairs of vertices, called edges. A graph is often represented by assigning vertices to positions in the plane and drawing a line segment between vertices i and j whenever $(i, j) \in E$. We say that vertices i and j are *connected*, or *neighbors*, if $(i, j) \in E$ and that i and j are *incident* to (i, j) . The *degree* of d_i of vertex i is the number of edges to which it is incident, or equivalently its number of neighbors. A graph on n vertices is called *complete* and denoted by K_n if $E = V \times V$, i.e. every pair of vertices is connected by an edge. The complete graph contains $\frac{1}{2}n(n-1)$ edges. Graphs can sometimes be defined with *self-edges*, where $(i, i) \in E$, or with *multiple edges* between two vertices. A *simple graph* is one without self-edges and multiple edges. This dissertation exclusively uses simple graphs.

A *path* is a sequence of vertices v_1, \dots, v_m with $(i, i+1) \in E \forall i \in \{1, \dots, m-1\}$. Vertices v_1 and v_m are said to be connected by a path. A graph is called *connected* if every pair of vertices is connected by a path. A graph is called *k-connected* if it remains connected after removing any $k-1$ edges.

A *subgraph* of a graph $G(V, E)$ is a graph $G'(V', E')$ with $V' \subseteq V$ and $E' \subseteq E$. The subgraph *induced* by a set of vertices V' is obtained by removing all vertices in $V \setminus V'$ (where $V \setminus V' = \{v \in V | v \in V \text{ and } v \notin V'\}$) and all edges incident to them.

A *directed graph* $G(V, E)$ is a set V of vertices and a set $E \subseteq V \times V$ of *ordered* pairs of vertices, called edges. An edge $(i, j) \in E$ is an *outgoing edge* from i and an *incoming edge* to j . A directed graph is often represented by drawing arrows to indicated edge directions. A *directed path* is a sequence of vertices v_1, \dots, v_m with $(i, i + 1) \in E \forall i \in \{1, \dots, m - 1\}$. Vertices v_1 and v_m are said to be connected by a directed path. A *cycle* is a directed path that starts and ends at the same vertex. A directed graph that contains at least one cycle is called *cyclic*; otherwise it is called *acyclic*. A graph is called *strongly connected* if every pair of vertices is connected by a directed path. A *directed spanning tree* is a directed graph that has one vertex, called the *root*, from which there is a directed path to every other vertex.

2.2 Rigid and Persistent Formations

2.2.1 Rigidity

The *information architecture* of a formation is modeled by a graph $G(V, E)$ where the vertex set V represents the agents and the edge set E represents the set of interagent distances to be controlled to maintain formation shape. A *representation* $p : V \rightarrow \mathbb{R}^{2n}$ is a function which assigns to each vertex a position in the plane, and we call $p_i \in \mathbb{R}^2$ the position of vertex i . Consider all continuous motions such that the distances between any two vertices connected by an edge remains constant. The graph is called *rigid* if for

almost all¹ representations, every such motion preserves the distance between *every* vertex pair. A *formation* $F(G, p)$ is an information architecture together with a representation and is called rigid if G is a rigid graph.

Rigidity is a generic property; that is, for a formation with generic agent positions, it is not the particular agent positions that matter in determining rigidity, but rather the distribution of the edges amongst the graph vertices. This leads us to the following paraphrase of Laman’s combinatorial characterization of rigid graphs in the plane [40].

Theorem 2.2.1 ([40]). *A graph $G(V, E)$ is rigid in the plane iff there is a subgraph $G'(V, E')$, $E' \subseteq E$ that satisfies*

- $|E'| = 2|V| - 3$
- *For any $V' \subseteq V$ and the associated induced subgraph $G''(V', E'')$ of G' with $E'' \subseteq E'$, there holds $|E''| \leq 2|V'| - 3$.*

The first condition gives the minimum number of edges required for a rigid graph: given $|V|$ vertices, one must have at least $2|V| - 3$ edges. The second condition gives the manner in which a minimum set of edges must be

¹The definition of rigidity given here differs slightly from standard definitions in the literature. This is done to simplify the presentation by making several subtly different rigidity concepts equivalent (namely rigidity, infinitesimal rigidity, and graph rigidity; see e.g. [3, 4, 73]). The term “almost all” is referring here to *generic* representations, which form an open, dense subset of \mathfrak{R}^{2n} . A representation is called generic if the set of coordinates of agent positions is algebraically independent over the rationals. Non-generic representations correspond to special agent configurations, e.g. all agents are collinear. The fact that rigidity is a generic property is nontrivial; for discussion on use of the terms “generic” and “almost all” in this context, see [3, 4, 73]

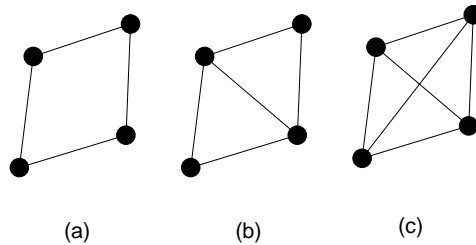


Figure 2.1: Illustration of a (a) non-rigid, (b) minimally rigid, and (c) non-minimally rigid formation.

distributed amongst the vertices to ensure rigidity. A graph is called *minimally rigid* if it is rigid and has exactly $2|V| - 3$ edges. The minimum number of required edges is linear in the number of vertices. In contrast, in a complete information architecture (i.e. every inter-vehicle distance is actively maintained), the number of required edges is quadratic in the number of vertices. This difference can be quite significant for large formations. For example, a 100 agent formation requires 197 distances to be maintained (and thus 197 communication/sensing links) whereas a complete architecture would require 4,950 links. Figure 2.1 illustrates non-rigid, minimally rigid, and non-minimally rigid formations with four vertices [2].

Additionally, there is a set of two basic operations, called Henneberg operations, that allow one to “grow” *every* minimally rigid graph in the plane from the complete graph on two vertices [34, 73]. Let j and k be two distinct vertices of a minimally rigid graph $G(V, E)$. A *vertex addition* operation involves adding a vertex i and edges (i, j) and (i, k) . Let x , y , and z be

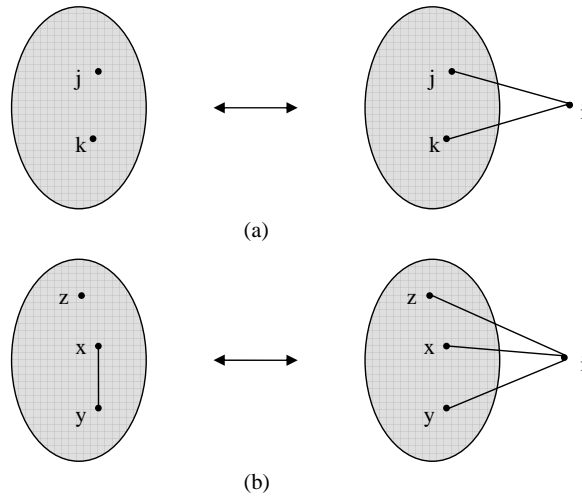


Figure 2.2: Representation of (a) vertex addition operation (b) edge splitting operation.

three distinct vertices of a minimally rigid graph with edge (x, y) . An *edge splitting* operation involves removing (x, y) and adding a vertex w and edges $(w, x), (w, y), (w, z)$. The operations are illustrated in Figure 2.2. They give an equivalent characterization of rigidity: a graph is minimally rigid iff it can be obtained from the complete graph on two vertices by applying a certain sequence of vertex addition and edge splitting operations.

There is a separate linear algebraic way to characterize rigidity involving the *rigidity matrix*. Let $F(G, p)$ be a formation in the plane and $p_i \in \mathbb{R}^2$ be the position of agent i . Let $\mathcal{F}(G, 2)$ denote the space of formations in the plane with a given graph G . Let $r : \mathcal{F}(G, 2) \rightarrow \mathbb{R}^{|E|}$ be the *rigidity function*

defined by

$$r(p) = \frac{1}{2}[\dots, \|p_j - p_k\|^2, \dots]^T \quad (2.1)$$

where the i th entry of r , viz. $\|p_j - p_k\|^2$, corresponds to the edge $e_i \in E$ connecting vertex j to vertex k in G . The rigidity matrix $R(p) \in \mathfrak{R}^{|E| \times 2|V|}$ is given by the Jacobian of r and has the following structure. The columns of R are regarded as $|V|$ sets of two columns, with each set of two columns corresponding to a vertex of G , i.e. columns $2i - 1$ and $2i$ correspond to vertex i . Each row of R corresponds to an edge of G . In the i th row corresponding to the edge connecting vertices j and k , all entries zero except in columns $2j - 1$, $2j$, $2k - 1$, $2k$, which are $x_j - x_k$, $y_j - y_k$, $x_k - x_j$, and $y_k - y_j$, respectively, with (x_j, y_j) denoting the coordinates of agent j . Because the rigidity matrix is the Jacobian of a rational function, it has the same rank for all points but a set of measure zero (via a nontrivial result of Sard [62]), corresponding to special vehicle configurations (e.g. there is a set of collinear or collocated vehicles) that cause the rank deficiency. The linear algebraic characterization is given by following result from [73].

Theorem 2.2.2 ([73]). *Let $F(G, p)$ be a formation in the plane with generic representation p and let $R(p)$ be the associated rigidity matrix. Then F is rigid iff the rank of $R(p)$ is $2|V| - 3$.*

Thus, a rigid formation has at least $2|V| - 3$ well-distributed edges and has a rigidity matrix with full row rank. Further, the dimension of the null space is exactly three. The vectors in the null space correspond to a set of infinitesimal displacements of the agents that preserve the formation shape, with

the three independent displacements spanning the null space corresponding to translation in two directions and rotation of the entire formation.

Rigid graph theory can be developed for representations in D dimensions (i.e. $p : V \rightarrow \mathfrak{R}^{Dn}$ with $p_i \in \mathfrak{R}^D$). The linear algebraic characterization given by Theorem 2.2.2 generalizes to any dimension: a formation in D -space with generic representation is rigid iff the associated rigidity matrix has rank $D|V| - \frac{1}{2}D(D+1)$ [73]. For example, in three dimensions, a rigid formation with $|V|$ agents has a rigidity matrix with rank $3|V| - 6$. Unfortunately, the Laman conditions given in Theorem 2.2.1 are only necessary for $D > 2$ [73]. Finding a necessary and sufficient combinatorial characterization for graphs in higher dimensions remains a significant and elusive open problem in rigid graph theory.

2.2.2 Persistence

An important distinction of rigid graph theory as applied to autonomous vehicle formations is that the distance corresponding to an edge is held constant by a control law rather than by some physical mechanism. This distinction gives rise to the notion of rigidity for directed graphs. In particular, there are two possible ways that a particular interagent distance can be controlled: either the two involved agents share the responsibility, or only one of the involved agents is given the responsibility. In the former case, the information architecture can be modeled by an undirected graph, and in the latter case, by a directed graph. We sometimes refer to the formation as being undirected or

directed, respectively. In a directed formation, a direction is assigned to every edge in E with an outgoing edge from the agent responsible for controlling the interagent distance.

Directed formations have the advantage of reducing the sensing and communication requirements by half. Also, they allow leader-follower formations that are prevalent in the literature and may be necessary when agents have limitations on sensing/communication range.

The concept of rigidity for directed graphs is not a simple transposition of rigidity for undirected graphs; therefore, the term *persistence* is used for directed graphs to distinguish from the undirected notion. It turns out that the formation shape control task becomes impossible for certain directed information flows. To preclude these situations, a further condition called *constraint consistency* is required in addition to rigidity [33]. Examples of a constraint consistent and non-constraint consistent graph are shown in Figure 2.3, taken from [83]. In the right-hand graph, agent 1 is free to move in the plane while agents 2 and 3 can move on circles around agent 1; thus, it may be impossible for agent 4 to maintain all of its distance constraints simultaneously. For further discussion and rigorous definitions, see [33, 83, 84].

Essentially, a graph is persistent if its underlying undirected graph (obtained simply by ignoring the edge directions) is rigid and the edge directions are constraint consistent. A formation is called persistent if its information architecture is persistent.

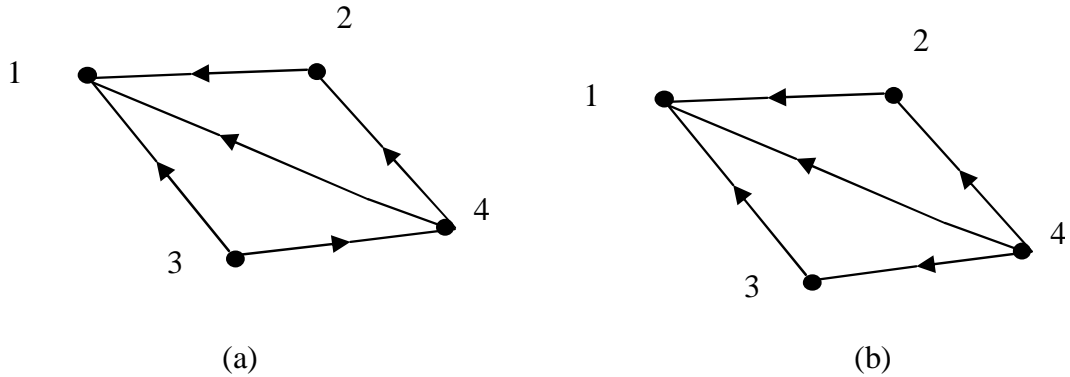


Figure 2.3: Constraint consistent and non-constraint consistent graphs with the same underlying undirected graph.

2.2.3 Minimally Persistent Formations

The focus in this dissertation will be on minimally persistent formations in the plane, which are persistent formations with the smallest possible number of edges in the graph. We have the following basic result from [33].

Theorem 2.2.3 ([33]). *Let $G(V, E)$ be a directed graph in the plane with at least two vertices. Then G is minimally persistent iff the underlying undirected graph is minimally rigid (rigid with exactly $2|V| - 3$ edges), and no vertex has more than two outgoing edges.*

This results in the following classification of minimally persistent formations in the plane.

- Type (A) [*Leader-First-Follower* (LFF)]: One agent known as the leader has no outgoing edge, i.e. zero distances to maintain and thus two degrees of freedom (DOF). Another known as the first follower has one

out going edge to the leader, i.e. one distance to maintain and thus one DOF. The remaining, ordinary followers have two outgoing edges each, i.e. two distances to maintain and thus zero DOF.

- Type (B) [*Leader-Remote-Follower* (LRF)]: One agent known as the leader has no outgoing edge (two DOF), another known as the remote follower has one outgoing edge to an agent other than the leader (one DOF), and the remaining ordinary followers have two outgoing edges each (zero DOF).
- Type (C) [*Coleader*]: Three agents (known as coleaders), have one outgoing edge each (one DOF each) and all others (known as ordinary followers), have exactly two such edges each (zero DOF).

Figure 2.4 illustrates examples LFF and LRF formations. Figure 2.5 illustrates examples of coleader formations with differing information flow patterns and coleader connectivity.

In directed formations, it becomes possible to have cycles in the information architectures. LFF formations can be either cyclic or acyclic, and LRF and coleader formations are inherently cyclic (see Theorem 5 of [33]). As will be seen in Chapter 4, cyclic information architectures can cause the desired formation shape to be locally unstable under a standard control law; achieving stabilizability requires a non-trivial modification of the control law.

When might the LRF or Coleader structures be used? There is currently no straightforward measure like a controllability gramian that might give

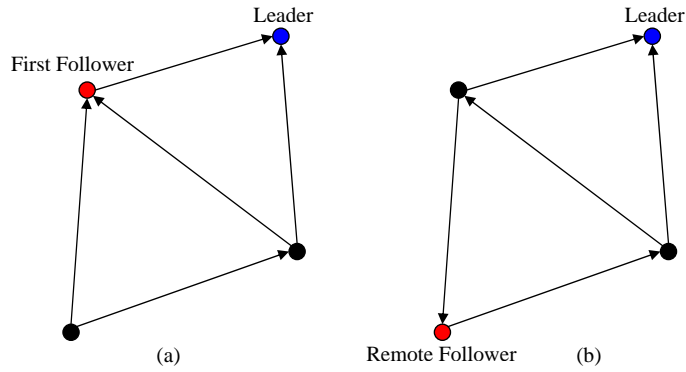


Figure 2.4: Examples of LFF and LRF formations with four agents: (a) in LFF formations the one-DOF agent is connected to the leader, and (b) in LRF formations the one-DOF agent is not connected to the leader.

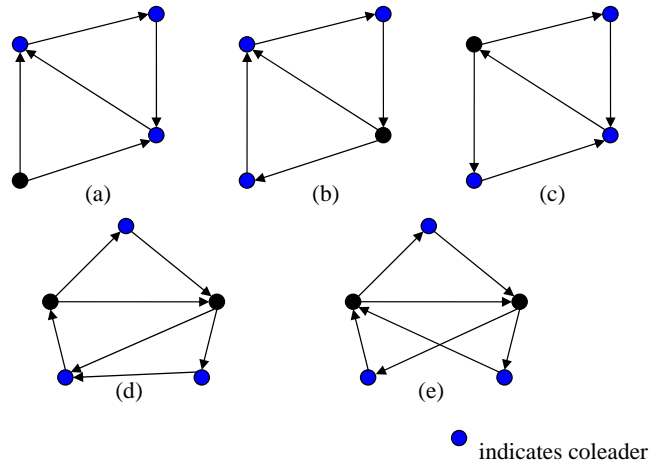


Figure 2.5: Examples of coleader formations with connected coleaders: (a) cyclic coleaders, (b) inline coleaders, (c) v-coleaders. Examples of coleader formations with non-connected coleaders: (d) one-two coleaders, (e) distributed coleaders. Each coleader has only one interagent distance to maintain and so has only one outgoing arrow.

guidance as to preferred information structures, and such a measure might well give guidance. Apart from that, one can readily contemplate intuitively the potential attractiveness of a cyclic coleader pattern in the case of a formation three of whose agents define a triangle, with all other agents in the interior of the triangle. The three agents defining the triangle would in some sense confine and lead the rest of the formation. The motion of the three agents in this case can be analyzed as in [1], and would be independent of the motion of other agents, though not conversely. In relation to a leader-remote-follower structure, one could conjecture its relevance for control of a formation whose shape was long and thin. At one end of the formation, the leader would move in the direction of a target. At the other end of the formation, the freedom of the remote follower would be used to rotate the formation, thereby aligning its longer axis with the direction of target motion.

The distinction between LFF, LRF, and coleader formations is important in the stability analysis for the formation shape control laws. In particular, for LFF formations it is possible to define a global coordinate basis to obtain a hyperbolic reduced-order system in which local stability can be ascertained via eigenvalue analysis of the linearized system [83]. This is so because in the framework of both [83], after its “small” initial move, the leader stops moving. Thereafter, the algorithm of [83] forces the first follower to move in the direction of the leader. Thus the direction of movement of the first follower in the LFF framework is fixed. This direction critically defines the stated coordinate basis in [83]. In contrast, for LRF formations the direction associated with

the remote follower's DOF is not fixed in space since it is following an agent other than the leader to satisfy its distance constraint. Similarly, for coleader formations the directions associated with the coleader DOFs are not fixed in space. Thus, the device used in [83] to obtain a global coordinate system that provides a hyperbolic reduced-order system no longer applies. Consequently, one cannot draw conclusions about the local stability of the nonlinear system near the desired formation shape by analyzing the linearized system alone; more sophisticated techniques are needed. Center manifold theory provides tools for determining stability near nonhyperbolic equilibrium points and is reviewed in Chapter 4.

In contrast to [83], [38] does use center manifold theory to establish stability of the closed-loop system, but their analysis is restricted to undirected graphs. It is possible to work with a reduced-order system, using the fact that for the laws in question, the centroid of the formation is stationary. This allows the full-order system to be reduced by 2 in dimension, and leaves one zero eigenvalue for the linearized system. A critical feature of the center manifold analysis of [38] is the observation that the set of equilibria of this reduced-order system is then compact. For LRF formations, one can fix the position of the leader to obtain a compact set of equilibria for a reduced-order system. However, this is not possible in the coleader setting. In either case, separate aspects of center manifold theory have to be used to establish a related *de facto* compactness condition. Stability analysis of the formation shape control laws for minimally persistent LRF and Coleader formations is taken up in Chapter

4.

2.3 Global Rigidity

A fundamental task for sensor networks is to determine uniquely the position of each agent from knowledge of certain inter-agent distances and the positions of a small number of agents. This task is related to a further concept called *global rigidity*. A graph in the plane is called *globally rigid* if two formations having the same inter-agent distances differ at most by translation, rotation, and reflection. In [5], Aspnes et al show that global rigidity is required for unique self-localization in sensor networks (and when the positions of any three non-collinear agents are known, global rigidity is sufficient for localizability of every agent). In [35], Jackson and Jordan prove a conjecture posed by Hendrickson in [30] that provides a complete characterization of global rigidity in the plane. The result is as follows:

Theorem 2.3.1. *A graph $G(V, E)$ in the plane is globally rigid if and only if it is 3-connected and redundantly rigid².*

A graph is called *minimally globally rigid* if it is globally rigid and there exists no globally rigid graph with the same number of vertices and a smaller number of edges, or equivalently, if removing any edge results in loss of global rigidity. This equivalency is related to the fact that the edge splitting

²A graph is redundantly rigid if it remains rigid after removing any edge.

operation described above can be used to “grow” *all* minimally globally rigid graphs from the complete graph on four vertices [10].

2.4 Conclusion

Rigidity, persistence and global rigidity are rich mathematical topics that feature extensively in modeling of autonomous vehicle formations and sensor networks in this dissertation. A demonstration of how persistence features in the information architecture and control law design is presented in the next chapter, which examines a practical scenario in which a team of unmanned aircraft are employed to cooperatively track a target.

Chapter 3

Coordinated Standoff Tracking: Control Laws and Information Architectures

3.1 Introduction

A primary use of unmanned aerial vehicles (UAVs) is for the surveillance and tracking of moving targets. Teams of UAVs could be employed for reconnaissance on unknown or adversarial targets, or for surveillance of the surrounding area for potential threats to a friendly convoy. This chapter examines a *coordinated standoff tracking problem*, in which the objective is to fly a team of UAVs in a planar circular orbit around a moving target with prescribed standoff radius and inter-vehicle angular spacing.¹ It demonstrates that persistent information architectures can be used to achieve the coordinated standoff tracking objective, and implements control laws based on these architectures.

The problem of designing a heading rate controller to enable a vehicle to maintain the prescribed standoff radius from the target was recently introduced by Frew, Lawrence, and Morris using a Lyapunov guidance vector field

¹A configuration that places vehicles at equal angular spacing around a perimeter is optimal for gathering information about a given target [50].

approach [24]. This study also proposed airspeed control laws for two vehicles to achieve a prescribed angular spacing while executing the circular orbit. However, this analysis left several important areas open for further work.

- It neglected an important timescale separation issue for heading and standoff radius convergence.
- Although target motion and wind were considered, these were assumed to be known so that a correction term could be added into the control law. In general, wind and target motion are unknown and necessitate an estimation process or adaptive control laws.
- The angular spacing analysis for two vehicles did not provide a formal proof of convergence to the desired configuration.
- The multi-vehicle analysis was restricted to two vehicles and did not consider information architectures that scale to any number of vehicles.

A Lyapunov guidance vector field approach was also adopted in a study by Kingston and Beard that used heading control exclusively to obtain the desired circular orbit and spacing [37]. This analysis also had limitations.

- It circumvents the timescale separation issue by using a sliding mode controller to guarantee heading convergence in finite time; however, sliding mode controllers are inherently discontinuous and known to produce actuator chatter.

- It utilizes an information architecture that scales to n vehicles, but this architecture contains more than the minimum necessary number of information links. Their stability results are local, though their Monte Carlo analysis also suggests global stability.

This chapter addresses several gaps in the above analyses to further develop the Lyapunov guidance vector field approach to steer vehicles to the desired planar circular orbit. Section 3.2 presents the dynamical model and Lyapunov guidance field approach. In the no-wind, stationary target case, we show that the guidance field admits a closed-form analytical solution and that this can be used in a path planning approach for a single vehicle. We analyze two approaches for heading convergence, including a novel approach that guarantees exact heading convergence in finite time, and demonstrate that the trajectory is entirely determined from the initial condition. Section 3.3 applies these results to the case of a moving target with unknown constant-velocity and unknown wind. Adaptive estimates are employed to account for wind and target motion to achieve the desired circular orbit. Section 3.4 presents a variable airspeed control law that achieves the desired angular spacing. The control laws are based on a persistent information architecture. We show convergence to the desired configuration for any number of vehicles. Section 3.5 shows numerical simulations that demonstrate the theoretical work, and Section 3.6 offers concluding remarks.

3.2 The Coordinated Standoff Tracking Problem

This section presents the dynamic model and the Lyapunov guidance vector field approach to guide a single vehicle to the desired circular orbit, as introduced by Frew, Lawrence, and Morris in [24]. We begin with the no-wind stationary target case and generalize the results to account for unknown wind and target motion in the following section.

We use the following unicycle model with kinematic constraints to describe the dynamics of a fixed-wing UAV:

$$\begin{aligned}\dot{x} &= u_1 \cos \psi \\ \dot{y} &= u_1 \sin \psi \\ \dot{\psi} &= u_2\end{aligned}\tag{3.1}$$

where $[x, y]^T \in \mathbb{R}^2$ is the inertial position of the aircraft, ψ is the heading, u_1 is the airspeed input, and u_2 is the heading rate input. This model, as with any model, represents a simplification of the physics of a real UAV. It is assumed that the UAV is capable of altitude stabilization, so the analysis is restricted to a flat-earth plane, and typically 2nd-order dynamics associated with the control inputs are neglected. However, the unicycle model is commonly used in the literature [24, 49, 65] and is a reasonable starting point for describing UAV motion. We do enforce kinematic constraints that would be an essential feature of any practical implementation. We assume that there are constraints on minimum and maximum airspeed according to

$$0 < v_{min} \leq u_1 \leq v_{max}\tag{3.2}$$

and a constraint on maximum heading rate magnitude according to

$$|u_2| \leq \omega_{max}. \quad (3.3)$$

The maximum heading rate constraint is equivalent to a minimum turning radius constraint, where $r_{min} = u_1/\omega_{max}$.

3.2.1 Lyapunov Guidance Vector Field Construction

This subsection describes the design of the heading rate control input $u_2(t)$ to guide a vehicle to the desired circular trajectory around the target. For the moment, we assume that the airspeed input is constant, i.e. $u_1(t) = u_0 \forall t$. The heading rate command is generated from a Lyapunov guidance vector field that guides the UAV to a circular orbit around the target, which is assumed to be stationary and centered at the origin. We assume here that the initial vehicle heading is aligned with the heading specified by the Lyapunov guidance vector field and discuss how to deal with arbitrary initial headings in the next subsection.

Consider the Lyapunov function

$$V(r) = (r^2 - r_d^2)^2 \quad (3.4)$$

where $r = \sqrt{x^2 + y^2}$ is the relative distance to the target and r_d is the desired standoff radius of the circular orbit. As shown in [24], the time derivative of V can be made non-positive and the the circular orbit can be achieved by choosing the desired inertial velocity according to the vector field

$$f(x, y) = \begin{bmatrix} \dot{x} \\ \dot{y} \end{bmatrix} = -\frac{u_0}{r(r^2 + r_d^2)} \begin{bmatrix} x(r^2 - r_d^2) + y(2rr_d) \\ y(r^2 - r_d^2) - x(2rr_d) \end{bmatrix}. \quad (3.5)$$

The desired heading along the vector field, denoted ψ_d , is determined from (3.5) via

$$\psi_d = \arctan\left(\frac{\dot{y}}{\dot{x}}\right) = \arctan\left(\frac{-y(r^2 - r_d^2) + x(2rr_d)}{-x(r^2 - r_d^2) - y(2rr_d)}\right). \quad (3.6)$$

Differentiating, we obtain the heading rate input along the guidance field

$$u_2 = \dot{\psi}_d = \frac{4u_0r_d^3}{(r^2 + r_d^2)^2}. \quad (3.7)$$

To satisfy the heading rate constraint, we require $\dot{\psi}_d \leq \omega_{max}$. Since the heading rate given by (3.7) is maximized when $r = 0$, the constraint is satisfied for any guidance field trajectory whenever $4u_0/r_d \leq \omega_{max}$. It will be shown below that if the guidance field trajectory begins outside the standoff radius, it converges globally asymptotically to the standoff radius without ever going inside the standoff radius. For such trajectories, the heading rate constraint is satisfied whenever $u_0/r_d \leq \omega_{max}$. Throughout this subsection, we assume that the parameters u_0, r_d , and ω_{max} are such that the heading rate constraint is satisfied along the guidance trajectories.

The guidance field may be expressed in polar coordinates as

$$g(r, \theta) = \begin{bmatrix} \dot{r} \\ r\dot{\theta} \end{bmatrix} = \frac{u_0}{r^2 + r_d^2} \begin{bmatrix} -(r^2 - r_d^2) \\ 2rr_d \end{bmatrix}. \quad (3.8)$$

Observe qualitatively that when $r > r_d$, r decreases toward the standoff radius, when $r < r_d$, r increases toward the standoff radius, and when $r = r_d$, r is constant and the vehicle moves around the standoff circle with constant angular velocity $\dot{\theta} = u_0/r_d$, which is the desired behavior. Evaluating the

derivative of (3.4) along these trajectories, then

$$\dot{V} = -\frac{4u_0r(r^2 - r_d^2)^2}{r^2 + r_d^2} \leq 0 \quad (3.9)$$

and LaSalle's Invariance Principle [41] may be invoked to conclude that $r \rightarrow r_d$ as $t \rightarrow \infty$, i.e. the trajectories converge asymptotically to the desired standoff radius [24].

In fact, the vector field admits a closed-form analytical solution. Observe that the dynamics in (3.8) are independent of θ and we can obtain

$$\frac{dr}{d\theta} = -\frac{r^2 - r_d^2}{2r_d} \quad (3.10)$$

which has the solution

$$r(\theta) = \begin{cases} \frac{1+k_r e^{-(\theta-\theta_0)}}{1-k_r e^{-(\theta-\theta_0)}} r_d, & r_0 \geq r_d \\ \frac{1-k_r e^{-(\theta-\theta_0)}}{1+k_r e^{-(\theta-\theta_0)}} r_d, & r_0 < r_d \end{cases} \quad k_r = \frac{r_0 - r_d}{r_0 + r_d} \quad (3.11)$$

where $r_0 = r(0)$ is the initial separation distance from the target and θ_0 is the initial polar coordinate ‘‘clock angle’’. This solution can be substituted into the $\dot{\theta}$ equation in (3.8), which can be integrated to give the following implicit solution for θ as a function of time

$$\begin{aligned} \theta - \theta_0 &= \frac{u_0}{r_d}(t - t_0) + 2k_r \left[\frac{e^{-(\theta-\theta_0)}}{1 - k_r e^{-(\theta-\theta_0)}} - \frac{1}{1 - k_r} \right] & r_0 \geq r_d \\ \theta - \theta_0 &= \frac{u_0}{r_d}(t - t_0) - 2k_r \left[\frac{e^{-(\theta-\theta_0)}}{1 + k_r e^{-(\theta-\theta_0)}} - \frac{1}{1 + k_r} \right] & r_0 < r_d. \end{aligned} \quad (3.12)$$

An example trajectory under the control law (3.7) is shown in Fig. 3.1 with $u_0 = 20m/s$, $r_d = 300m$, $x_0 = 800m$, $y_0 = 800m$, and assuming $\psi_0 = -2.8746rad$ in accordance with (3.6).

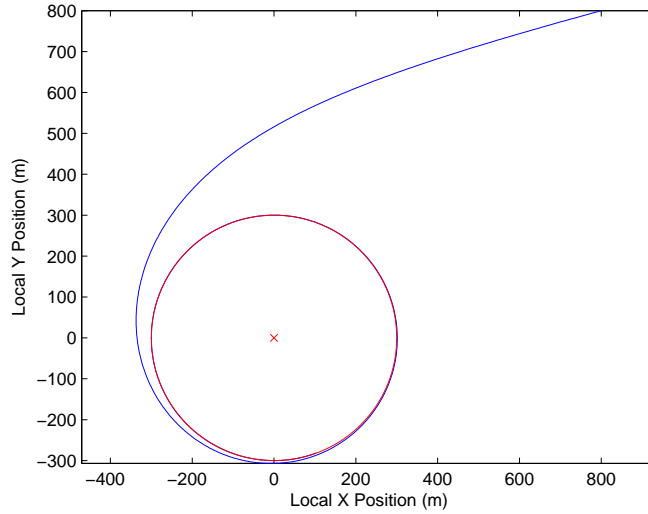


Figure 3.1: Lyapunov guidance field trajectory with heading initially aligned with the field.

The solutions given by (3.11) and (3.12) constitute the complete analytical solution to the guidance vector field. A vehicle with heading rate commanded according to (3.7) will converge to the desired circular orbit, provided that the initial heading is aligned with the guidance field. However, in general the initial vehicle heading will not be aligned with the guidance field, and we need an approach to converge to the desired heading. In the next subsection, we analyze two approaches for heading convergence. We show that a heading feedback approach from the literature has some theoretical and practical limitations and propose an alternative that avoids these limitations.

3.2.2 Heading Convergence

A heading feedback approach to obtain exponential heading convergence is used by Frew, Lawrence, and Morris [24]; however, a complete proof that accounts for the timescale separation between heading convergence and standoff radius convergence is absent from their analysis. Other studies use a sliding mode controller to guarantee heading convergence in finite time, [28,37] which is inherently discontinuous and known to produce actuator chatter. This problem is typically circumvented in practice by an approximation via a saturation function, but this has the effect of diluting the theoretical convergence properties.

In this subsection, we present a proof of heading convergence using the feedback approach that explicitly addresses the timescale separation issue. We also identify two theoretical and practical problems with this approach. First, the proof of convergence is restricted to a certain set of initial headings, and second, the kinematic constraints are not always satisfied.

As an alternative, we propose a novel, yet simple, approach to heading convergence, which involves an initial minimum radius loiter circle. The vehicle converges exactly to the desired heading in finite time for any initial heading and does not violate the kinematic constraints. Further, the time and location of convergence are analytically computable, and this allows the entire trajectory to be exactly known for any arbitrary initial heading.

3.2.2.1 Heading Feedback

Before proceeding with the heading error analysis, we introduce some additional notation for the guidance trajectories. Since $x = r \cos \theta$ and $y = r \sin \theta$, and defining the angle ϕ via

$$\cos \phi = \frac{r^2 - r_d^2}{r^2 + r_d^2}, \quad \sin \phi = \frac{2rr_d}{r^2 + r_d^2}, \quad (3.13)$$

we can write the vehicle dynamics (3.5) as

$$\begin{aligned} \dot{x} &= -\frac{u_0}{r^2 + r_d^2} \left[(r^2 - r_d^2) \frac{x}{r} + (2rr_d) \frac{y}{r} \right] \\ &= -u_0 [\cos \theta \cos \phi + \sin \theta \sin \phi] \\ &= -u_0 \cos(\theta - \phi) \end{aligned} \quad (3.14)$$

and similarly

$$\begin{aligned} \dot{y} &= -\frac{u_0}{r^2 + r_d^2} \left[(r^2 - r_d^2) \frac{y}{r} - (2rr_d) \frac{x}{r} \right] \\ &= -u_0 [\sin \theta \cos \phi - \cos \theta \sin \phi] \\ &= -u_0 \sin(\theta - \phi). \end{aligned} \quad (3.15)$$

Accordingly, from (3.6) we obtain the following angle relationship

$$\psi_d = \theta - \phi + \pi. \quad (3.16)$$

Now, suppose the vehicle has some initial heading error $\psi_e(0)$ defined by

$$\psi_e(t_0) = \psi(t_0) - \psi_d(t_0) \quad (3.17)$$

where $\psi(t_0)$ is the actual initial heading and $\psi_d(t_0)$ is the desired initial heading along the guidance solution. If the heading rate input u_2 is given by

$$u_2(t) = -k\psi_e(t) + \dot{\psi}_d(t) \quad (3.18)$$

for some feedback gain $k > 0$, then we obtain exponential convergence of the feedback error as $\psi_e(t) = \psi_{e0}e^{-k(t-t_0)}$, wherein $\psi_{e0} = \psi_e(t_0)$. Note that the parameter k explicitly governs the heading error convergence rate and that k must be chosen so that the turn rate constraint given by (3.3) is not violated. This requires striking a proper balance between the feedback and feedforward terms in (3.18).

From (3.1) and (3.17), the vehicle dynamics may be expressed as

$$\begin{bmatrix} \dot{x} \\ \dot{y} \end{bmatrix} = \begin{bmatrix} \cos(\psi_e) & -\sin(\psi_e) \\ \sin(\psi_e) & \cos(\psi_e) \end{bmatrix} \begin{bmatrix} u_0 \cos(\psi_d) \\ u_0 \sin(\psi_d) \end{bmatrix}. \quad (3.19)$$

Note that the matrix involving heading error has the structure of a rotation matrix. Further, as the heading error $\psi_e(t)$ converges to zero, this matrix exponentially becomes the identity matrix, and the ideal dynamics along the guidance field are recovered. From (3.19) we obtain the desired heading rate when there is heading error

$$\dot{\psi}_d = \frac{4u_0r_d^3}{(r^2 + r_d^2)^2} - \frac{2u_0}{r} \sin\left(\frac{\psi_e}{2}\right) \left[\cos\left(\phi - \frac{\psi_e}{2}\right) - \sin(\phi) \sin\left(\phi - \frac{\psi_e}{2}\right) \right]. \quad (3.20)$$

The desired heading rate here consists of the ideal heading rate along the guidance field given in (3.7) and a term involving $\sin(\psi_e/2)$ that goes to zero as ψ_e goes to zero. This additional term involves r in the denominator and

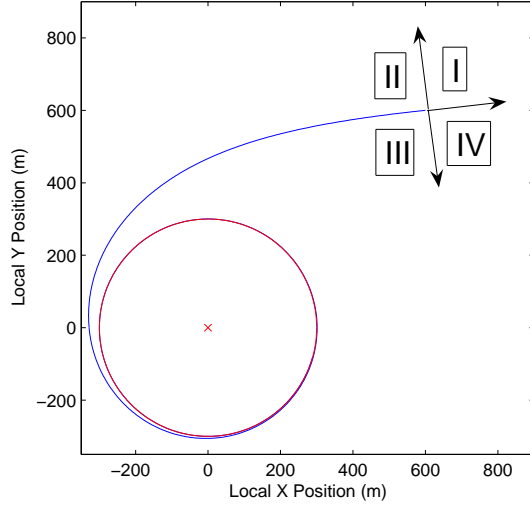


Figure 3.2: Heading Error Quadrants

may produce large heading rate commands that would violate the heading rate constraint when r becomes small.

The results for boundedness and convergence with the heading feedback approach depend on the quadrant of the initial heading error, illustrated in Fig. 3.2 where the curve represents the analytical guidance trajectory with $u_0 = 20m/s$, $r_d = 300m$, $x_0 = 600m$, and $y_0 = 600m$. The desired heading is tangent to this trajectory; in general, the actual initial heading will not be aligned with the guidance field, but instead pointed in one of the quadrants shown. The result is provided by the following theorem.

Theorem 3.2.1. *Suppose the vehicle dynamics are given by (3.1) and subject to kinematic constraints (3.2) and (3.3). Suppose the airspeed input is set*

to a constant u_0 , and the heading rate input is given by (3.18) and (3.20). Then when the initial heading error satisfies $-\pi/2 \leq \psi_{e0} \leq \pi/2$ (i.e. heading error is in quadrant II or III, as shown in Fig. 3.2), the vehicle asymptotically converges to the standoff radius and circles the target with constant angular velocity, i.e. $\lim_{t \rightarrow \infty} r(t) = r_d$ and $\lim_{t \rightarrow \infty} \dot{\theta}(t) = u_0/r_d$.

Proof. The vehicle dynamics may be expressed in polar coordinates as

$$\begin{bmatrix} \dot{r} \\ r\dot{\theta} \end{bmatrix} = \frac{u_0}{r^2 + r_d^2} \begin{bmatrix} \cos(\psi_e) & -\sin(\psi_e) \\ \sin(\psi_e) & \cos(\psi_e) \end{bmatrix} \begin{bmatrix} -(r^2 - r_d^2) \\ 2rr_d \end{bmatrix}. \quad (3.21)$$

We can express the r dynamics more compactly as

$$\dot{r} = -u_0 \cos(\phi - \psi_e). \quad (3.22)$$

Let us first establish an upper bound for r . Note from (3.13) that $\phi \in [0, \pi)$ (since $r \geq 0$) and $\phi \rightarrow 0$ as $r \rightarrow \infty$, $\phi = \pi/2$ when $r = r_d$, and $\phi \rightarrow \pi$ as $r \rightarrow 0$.

For the first case, suppose that the initial heading error is $-\pi/2 \leq \psi_{e0} < 0$ (i.e. the heading error is in quadrant II). Then we obtain the following upper bound on r (assuming $r_0 > r_d$),

$$r(t) \leq r_0 + u_0 t^* \triangleq r_{sup} \quad (3.23)$$

where t^* is the time at which r achieves its maximum value, which may be bounded as

$$t^* \leq \frac{1}{k} \ln \left(\frac{-\psi_{e0}}{\frac{\pi}{2} - \phi(0)} \right). \quad (3.24)$$

From (3.22) we have $r(t) \geq r_d$ for all $t \geq 0$.

For the second case, suppose that $0 \leq \psi_{e0} \leq \pi/2$ (i.e. the initial heading error is in quadrant III). From (3.22) we obtain $r(t) \leq r_0 \leq r_{sup} \forall t$. For this case, it is possible for $r(t)$ to become smaller than the prescribed stand-off radius r_d . The actual size of this standoff distance violation effectively depends on the initial distance to the target r_0 and the feedback gain parameter k .

Now consider the Lyapunov function candidate

$$V = \frac{1}{2}(r^2 - r_d^2)^2 + \frac{\lambda}{2}\psi_e^2, \quad (3.25)$$

for some $\lambda > 0$. Evaluating \dot{V} along the trajectories given by (3.21) and (3.22), then

$$\dot{V} = \frac{-2u_0r(r^2 - r_d^2)^2}{r^2 + r_d^2} + 4u_0r(r^2 - r_d^2)\sin\left(\frac{\psi_e}{2}\right)\sin\left(\frac{\psi_e}{2} - \phi\right) - \lambda k\psi_e^2. \quad (3.26)$$

Now, provided that $-\pi/2 \leq \psi_{e0} \leq \pi/2$, we can bound \dot{V} as

$$\dot{V} \leq \frac{-u_0r(r^2 - r_d^2)^2}{r^2 + r_d^2} + [u_0r_{sup}(r_{sup}^2 + r_d^2) - \lambda k]\psi_e^2 \quad (3.27)$$

and choosing λ according to

$$\lambda > \frac{1}{k}u_0r_{sup}(r_{sup}^2 + r_d^2) \quad (3.28)$$

we then obtain

$$\dot{V} \leq \frac{-u_0r(r^2 - r_d^2)^2}{r^2 + r_d^2} - \alpha\psi_e^2 \leq 0 \quad (3.29)$$

where $\alpha > 0$. Thus, $\lim_{t \rightarrow \infty} r(t) = r_d$, and $\lim_{t \rightarrow \infty} \dot{\theta}(t) = u_0/r_d$ follows from (3.21). When $|\psi_{e0}| > \pi/2$ (i.e. heading error is in quadrant I or IV), we cannot

bound \dot{V} as above. Consequently, the proof does not encompass this range of initial headings. \square

Our proof of convergence addresses the timescale separation issue between heading convergence and standoff radius convergence. The theoretical problem with this approach is that the proof is restricted to initial headings in quadrants II and III. It is not necessarily impossible to prove convergence for the remaining quadrants, though it would likely require a nontrivial modification to what we have shown. The practical problem with this approach is that for initial headings in quadrant III, where $r(t)$ could possibly become smaller than the prescribed standoff distance r_d , it is not straightforward to choose the heading feedback gain k in such a way to satisfy the heading rate constraint. The lower bound of r for initial headings in quadrant III is a function of k , and there is potential to violate the heading rate constraint. A particular case is shown in Fig. 3.3 with $u_0 = 20m/s$, $r_d = 300m$, $x_0 = 325m$, $y_0 = 0m$, $\psi_0 = \pi$, and $k = 0.001$. Although the trajectory will eventually converge to the standoff radius via Theorem 3.2.1, it gets close to the target in the process, and potentially violates the turn rate constraint due to tighter loops the vehicle must execute around the target.

3.2.2.2 Initial Loiter Circle

The availability of an analytical solution for the guidance vector field motivates a novel approach for aligning the heading with the field. In particular, we show in this section that the desired heading can be exactly achieved

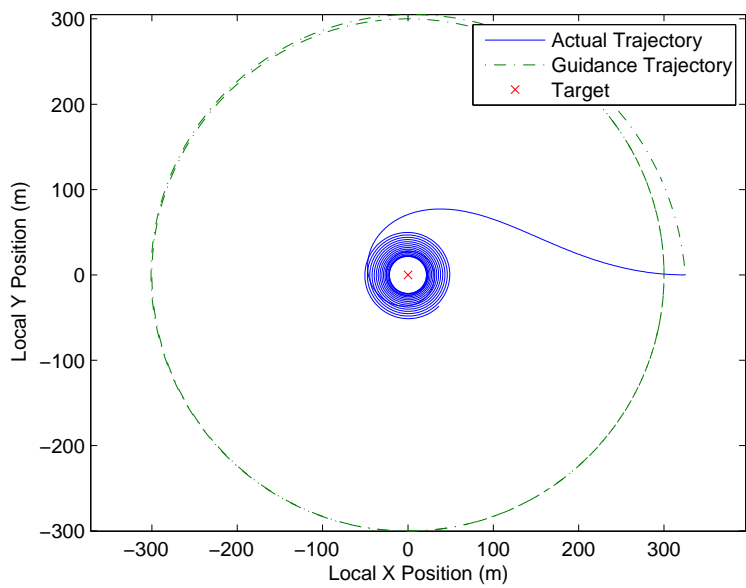


Figure 3.3: Trajectory using heading feedback with initial heading in quadrant III and small feedback gain.

without the use of continuous heading feedback. The approach is to fly an initial loiter circle of minimum radius r_{min} that is consistent with the heading rate constraint (3.3). Whenever the desired heading is exactly achieved, the vehicles can switch onto the guidance field solution, which is analytically known from (3.11) and (3.12). The time and location of convergence are analytically available. The result is given by the following theorem.

Theorem 3.2.2. *Any minimum radius loiter circle that does not contain the target will necessarily obtain the desired heading defined by the guidance vector field (3.6) within finite time.*

Proof. Consider a minimum radius loiter circle on which a vehicle is traveling initially. This trajectory continuously takes on all values in $[0, 2\pi]$ from initial time to the time it takes to complete the loiter circle. Note that the desired heading on the loiter circle is the same at initial time and at the time at which a loiter circle has been completed (since this is the same point in space). Assuming that the loiter circle does not contain the target, we can show that the desired heading along the loiter circle takes on only a subset of values in $[0, 2\pi]$. Then along the lines of the Intermediate Value Theorem, the headings will match at some point between initial time and the time at which a loiter circle has been completed. We make the argument for the open right half-plane. By the radial symmetry of the guidance vector field, the argument will hold for any rotated open half-plane. Thus, the result holds for any loiter circle that does not contain the target.

Let us show that in the open right half-plane, the guidance vector field (3.5) never points down, i.e. when the \dot{x} -component is zero the \dot{y} -component is positive. Ignoring the scalar parts since they do not contribute to direction, when the \dot{x} -component is zero, the \dot{y} -component is given by

$$\dot{y} = 2r_d(x + \frac{y^2}{x})\sqrt{x^2 + y^2} \quad (3.30)$$

Since in the open right half-plane $x > 0$, then $\dot{y} > 0$. By radial symmetry of the vector field, the same argument is valid for any rotated open half-plane, and hence the desired heading can be attained by any trajectory in this plane that acquires all headings. \square

Thus, it suffices to simply execute an initial loiter circle of minimum radius in accordance with the initial heading, and the desired heading will be exactly attained in finite time at some point on the circle. In fact, in the stationary target with no wind case, we can determine the point of heading convergence as follows. Consider an initial loiter circle defined by

$$(x - x_l)^2 + (y - y_l)^2 = r_{min}^2 \quad (3.31)$$

where (x_l, y_l) defines the center of the initial loiter circle and r_{min} denotes the minimum turn radius according to the heading rate constraint (3.3). We can rewrite this equation in polar coordinates as

$$r^2 + r_{min}^2 - r_l^2 - 2rr_{min} \cos(\theta - \alpha) = 0 \quad (3.32)$$

where $r_l = \sqrt{x_l^2 + y_l^2}$ and α is the clock angle relative to horizontal reference direction on the initial loiter circle, defined by

$$\begin{aligned} x - x_l &= r_{min} \cos \alpha \\ y - y_l &= r_{min} \sin \alpha. \end{aligned} \tag{3.33}$$

The angle α is related to the heading as

$$\psi = \alpha + \frac{\pi}{2}. \tag{3.34}$$

We are seeking the point where $\psi_d = \psi$, and from (3.16) and (3.34) we can obtain the following relationship

$$\theta - \alpha = \phi - \frac{\pi}{2} \tag{3.35}$$

which implies

$$\cos(\theta - \alpha) = \sin \phi. \tag{3.36}$$

From the definition of ϕ , (3.32) can be written as

$$r^4 + (r_{min}^2 - r_l^2 + r_d^2 + 4r_d r_{min})r^2 + r_d^2(r_{min}^2 - r_l^2) = 0 \tag{3.37}$$

and the real, positive solution to this equation corresponds to the point on (3.31) at which the desired heading will be obtained. An example trajectory using this approach is shown in Fig. 3.4.

Further, we can implement logic on the turn direction of the initial loiter circle to minimize the time to heading convergence and also the penetration depth of the standoff radius, which may be desired for adversarial targets where

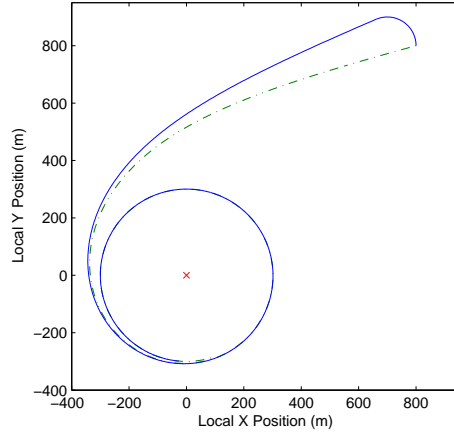


Figure 3.4: Trajectory using initial left-turn loiter circle to converge exactly to the desired heading. The dashed line represents the guidance trajectory if the vehicle's initial heading was aligned with the guidance field.

stealth is needed. Referring back to the heading error quadrants defined in Fig. 3.2, it is reasonable to choose a left-turn loiter when the heading error is in quadrants I and II, and a right-turn loiter when the heading error is in quadrants III and IV. As examples, Fig. 3.4 shows a case where a left-turn loiter is executed with $u_0 = 20m/s$, $r_d = 300m$, $x_0 = 800m$, and $y_0 = 800m$ and $\psi_0 = \pi/2$, and Fig. 3.5 shows a case where a right-turn loiter is executed with $u_0 = 20m/s$, $r_d = 300m$, $x_0 = 800m$, and $y_0 = 800m$ and $\psi_0 = -\pi/2$. Moreover, when the initial radius satisfies $r_0 < r_d + 2r_{min}$ and it is desirable to avoid penetrating the standoff radius, a left-turn loiter may be executed with quadrant IV headings. This case is shown in Fig. 3.6 with $u_0 = 20m/s$, $r_d = 300m$, $x_0 = 230m$, and $y_0 = 230m$ and $\psi_0 = -3\pi/4$. However, there are certain initial conditions from which it is impossible to avoid penetrating the

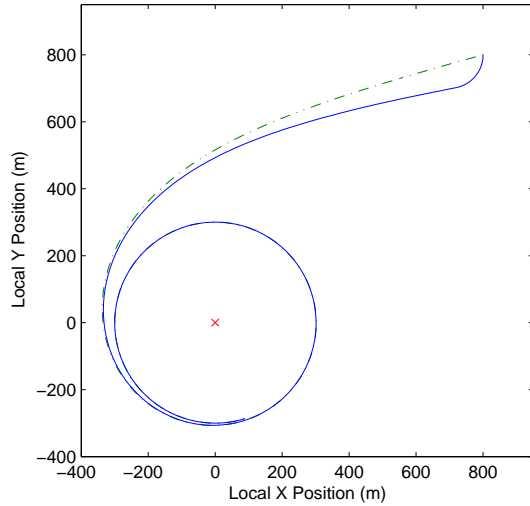


Figure 3.5: Trajectory using initial right-turn loiter circle to converge exactly to the desired heading.

standoff radius without violating the heading rate constraint.

There are several advantages of using this approach instead of heading feedback. First, the convergence to the guidance field heading is exact, not asymptotic. As a consequence, the entire trajectory, including the analytical guidance solution, is exactly known at initial time for arbitrary initial heading errors. Therefore, there is no need to continuously measure heading for feedback. Measurements of deviations from this trajectory may be used to estimate unknown wind and target motion, which we show in the following section. Finally, the heading rate constraint (3.3) is always satisfied.

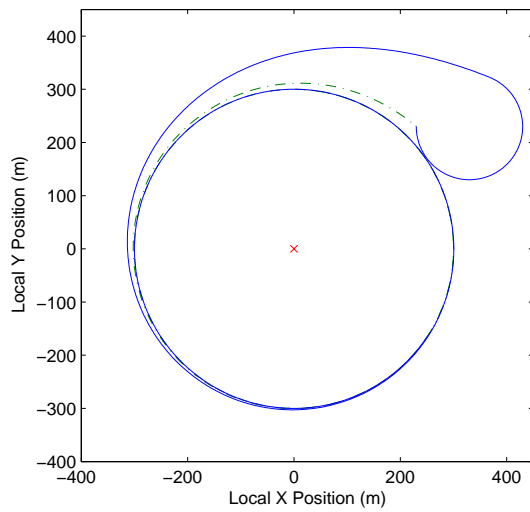


Figure 3.6: Trajectory using initial left-turn loiter circle with quadrant IV heading to avoid penetrating the standoff radius. The trajectory get close to, but does penetrate, the standoff radius. However, there are certain initial conditions from which it is impossible to avoid penetrating the standoff radius without violating the heading rate constraint.

3.3 Moving Target Tracking with Wind

In this section we extend the Lyapunov guidance vector field approach to account for unknown wind and target motion. Specifically, we use variable airspeed control and adaptive estimates of wind and target motion to maintain stability of the circular orbit pattern. We restrict consideration to targets moving with constant velocity, though the same principles could in theory be applied to more general target motion. We also discuss theoretical and practical limitations on what can be achieved given the kinematic constraints on the controllers.

3.3.1 Variable Airspeed Controller with Adaptive Wind/Target Motion Estimates

Consider the vehicle dynamics given by (3.1) expressed relative to a moving target and incorporating a wind term

$$\begin{aligned}\dot{x} &= u_1 \cos \psi + W_x - V_{xT} \\ \dot{y} &= u_1 \sin \psi + W_y - V_{yT} \\ \dot{\psi} &= u_2\end{aligned}\tag{3.38}$$

where $[W_x, W_y]^T$ are components of a constant wind velocity and $[V_{xT}, V_{yT}]^T$ are components of the constant inertial target velocity. The wind and target velocity both affect the dynamics additively, and this allows us to combine the

two effects into one variable as

$$\begin{aligned} T_x &= V_{xT} - W_x \\ T_y &= V_{yT} - W_y. \end{aligned} \quad (3.39)$$

We treat T_x and T_y as *unknown* constants, and assume a priori availability of an upper bound T^* satisfying

$$\max(T_x, T_y) \leq T^* \quad (3.40)$$

which encompasses worst case combined effect of wind and target velocities.

Consider the following controller construction

$$\begin{aligned} u_1 \cos \psi &= -u_0 \cos(\theta - \phi) + \hat{T}_x - \nu_s \sin \theta \\ u_1 \sin \psi &= -u_0 \sin(\theta - \phi) + \hat{T}_y + \nu_s \cos \theta \end{aligned} \quad (3.41)$$

where \hat{T}_x and \hat{T}_y are adaptive estimates for the unknown wind and target motion, ν_s is a yet-to-be-specified signal, and all other variables have the same meaning as before. This construction defines a heading given by

$$\tan \psi = \frac{-u_0 \sin(\theta - \phi) + \hat{T}_y + \nu_s \cos \theta}{-u_0 \cos(\theta - \phi) + \hat{T}_x - \nu_s \sin \theta} \quad (3.42)$$

and an airspeed input given by

$$u_1^2 = [-u_0 \cos(\theta - \phi) + \hat{T}_x - \nu_s \sin \theta]^2 + [-u_0 \sin(\theta - \phi) + \hat{T}_y + \nu_s \cos \theta]^2. \quad (3.43)$$

The heading equation (3.42) may be differentiated to obtain the heading rate input.

Using (3.41) with (3.38) we obtain

$$\begin{aligned}\dot{r} &= -u_0 \frac{r^2 - r_d^2}{r^2 + r_d^2} + \tilde{T}_x \cos \theta + \tilde{T}_y \sin \theta \\ r\dot{\theta} &= -u_0 \frac{2rr_d}{r^2 + r_d^2} - \tilde{T}_x \sin \theta + \tilde{T}_y \cos \theta + \nu_s.\end{aligned}\quad (3.44)$$

where $\tilde{T}_x = \hat{T}_x - T_x$ and $\tilde{T}_y = \hat{T}_y - T_y$ are the adaptive estimation errors. We now use the same Lyapunov guidance field as before to define the perfect case *relative* motion as

$$\begin{aligned}\dot{r}_p &= -u_0 \frac{r_p^2 - r_d^2}{r_p^2 + r_d^2} \\ r_p \dot{\theta}_p &= -u_0 \frac{2r_p r_d}{r_p^2 + r_d^2}.\end{aligned}\quad (3.45)$$

We define the error signals as

$$\begin{aligned}e_r &= r - r_p \\ e_\theta &= \theta - \theta_p\end{aligned}\quad (3.46)$$

and the corresponding error dynamics are then given by

$$\begin{aligned}\dot{e}_r &= -u_0 \frac{2r_d^2(r^2 - r_p^2)e_r}{(r^2 + r_d^2)(r_p^2 + r_d^2)} + \tilde{T}_x \cos \theta + \tilde{T}_y \sin \theta \\ \dot{e}_\theta &= -u_0 \frac{2r_d(r + r_p)e_r}{(r^2 + r_d^2)(r_p^2 + r_d^2)} + \frac{1}{r}(-\tilde{T}_x \sin \theta + \tilde{T}_y \cos \theta + \nu_s).\end{aligned}\quad (3.47)$$

The actual and guidance trajectories are defined from the same point, which implies $r_p(0) = r(0)$ and $\theta_p(0) = \theta(0)$. Consequently, the error signals are zero at the initial time (after heading convergence to the desired Lyapunov guidance field is achieved).

Remark. It is important to note that we assume throughout this analysis that the desired heading can be obtained before the adaptation process is initialized. Via Theorem 3.2.2, the exact heading can be achieved provided that the target does not penetrate the initial loiter circle before the correct heading has been obtained.

There are some initial conditions and target trajectories where the vehicle heading does not converge to the desired heading within a single loiter circle. This situation would arise if a moving target penetrates the initial loiter circle before the desired heading has been obtained. However, since we are assuming that the target moves with constant velocity, the target will eventually exit the initial loiter trajectory. Thus, the desired heading will still be achieved, but it may require more than one initial loiter circle. For simplicity, we assume that we have sufficient initial separation such that the desired heading will be reached within one orbit of the initial loiter circle. As a consequence, the time required for one orbit can be used to initiate the variable airspeed angular spacing control scheme.

3.3.2 Stability Analysis

Before commencing the stability analysis, we introduce a smooth parameter projection construction to ensure that the estimates for wind and target motion evolve within the known bounds give by T^* . We define the

estimates as follows

$$\begin{aligned}\hat{T}_x &= T^* \tanh \hat{\phi}_x \\ \hat{T}_y &= T^* \tanh \hat{\phi}_y\end{aligned}\tag{3.48}$$

where $\hat{\phi}_x$ and $\hat{\phi}_y$ are estimates that can adapt free of any restrictive bounds.

The corresponding true parameter values are

$$\begin{aligned}T_x &= T^* \tanh \phi_x^* \\ T_y &= T^* \tanh \phi_y^*.\end{aligned}\tag{3.49}$$

Now consider the Lyapunov function candidate

$$V = \frac{1}{2}e_r^2 + \frac{\mu}{2}e_\theta^2 + \frac{T^*}{\gamma}(\log \cosh \hat{\phi}_x - \hat{\phi}_x \tanh \phi_x^*) + \frac{T^*}{\gamma}(\log \cosh \hat{\phi}_y - \hat{\phi}_y \tanh \phi_y^*) + c^*\tag{3.50}$$

for any $\mu > 0$ and $\gamma > 0$. The term c^* is a to-be-determined fixed constant to ensure positive definiteness of V . Evaluating \dot{V} along the trajectories defined by (3.47) and defining the adaptive update laws

$$\begin{aligned}\dot{\hat{\phi}}_x &= -\gamma \left[e_r \cos \theta - \mu \frac{e_\theta \sin \theta}{r} \right] \\ \dot{\hat{\phi}}_y &= -\gamma \left[e_r \sin \theta + \mu \frac{e_\theta \cos \theta}{r} \right] \\ \nu_s &= -\frac{k_\theta u_0}{\gamma} \tanh e_\theta + \beta\end{aligned}\tag{3.51}$$

for some signal β and constant $k_\theta > 0$, we obtain

$$\dot{V} = -u_0 \frac{2r_d^2(r+r_p)e_r^2}{(r^2+r_d^2)(r_p^2+r_d^2)} - \frac{k_\theta}{r} e_\theta \tanh e_\theta - \mu u_0 \frac{2r_d(r+r_p)e_r e_\theta}{(r^2+r_d^2)(r_p^2+r_d^2)} + \frac{\mu \beta e_\theta}{r}.\tag{3.52}$$

The parameter γ has the interpretation of a “learning rate” that governs how fast the adaptation process in (3.51) evolves. To cancel the sign-indefinite term in (3.52), we choose

$$\beta = \frac{2u_0 r_d (r + r_p) r e_r}{(r^2 + r_d^2)(r_p^2 + r_d^2)} \quad (3.53)$$

and thus

$$\dot{V} = -u_0 \frac{2r_d^2 (r + r_p) e_r^2}{(r^2 + r_d^2)(r_p^2 + r_d^2)} - \frac{k_\theta u_0}{\gamma r} e_\theta \tanh e_\theta \leq 0 \quad (3.54)$$

provided that $r > 0$, which can be readily established from (3.44) and (3.48). It still remains to determine the constant c^* . Since the error signals e_r and e_θ are initially zero, and if we set the adaptive estimates $\hat{\phi}_x$ and $\hat{\phi}_y$ to be initially zero, then the third and fourth terms in (3.50) have a minimum value whenever $\hat{\phi}_x = \phi_x^*$ and $\hat{\phi}_y = \phi_y^*$. Accordingly, we can define c^* as

$$c^* = \frac{T^*}{\gamma} [|\log \cosh \phi_x^* - \phi_x^* \tanh \phi_x^*| + |\log \cosh \phi_y^* - \phi_y^* \tanh \phi_y^*|] \quad (3.55)$$

to ensure positive definiteness of V . Finally, note that c^* is inversely proportional to γ and that $1/2e_r^2(t) \leq V(t) \leq V(0) = c^*$. This implies $|e_r(t)| \leq \sqrt{2c^*}$. Thus, the maximum radial error from the guidance trajectory can be reduced by increasing the learning rate γ .

Equation (3.54) implies that all closed-loop signals are bounded and that $e_r \rightarrow 0$ and $e_\theta \rightarrow 0$, which achieves the desired circular orbit.

3.3.3 Kinematic Constraints

There are theoretical and practical limitations to what can be achieved given the kinematic constraints (3.2) and (3.3) on the controllers. For example,

if either wind or target speed (or their combined effect) is too large, then it will be impossible to maintain the circular trajectory around the target. Moreover, even when it is possible to maintain the circular trajectory, there may be large demands on airspeed variation that are undesirable or infeasible from a fuel efficiency point of view.

Let us examine the vehicle airspeed command in order to establish a parameter $\alpha > 0$ such that

$$T^* = \alpha u_0 \quad (3.56)$$

for the maximum target speed T^* that we can accommodate given the airspeed constraint (3.2). From (3.43), we establish

$$\begin{aligned} u_1^2 = & u_0^2 + \nu_s^2 + \hat{T}_x^2 + \hat{T}_y^2 + 2u_0\nu_s \sin \phi + 2\nu_s(\hat{T}_y \cos \theta - \hat{T}_x \sin \theta) \\ & - 2u_0(\hat{T}_x \cos(\theta - \phi) + \hat{T}_y \sin(\theta - \phi)). \end{aligned} \quad (3.57)$$

Using (3.40) and (3.56), we obtain the following upper bound

$$u_1^2 \leq [|\nu_s| + u_0(1 + 2\alpha)]^2. \quad (3.58)$$

To satisfy the airspeed constraint, we require $u_1^2 \leq v_{max}^2$ and so

$$|\nu_s| \leq v_{max} - u_0(1 + 2\alpha). \quad (3.59)$$

For (3.59) to be meaningful, we need the right hand side to be positive, which yields an upper bound for α

$$\alpha < \frac{1}{2} \left[\frac{v_{max}}{u_0} - 1 \right]. \quad (3.60)$$

Next, from (3.57), we also establish the following lower bound on the commanded airspeed

$$u_1^2 \geq |\nu_s|^2 - 2u_0(1 + 2\alpha)|\nu_s| + (1 - 4\alpha)u_0^2. \quad (3.61)$$

To satisfy the airspeed constraint (3.2), we require $u_1^2 \geq v_{min}^2$, and so we need

$$|\nu_s|^2 - 2u_0(1 + 2\alpha)|\nu_s| + (1 - 4\alpha)u_0^2 - v_{min}^2 \geq 0. \quad (3.62)$$

Let r^+ and r^- be the two roots of

$$|\nu_s|^2 - 2u_0(1 + 2\alpha)|\nu_s| + (1 - 4\alpha)u_0^2 - v_{min}^2 = 0 \quad (3.63)$$

which are given by

$$\begin{aligned} r^+ &= u_0(1 + 2\alpha) + \sqrt{4\alpha^2 u_0^2 + 8\alpha u_0^2 + v_{min}^2} \\ r^- &= u_0(1 + 2\alpha) - \sqrt{4\alpha^2 u_0^2 + 8\alpha u_0^2 + v_{min}^2}. \end{aligned} \quad (3.64)$$

Clearly, these are two real distinct roots with $r^+ > r^-$. Now we can write (3.62) as

$$(|\nu_s| - r^+)(|\nu_s| - r^-) \geq 0 \quad (3.65)$$

and to satisfy this we need $|\nu_s| \geq r^+$ or $|\nu_s| \leq r^-$. Since we are interested in upper bounding $|\nu_s|$, we adopt $|\nu_s| \leq r^-$, which leads to

$$|\nu_s| \leq u_0(1 + 2\alpha) - \sqrt{4\alpha^2 u_0^2 + 8\alpha u_0^2 + v_{min}^2}. \quad (3.66)$$

For (3.66) to be meaningful, we need the right hand side to be positive, which yields a separate upper bound for α given by

$$\alpha < \frac{1}{4} \left[1 - \frac{v_{min}^2}{u_0^2} \right]. \quad (3.67)$$

Combining (3.60) and (3.67), then

$$\alpha < \min \left[\frac{1}{2} \left(\frac{v_{max}}{u_0} - 1 \right), \frac{1}{4} \left(1 - \frac{v_{min}^2}{u_0^2} \right) \right] = \alpha_{max} \quad (3.68)$$

in order to satisfy the airspeed constraint (3.2). Thus, we have $0 \leq \alpha < \alpha_{max}$ such that $T^* = \alpha u_0$. From (3.68), we can see that there is a tradeoff between allowable airspeed variation and maximum allowable wind and target speed: a larger allowable variation in airspeed (i.e. large v_{max} and small v_{min}) means that a faster target or stronger wind can be accommodated.

We must also establish a lower bound for the learning rate γ such that the airspeed constraint (3.2) is satisfied. Since $r = e_r + r_p$ then $|r| \leq |e_r| + |r_p|$. Also, $r_0 \geq |r_p| \geq r_d \forall t$ and, as we have already noted, $|e_r| \leq \sqrt{2c^*}$. Then, we obtain the following upper bound on the β term in ν_s from (3.51) as

$$|\beta| \leq \frac{2u_0\sqrt{2c^*}(\sqrt{2c^*} + r_0)(\sqrt{2c^*} + 2r_0)}{r_d^3} \quad (3.69)$$

Combining (3.51), (3.59), (3.66), and (3.69) we establish

$$\frac{k_\theta}{\gamma} + \frac{2\sqrt{2c^*}(\sqrt{2c^*} + r_0)(\sqrt{2c^*} + 2r_0)}{r_d^3} \leq \min \left[\frac{v_{max}}{u_0} - (1 + 2\alpha), (1 + 2\alpha) - \sqrt{4\alpha^2 + 8\alpha + \frac{v_{min}^2}{u_0^2}} \right] \quad (3.70)$$

Solving (3.70) yields a lower bound for γ where if we choose $\gamma > \gamma_{min}$, then the airspeed constraint will be readily satisfied.

However, we cannot choose an arbitrarily large learning rate γ because there is potential to violate the heading rate constraint. This can be seen by observing that the heading rate is given by the derivative of (3.42), which via

(3.48) is proportional to the adaptive estimates given in (3.51) that are directly scaled by the learning rate γ . Therefore, we must choose an appropriate learning rate γ such that the heading rate constraint is satisfied.

As an example, take $u_0 = 20m/s$, $r_d = 300m$, $r_0 = 800$, $k_\theta = 0.001$, $v_{max} = 25m/s$, and $v_{min} = 15m/s$. Then we have $\alpha_{max} = 7/64 \approx 0.1095$ and $T^* \approx 2m/s$, i.e., we can accommodate a target speed of approximately one tenth of the nominal vehicle airspeed u_0 . Also, $\gamma_{min} \approx 202.5$ so any $\gamma > \gamma_{min}$ will satisfy the airspeed constraint.

It is important to note that while the bounds derived in this section are sufficient to guarantee satisfaction of the airspeed constraint, they may not be necessary. Indeed, the process of bounding the various terms is conservative, which is apparent in the simulations we report subsequently. In practice, the design choices for the various tradeoffs will ultimately depend on mission particulars and individual UAV capabilities. The controller construction we have proposed allows adjustable parameters to be tuned so that the coordinated standoff tracking objective can be achieved despite uncertainties while also accounting for kinematic constraints.

3.4 Stationary Target Tracking: Multiple Vehicle Spacing

This section develops control laws to achieve desired angular spacing when multiple vehicles engage a stationary target. The control laws are based on a persistent information architecture. The coordinated standoff tracking

problem naturally suggests a leader-follower structure: the target is the leader since it is not constrained to maintain any relative distances, and the engaging vehicles are followers that maintain their distances to the target and to one another. We consider minimally persistent leader-first-follower, with the minimum possible number of distances actively controlled, and show global asymptotic stability of the desired formation.

Each vehicle uses a variable airspeed controller to obtain the desired spacing. We explicitly account for the airspeed constraint (3.2) by introducing a design variable that adjusts the amount of allowable airspeed variation without diluting our convergence properties. In this way, the fuel expenditure required to obtain desired angular spacing can be minimized. There is a trade-off: larger allowable airspeed variation means faster convergence and smaller allowable airspeed variation means slower convergence.

The angular spacing control can commence once all of the UAVs complete their initial respective loiter arcs. The required time for all of the vehicles to match headings with the guidance field is analytically determined through only knowledge of the initial conditions of all of the vehicles when there is no wind or target motion; the time can be upper-bounded according to Theorem 3.2.2 by the time required to execute a loiter circle. Accordingly, we assume in this section without loss of generality that all of the vehicles have already matched their heading with the guidance field. For simplicity in the analysis, we also assume that the vehicles align their headings with the guidance field outside of the standoff radius, though in principle the results would still

extend to the case where heading alignment occurs inside the standoff radius with some minor modifications.

Minimally Persistent Information Architecture

This subsection develops control laws based on a minimally persistent leader-first-follower information architecture. The target is the leader since it does not maintain any distances to the engaging UAVs. One of the engaging UAVs maintains the circular orbit around the target and has no other distances to maintain. The remaining vehicles maintain the circular orbit around the target and, through adjustments in airspeed, maintain a prescribed angular spacing with the neighboring vehicle ahead of it in the circular orbit. This structure requires the minimum possible number of communication/sensing links to achieve the circular orbit and angular spacing.

Control Laws and Stability Analysis

The dynamics for the i^{th} vehicle in polar coordinates are given by

$$\dot{r}_i = -u_{1i} \frac{r_i^2 - r_d^2}{r_i^2 + r_d^2} \quad (3.71)$$

$$r_i \dot{\theta}_i = u_{1i} \frac{2r_i r_d}{r_i^2 + r_d^2}, \quad i = 1, \dots, n. \quad (3.72)$$

We designate vehicle n to have a constant airspeed

$$u_{1n} = u_0. \quad (3.73)$$

Let the airspeed input of the remaining $n - 1$ vehicles be given by

$$u_{1i} = u_0 + \Delta V_{max} \tanh(\theta_{i+1} - \theta_i - \theta_d) \frac{r_i^2 + r_d^2}{r_{i+1}^2 + r_i^2} \quad (3.74)$$

where $\Delta V_{max} > 0$ is a design parameter to be chosen such that (3.74) satisfies the airspeed constraint, and θ_d is the desired angular spacing between each pair of vehicles. To satisfy the airspeed constraint, we require $u_0 - \Delta V_{max} > v_{min} > 0$. When the angular spacing is different from desired, the second term adjusts the airspeed to compensate. When the desired spacing is achieved, the second term goes to zero, and the airspeed becomes the constant nominal u_0 . We emphasize that any positive value for ΔV_{max} is sufficient to achieve the desired spacing. Therefore the amount of allowable airspeed variation can be adjusted in order to maximize fuel efficiency. The tradeoff for choosing a small ΔV_{max} is that convergence to the desired angular spacing may be slower. We note that all feedback signals for vehicle i , viz. $r_i, r_{i+1}, \theta_{i+1} - \theta_i$ are computable from relative position measurements in an arbitrary local coordinate basis from the target and from vehicle i 's neighboring vehicle.

We define the angular spacing errors as $\delta\theta_i = \theta_{i+1} - \theta_i - \theta_d$. We then differentiate and use (3.71) with (3.74) to obtain angular spacing error dynamics as

$$\begin{aligned} \delta\dot{\theta}_{n-1} &= \frac{2u_0r_d(r_{n-1}^2 - r_n^2)}{(r_n^2 + r_d^2)(r_{n-1}^2 + r_d^2)} - \frac{2r_d\Delta V_{max}}{(r_n^2 + r_{n-1}^2)} \tanh(\delta\theta_{n-1}), \quad i = n - 1 \quad (3.75) \\ \delta\dot{\theta}_i &= \frac{2u_0r_d(r_i^2 - r_{i+1}^2)}{(r_{i+1}^2 + r_d^2)(r_i^2 + r_d^2)} + \frac{2r_d\Delta V_{max}}{(r_{i+2}^2 + r_{i+1}^2)} \tanh(\delta\theta_{i+1}) - \frac{2r_d\Delta V_{max}}{(r_{i+1}^2 + r_i^2)} \tanh(\delta\theta_i), \\ & \quad i = 1, \dots, n - 2. \end{aligned} \quad (3.76)$$

Now consider the Lyapunov function candidate

$$V = \sum_{i=1}^{n-1} \log \cosh \delta\theta_i + \frac{1}{2} \sum_{i=1}^n \lambda_i r_i^2 \quad (3.77)$$

with some suitably chosen $\lambda_i > 0$. Evaluating \dot{V} along the trajectories defined by (3.71) and (3.75), we obtain

$$\begin{aligned} \dot{V} = & \sum_{i=1}^{n-1} \left[\frac{2u_0 r_d (r_i^2 - r_{i+1}^2)}{(r_{i+1}^2 + r_d^2)(r_i^2 + r_d^2)} \tanh(\delta\theta_i) - \frac{2r_d \Delta V_{max}}{(r_{i+1}^2 + r_i^2)} \tanh^2(\delta\theta_i) - \lambda_i r_i u_{1i} \frac{r_i^2 - r_d^2}{r_i^2 + r_d^2} \right] \\ & + \sum_{i=1}^{n-2} \left[\frac{2r_d \Delta V_{max}}{(r_{i+2}^2 + r_{i+1}^2)} \tanh(\delta\theta_{i+1}) \tanh(\delta\theta_i) \right] - \lambda_n r_n u_0 \frac{r_n^2 - r_d^2}{r_n^2 + r_d^2} \end{aligned} \quad (3.78)$$

Using the fact that $r_d \leq r_i(t) \leq r_{i0}$ from (3.71) and $u_{12} \geq u_0 - \Delta V_{max}$ from (3.74), we can bound \dot{V} as

$$\dot{V} \leq \sum_{i=1}^{n-1} \left[-\frac{\Delta V_{max} r_d}{\bar{r}_0^2} \tanh^2 \delta\theta_i + \frac{u_0 (r_i^2 - r_d^2)}{r_d (r_i^2 + r_d^2)} + \frac{u_0 (r_{i+1}^2 - r_d^2)}{r_d (r_{i+1}^2 + r_d^2)} \right] \quad (3.79)$$

$$\begin{aligned} & - \sum_{i=1}^{n-1} \left[\lambda_i r_d (u_0 - \Delta V_{max}) \frac{(r_i^2 - r_d^2)}{(r_i^2 + r_d^2)} \right] \\ & + \sum_{i=1}^{n-2} \left[\frac{\Delta V_{max}}{r_d} \tanh(\delta\theta_{i+1}) \tanh(\delta\theta_i) \right] - \lambda_n r_n u_0 \frac{r_n^2 - r_d^2}{r_n^2 + r_d^2}. \end{aligned} \quad (3.80)$$

We can rewrite as

$$\begin{aligned} \dot{V} \leq & -\tanh \delta\theta^T C \tanh \delta\theta - \sum_{i=1}^{n-1} \left[\lambda_i r_d (u_0 - \Delta V_{max}) - \frac{2u_0}{r_d} \right] \frac{(r_i^2 - r_d^2)}{(r_i^2 + r_d^2)} \\ & - (\lambda_n r_n u_0 - \frac{u_0}{r_d}) \frac{(r_n^2 - r_d^2)}{(r_n^2 + r_d^2)} \end{aligned} \quad (3.81)$$

where $\tanh \delta\theta = [\tanh(\delta\theta_1), \dots, \tanh(\delta\theta_{n-1})]$ and the matrix C has the positive-definite structure

$$C = \begin{bmatrix} \frac{\Delta V_{max} r_d}{\bar{r}_0^2} & -\frac{\Delta V_{max}}{r_d} & 0 & \dots & 0 \\ 0 & \frac{\Delta V_{max} r_d}{\bar{r}_0^2} & -\frac{\Delta V_{max}}{r_d} & \dots & 0 \\ 0 & \dots & \ddots & \dots & 0 \\ 0 & \dots & 0 & \frac{\Delta V_{max} r_d}{\bar{r}_0^2} & -\frac{\Delta V_{max}}{r_d} \\ 0 & 0 & \dots & 0 & \frac{\Delta V_{max} r_d}{\bar{r}_0^2} \end{bmatrix}. \quad (3.82)$$

The positive-definiteness of C is directly related to the information architecture being minimally persistent leader-first-follower. Choosing

$$\lambda_n > \frac{1}{r_d^2}, \quad \lambda_i > \frac{u_0}{r_d^2}(u_0 - \Delta V_{max}), \quad i = 1, \dots, n-1 \quad (3.83)$$

we obtain $\dot{V} \leq 0$. This implies

$$\lim_{t \rightarrow \infty} r_i(t) = r_d, \quad \forall i \quad (3.84)$$

which achieves the circular standoff radius, and

$$\lim_{t \rightarrow \infty} \delta\theta_i(t) = 0, \quad \forall i \quad (3.85)$$

which achieves the angular spacing objective.

3.5 Simulations

In this section, we present simulations to demonstrate our control laws for the coordinated standoff tracking problem with minimally persistent information architecture. The simulations show four UAVs engaging a stationary target and two UAVs engaging a moving target.

Fig. 3.7 shows four UAVs engaging a stationary target with $u_0 = 20m/s$, $r_d = 300m$, $\Delta V_{max} = 5m/s$, $x_{10} = 1000m$, $y_{10} = 1000m$, $\psi_{10} = 0$, $x_{20} = -800m$, $y_{20} = -700m$, $\psi_{20} = \pi/2$, $x_{30} = -500m$, $y_{30} = 900m$, $\psi_{30} = \pi$, $x_{40} = 700m$, $y_{40} = -100m$, and $\psi_{40} = -\pi/4$. The vehicles initially have arbitrary headings and execute the initial loiter circle to converge to the desired heading along the Lyapunov guidance vector field. When all vehicles arrive

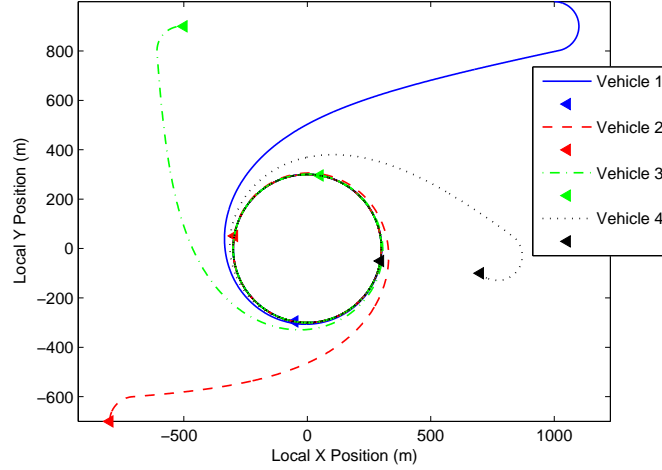


Figure 3.7: Four UAVs engaging a stationary target in local coordinates.

within a prescribed distance from the standoff radius, the variable airspeed controllers commence to achieve the desired angular spacing. The airspeed commands are shown in Fig. 3.8. The airspeed of the first follower remains constant while the other vehicles adjust their airspeeds to achieve the spacing. The relative spacing errors (we show relative distances here, which is equivalent to relative angles in this case) are shown in Fig. 3.9 and all converge to zero.

Fig. 3.10 shows two UAVs engaging a target moving with constant velocity in inertial coordinates where $u_0 = 20m/s$, $r_d = 400m$, $\Delta V_{max} = 5m/s$, $\gamma = 0.01$, $\mu = 1$, $k_\theta = 0.01$, $x_{10} = 1100m$, $y_{10} = 800m$, $\psi_{10} = 0$, $x_{20} = 800m$, $y_{20} = -800m$, $\psi_{20} = 0$, $T_x = 3m/s$, and $T_y = 3m/s$. The target speeds T_x and T_y and the learning rate γ are outside the range of values established in our analysis in section 3.3. Despite this, the vehicles

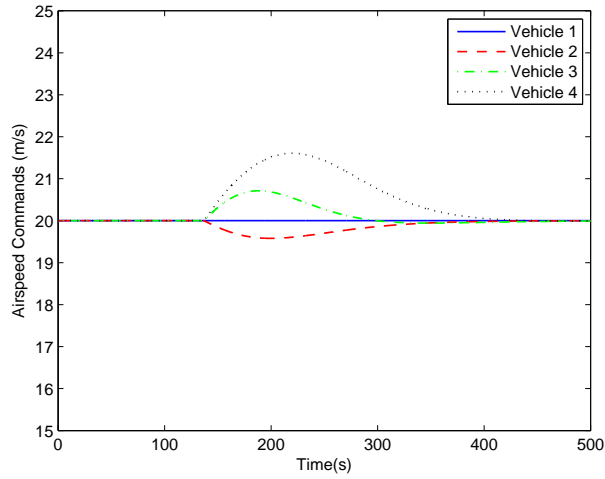


Figure 3.8: Airspeed commands for spacing.

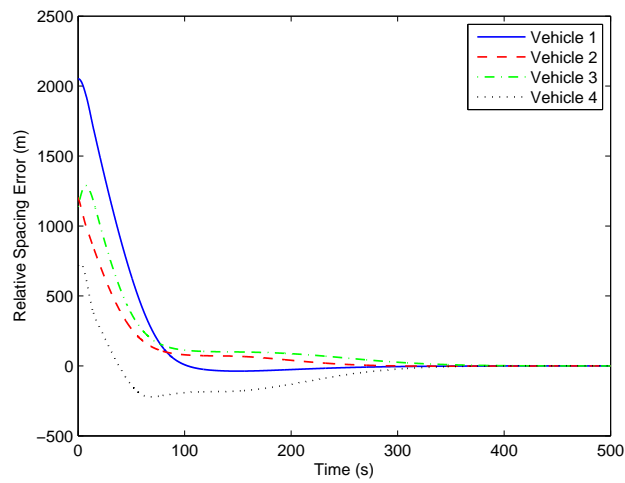


Figure 3.9: Relative spacing errors for four UAVs engaging a stationary target.

accomplish the coordinated standoff tracking objectives, which highlights the conservatism inherent in the various upper bounds that were derived. The vehicles again initially have arbitrary headings and execute the same initial loiter circle at constant airspeed to converge to the desired heading. When the desired heading is achieved, the variable airspeed control commences, which adapts for the unknown wind and target motion. After a prescribed time, the variable airspeed angular spacing control commences for the vehicles to obtain a prescribed angular separation of π . The trajectories are shown in local target frame coordinates in Fig. 3.11, where it can be seen that the circular orbit pattern is achieved despite the unknown wind and target motion. The airspeed commands for spacing and maintaining the circular orbit are shown in Fig. 3.12 and the variations are within 25% of the nominal airspeed. The relative spacing error (we show relative distance here, which is equivalent to relative angle in this case) is shown in Fig. 3.13 and converges to zero.

3.6 Conclusions

This chapter has progressed the Lyapunov guidance vector field approach to the coordinated standoff tracking problem. For single vehicle path planning, we presented a proof of heading convergence that addresses a previously neglected timescale separation issue. We then proposed a novel approach for heading convergence that utilizes an analytical solution to the guidance vector field and offers theoretical and practical advantages. To accommodate unknown target motion and wind, adaptive estimates were introduced to ensure

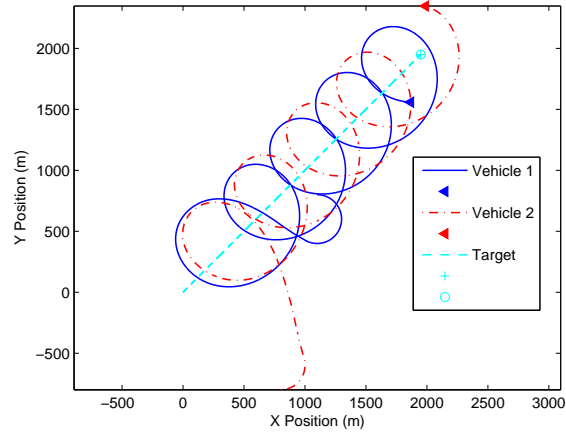


Figure 3.10: Two UAVs engaging a moving target in inertial coordinates (m).

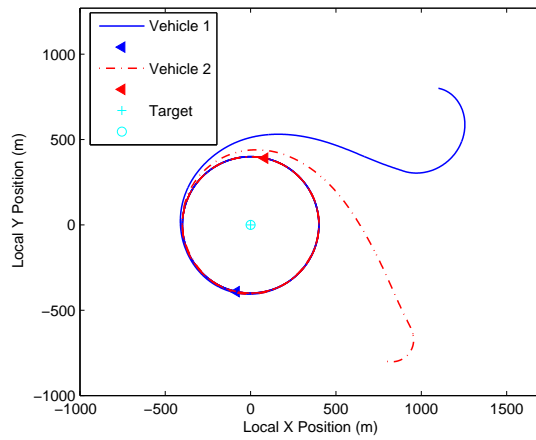


Figure 3.11: Two UAVs engaging a moving target in local target frame coordinates (m).

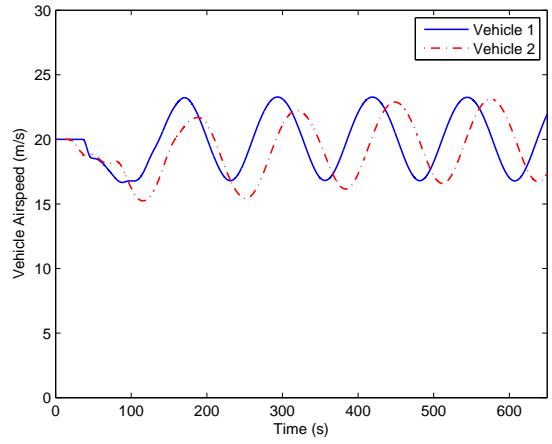


Figure 3.12: Airspeed commands for spacing and maintaining circular orbit around a moving target.

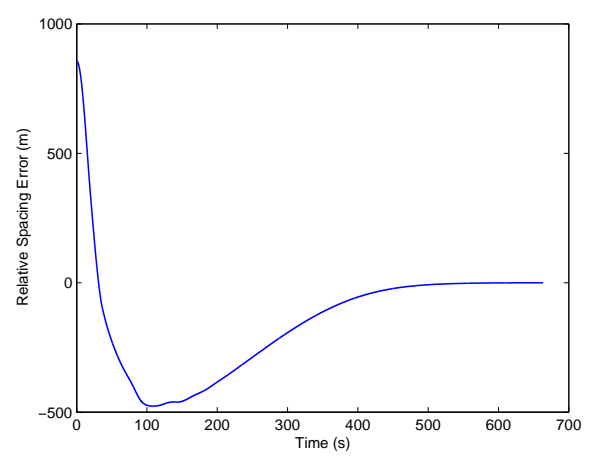


Figure 3.13: Relative spacing error for two UAVs engaging a moving target.

stability of the circular trajectory. For multiple vehicle coordination, a variable airspeed controller was implemented to achieve prescribed inter-vehicle angular spacing. We established a connection with recent work on persistent information architectures and based our control laws on an architecture which was derived from that theory. We showed asymptotic stability the desired formation configuration.

The connection between the stability of the desired formation shape and graph theoretic properties of the information architecture motivates a study of more general information architectures. The next chapter studies the stabilizability of two types of minimally persistent formations: leader-remote-follower and coleader.

Chapter 4

Control of Minimally Persistent Leader-Remote-Follower and Coleader Formations in the Plane

4.1 Introduction

The previous chapter used an *instance* of a persistent information architecture to solve a coordinated standoff tracking problem. This chapter addresses the more general problem of solving an n -agent formation shape control problem in the plane for a *class* of persistent architectures. The objective of this problem is to design decentralized control laws for each agent to restore a desired formation shape. We use relative position measurements to control certain interagent distances according to a directed graph.

The persistent architectures considered in this chapter are *minimally persistent* formations in the plane, which fall into three categories: Leader-First-Follower (LFF), Leader-Remote-Follower (LRF) and Coleader. This chapter extends the results of [83] to minimally persistent *LRF* and *coleader* formations. In [83], Yu et al prove for minimally persistent LFF formations in the plane *with cycles* that choosing locally stabilizing control gains is possible if a certain submatrix of the *rigidity matrix* has all leading principal minors

nonzero. They also prove that all minimally persistent LFF formations generically obey this principal minor condition.

The contribution of this chapter is non-trivial because the nonlinear closed-loop system has a manifold of equilibria, which implies that the linearized system is nonhyperbolic. Center manifold theory is thus required in the stability analysis. Yu et al obtain a hyperbolic system for LFF formations via the choice of a particular global coordinate system and prove local exponential stability of the formation shape through eigenvalue analysis. Such a choice of global coordinate system is not possible for LRF and Coleader formations. Accordingly, we apply a new result based on center manifold theory to show local exponential stability of the desired formation shape. In [38] Krick et al also show local exponential stability of the desired formation shape using center manifold theory, but their analysis is restricted to undirected rigid formations. A further challenge of our argument, in contrast to that of [38], is to circumvent the non-compactness of the equilibrium manifold. We show that it is again possible to choose stabilizing control gains whenever a certain submatrix of the rigidity matrix has all leading principal minors nonzero and show that this condition holds for all LRF and coleader formations.

Together with [83], this chapter effectively demonstrates local stabilizability of the desired shape for all minimally persistent formations. Section 4.2 presents background on center manifold theory. Section 4.3 proves a new center manifold theory result for systems with an equilibrium manifold. Section 4.4 describes the nonlinear equations of motion and shows how center

manifold theory can be applied to prove that the desired formation shape is locally exponentially stable. Section 4.5 shows that the principal minor condition holds for all LRF and coleader formations. Section 4.6 illustrates the results with numerical simulations. Section 4.7 gives concluding remarks.

4.2 Center Manifold Theory

Center manifold theory offers tools for analyzing stability of dynamical systems near nonhyperbolic equilibrium points of a nonlinear system (that is, equilibrium points about which the linearization has one or more eigenvalues with zero real part). Effectively, the theory allows one to reduce the dimension of the nonlinear system. The motions tend asymptotically toward trajectories on the center manifold rather than to a point. Standard treatments of center manifold theory can be found in e.g [15], [64], or [79]. These concentrate on isolated equilibria. In the formation shape maintenance problem, the dynamic system has a manifold of non-isolated equilibrium points corresponding to the desired formation shape that for the coleader case is not even compact. In [47], Malkin proves a local stability result where trajectories converge to a point on an equilibrium manifold. More general results for equilibrium manifolds are presented by Aulbach in [6]. In [38], Krick et al emphasize the importance of compactness for proving stability of the entire equilibrium manifold. Here, we state a new result for stability of equilibrium manifolds and offer a concise proof using center manifold theory.

Consider the nonlinear autonomous dynamic system

$$\dot{x} = f(x), \quad x \in \mathfrak{R}^n \quad (4.1)$$

where the function f is \mathbf{C}^r , $r \geq 2$ almost everywhere including a neighbourhood of the origin. Without loss of generality, suppose the origin is an equilibrium point and that the Jacobian of f (we will use the notation $J_f(x)$) at the origin has m eigenvalues with zero real part and $n - m$ eigenvalues with negative real part. Then (4.1) can be locally transformed into the following form

$$\begin{aligned} \dot{\theta} &= A_c \theta + g_1(\theta, \rho) \\ \dot{\rho} &= A_s \rho + g_2(\theta, \rho), \quad (\theta, \rho) \in \mathfrak{R}^m \times \mathfrak{R}^{n-m} \end{aligned} \quad (4.2)$$

where A_c is a matrix having eigenvalues with zero real parts, A_s is a matrix having eigenvalues with negative real parts, and the functions g_1 and g_2 satisfy

$$\begin{aligned} g_1(0, 0) &= 0, \quad J_{g_1}(0, 0) = 0 \\ g_2(0, 0) &= 0, \quad J_{g_2}(0, 0) = 0. \end{aligned} \quad (4.3)$$

Definition 4.2.1. An invariant manifold is called a *center manifold* for (4.2) if it can be locally represented as follows

$$W^c(0) = \{(\theta, \rho) \in U \subset \mathfrak{R}^m \times \mathfrak{R}^{n-m} \mid \rho = h(\theta)\} \quad (4.4)$$

for some sufficiently small neighbourhood of the origin U where the function h satisfies $h(0) = 0$ and $J_h(0) = 0$.

We have the following standard result.

Theorem 4.2.1 ([79]). *Consider (4.2) where A_c has eigenvalues with zero real part, A_s has eigenvalues with negative real part, and g_1 and g_2 satisfy (4.3). There exists a \mathbf{C}^r center manifold for (4.2) with local representation function $h : \mathfrak{R}^m \rightarrow \mathfrak{R}^{n-m}$. The dynamics of (4.2) restricted to any such center manifold is given by the following m -dimensional nonlinear system for ξ sufficiently small*

$$\dot{\xi} = A_c \xi + g_1(\xi, h(\xi)), \quad \xi \in \mathfrak{R}^m. \quad (4.5)$$

If the origin of (4.5) is stable (asymptotically stable) (unstable), then the origin of (4.2) is stable (asymptotically stable) (unstable). Suppose the origin of (4.5) is stable. Then if $(\theta(t), \rho(t))$ is a solution of (4.2) for sufficiently small $(\theta(0), \rho(0))$, there is a solution $\xi(t)$ of (4.5) such that as $t \rightarrow \infty$

$$\begin{aligned} \theta(t) &= \xi(t) + O(e^{-\gamma t}) \\ \rho(t) &= h(\xi(t)) + O(e^{-\gamma t}) \end{aligned} \quad (4.6)$$

where γ is a positive constant.

This result shows that in order to determine stability near the nonhyperbolic equilibrium point of (4.1), one can analyze a reduced-order system, viz. (4.5). If the origin of the reduced-order system (4.5) is stable, then the solutions of the original system converge exponentially to a trajectory on the center manifold. This result however only applies when the nonhyperbolic equilibrium point is isolated. In our formation shape control problem, we will

see that there is a smooth manifold of equilibrium points. This requires a new center manifold result, which we provide in the following section.

4.3 Center Manifold Result for a System with an Equilibrium Manifold

We have the following result when there is a manifold of equilibria, and we will contrast it with the result of [38]. There are two essential differences with the result of [38], both related to the fact that [38] deals with undirected formations and the simplifications they engender.

First the undirected nature of the formations renders the center manifold underlying [38] compact. This is in fact quite crucial to the argument in [38]. Ultimately the goal of [38], and indeed our goal, is to demonstrate exponential convergence to the center manifold. The lack of compactness of this manifold, that unlike the setting of [38] is the case here, causes difficulties.¹

The second difference stems from the fact that the undirected nature of the formation considered in [38] makes the *entire* center manifold, under the control law of [38], exponentially stable. In the directed formation case considered here that does not necessarily happen. This requires a fundamentally new result provided in the theorem below. Observe that although the theorem

¹Saying that a manifold is locally exponentially stable means that there is a single exponent γ such that all trajectories converge to the manifold from a sufficiently small neighbourhood at least as fast as $e^{-\gamma t}$. One could envisage a non-compact manifold where any single trajectory approaches the manifold exponentially fast but no single γ could be found applicable to all trajectories.

postulates and proves the existence of a center manifold, it makes no explicit compactness assumptions, in contrast to [38].

Theorem 4.3.1. *Consider (4.1) with $f \in \mathbf{C}^r$, $r \geq 2$ almost everywhere including a neighbourhood of the origin. Suppose there is a smooth m -dimensional ($m > 0$) manifold of equilibrium points $M_1 = \{x \in \mathfrak{R}^n | f(x) = 0\}$ for (4.1) that contains the origin. Suppose at the origin the Jacobian of f has m eigenvalues with zero real part and $n - m$ eigenvalues with negative real part. Then we have the following*

- M_1 is a center manifold for (4.1).
- There are compact neighbourhoods Ω_1 and Ω_2 of the origin such that $M_2 = \Omega_2 \cap M_1$ is locally exponentially stable and for each $x(0) \in \Omega_1$ there is a point $q \in M_2$ such that $\lim_{t \rightarrow \infty} x(t) = q$.

We shall prove Theorem 4.3.1 with the aid of the following lemma.

Lemma 4.3.2. *Consider (4.2) where A_c has eigenvalues with zero real part, A_s has eigenvalues with negative real part, and g_1 and g_2 satisfy (4.3). Suppose that the equilibrium set is a smooth m -dimensional manifold M_1 . Then there exists a smooth function $h_1 : \mathfrak{R}^m \rightarrow \mathfrak{R}^{n-m}$ such that $h_1(0) = 0$, $J_{h_1}(0) = 0$ and in a suitably small neighborhood U of the origin, the equilibrium set can be represented as $\rho = h_1(\theta)$.*

Proof. Consider the equation

$$\tilde{g}_2(\theta, \rho) = A_s \rho + g_2(\theta, \rho) = 0 \tag{4.7}$$

As A_s is nonsingular and (4.3) holds, then by the implicit function theorem, for any suitably small θ , there exists ρ , expressible as $\rho = h_1(\theta)$, for a smooth h_1 satisfying $h_1(0) = 0$, $J_{h_1}(0) = 0$, and such that (4.7) holds.

Note that to prove $(\theta, \rho = h_1(\theta))$ lies on the equilibrium manifold, we must show in addition to (7) that the following equation holds:

$$A_c \theta + g_1(\theta, h_1(\theta)) = 0 \quad (4.8)$$

To do this, we now appeal to the fact that M_1 is an m -dimensional manifold. As a result, there exists a neighborhood W of the origin in R^m and a diffeomorphism $\phi = (\phi_1, \phi_2)$ such that for $w \in W$

$$\begin{bmatrix} \phi_1 \\ \phi_2 \end{bmatrix} : w \rightarrow \begin{bmatrix} \theta \\ \rho \end{bmatrix} \in M_1 \cap U. \quad (4.9)$$

Then the set of equilibria include $\theta = \phi_1(w)$, $\rho = \phi_2(w)$ for all $w \in W$. Because an equilibrium point necessarily satisfies (4.7), it is necessary that the function $h_1(\cdot)$ identified above is such that $\phi_2(w) = h_1(\phi_1(w)) \forall w \in W$. The mapping from w to the set of equilibria is then $(\phi_1(w), h_1(\phi_1(w)))$, and it is invertible, being a diffeomorphism. Therefore, $\phi_1 : w \rightarrow \theta$ itself must be invertible. Let $w = \psi(\theta)$. Then the equilibria are $(\phi_1(\psi(\theta)), h_1(\phi_1(\psi(\theta)))) = (\theta, h_1(\theta))$. This establishes the claim of the lemma. \square

Proof of Theorem 4.3.1. By assumption, there exists a similarity transformation Q and a neighborhood U of the origin, such that for each $\bar{x} \in U \cap M_1$, we can write

$$QJ_f(\bar{x})Q^{-1} = \begin{bmatrix} A_c & 0 \\ 0 & A_s \end{bmatrix}. \quad (4.10)$$

Therefore, for any equilibrium point $\bar{x} \in U \cap M_1$, we can write (4.1) in the form given by (4.2). The first part of the theorem is then immediate, for M_1 , being an equilibrium manifold, is invariant, and Lemma 4.3.2 demonstrates the local representation condition required for M_1 to be a center manifold.

Now, we turn to the second part of the theorem. Since M_1 is a center manifold, the dynamics restricted to M_1 are stationary. Therefore, from (4.5) we have $\dot{\xi} = 0$, which implies $\xi(t) = \xi(0) \forall t$. Thus, the reduced-order system is stable. Theorem 4.2.1 then mandates that the origin is locally stable. This together with the stated conditions of the Jacobian, ensures that there exist compact neighbourhoods Ω_1 and Ω_2 of the origin such that (a) all trajectories starting in Ω_1 remain in Ω_2 , (b) with M_2 defined in the theorem statement, the Jacobian of f has m eigenvalues with zero real part and $n - m$ eigenvalues with negative real part everywhere in M_2 , and (c) there is a $\gamma > 0$ such that for each $\bar{x} \in M_2$, $Re[eig(A_s(\bar{x}))] < -\gamma$. (The compactness of M_2 is crucial.) The exponential convergence mandated by Theorem 4.2.1 implies that Ω_1 and Ω_2 can be chosen to have the additional property that trajectories starting in Ω_1 converge exponentially to a point on the center manifold and thus to a point in M_2 (though not necessarily to the origin).

Finally, this argument is valid for any point in M_2 . For each point in M_2 , there is an open neighbourhood of attraction U_i . Further, M_2 is a compact subset of M_1 . By the Heine-Borel Theorem, there is a finite subcover Ω_3 of M_2 constructible from a finite union of these neighbourhoods. The smallest exponential convergence rate associated with the neighbourhoods of the finite

subcover is valid to bound the speed of convergence for all trajectories starting in Ω_3 . The final part immediately follows. \square

The distinction between LFF, LRF, and coleader formations is important in the stability analysis for the formation shape maintenance control laws. In particular, for LFF formations it is possible to define a global coordinate basis to obtain a hyperbolic reduced-order system in which local stability can be ascertained via eigenvalue analysis of the linearized system [83]. This is so because in the framework of both [83] and this chapter, after its “small” initial move, the leader stops moving. Thereafter, the algorithm of [83] forces the first follower to move in the direction of the leader. Thus the direction of movement of the first follower in the LFF framework is fixed. This direction critically defines the stated coordinate basis in [83]. In contrast, for LRF formations the direction associated with the remote follower’s DOF is not fixed in space since it is following an agent other than the leader to satisfy its distance constraint. Similarly, for coleader formations the directions associated with the coleader DOFs are not fixed in space. Thus, the device used in [83] to obtain a global coordinate system that provides a hyperbolic reduced-order system no longer applies. Consequently, one cannot draw conclusions about the local stability of the nonlinear system near the desired formation shape by analyzing the linearized system alone; more sophisticated techniques are needed.

In contrast to [83], [38] does use center manifold theory to establish stability of the closed-loop system, but their analysis is restricted to undirected

graphs. It is possible to work with a reduced-order system, using the fact that for the laws in question, the centroid of the formation is stationary. This allows the full-order system to be reduced by 2 in dimension, and leaves one zero eigenvalue for the linearized system. A critical feature of the center manifold analysis of [38] is the observation that the set of equilibria of this reduced-order system is then compact. For LRF formations, one can fix the position of the leader to obtain a compact set of equilibria for a reduced-order system. However, this is not possible in the coleader setting. In either case, separate aspects of center manifold theory have to be used to establish a related *de facto* compactness condition.

In the formation shape maintenance problem, the manifold of equilibria will correspond to formation positions with the desired shape. In the plane, the manifold is three-dimensional due to the three possible Euclidean motions of the formation in the plane (two translational and one rotational). In the following section, we develop equations of motion and apply Theorem 4.3.1 to show local exponential stability of the desired shape.

4.4 Equations of Motion

In this section, we present equations of motion for the formation shape maintenance problem and study the local stability properties of the desired formation shape. Suppose the formation is initially in the desired shape. Then the position of each agent is perturbed by a small amount and all agents (except for the leader in a LRF formation) move under distance control laws

to meet their distance specifications in order to restore the desired formation shape. This shape is realized by every point on a smooth three-dimensional equilibrium manifold. For LRF and coleader formations, we show that a direct application of Theorem 4.3.1 proves local exponential convergence to the invariant manifold, whether or not the equilibrium manifold is compact.

4.4.1 Nonlinear Equations of Motion

Consider a minimally persistent formation $F(G, p)$ of n agents in the plane. For LRF formations the leader and remote follower are agents n and $n - 1$, respectively. For coleader formations the coleaders are agents $n - 2$, $n - 1$, and n . Recall the rigidity function r from (2.1) and let $d = [\dots, d_{jk}^2, \dots]$ represent a vector of the squares of the desired distances corresponding to each edge of G . We assume that there exist agent positions p such that $p = r^{-1}(d)$, i.e. the set of desired interagent distances is realizable. Formation shape is controlled by controlling the interagent distance corresponding to each edge.

Following [83] and [38], we adopt a single integrator model for each agent:

$$\dot{p}_i = u_i. \tag{4.11}$$

Consider an ordinary follower agent denoted by i that is required to maintain constant distances d_{ij}^* and d_{ik}^* from agents j and k , respectively, and can measure the instantaneous relative positions of these agents. We use the same law as in [83] for ordinary followers:

$$u_i = K_i(p_i^* - p_i) = K_i f_i(p_j - p_i, p_k - p_i, d_{ij}^*, d_{ik}^*) \tag{4.12}$$

where K_i is a gain matrix and p_i^* is the closest instantaneous target position for agent i in which its distances from agents j and k are correct. Since the perturbations from the desired shape are small, these instantaneous target positions are well-defined and unique. For the remote follower ($i = n - 1$) or the coleaders ($i = n - 2, n - 1, n$), we have

$$\begin{aligned} u_i &= K_i(p_i^* - p_i) \\ &= K_i \frac{\|p_{j(i)} - p_i\| - d_{ij(i)}^*}{\|p_{j(i)} - p_i\|} (p_{j(i)} - p_i) \end{aligned} \quad (4.13)$$

where K_i is a gain matrix and agent $j(i)$ is the agent from which the remote follower or coleader i is maintaining the constant distance $d_{ij(i)}^*$ (note that each coleader may follow a different agent). For the leader, we have

$$\dot{p}_n = 0. \quad (4.14)$$

For a LRF formation, equations (4.12), (4.13), and (4.14) represent the dynamics of the autonomous closed-loop system, which may be written in the form

$$\dot{p} = \begin{bmatrix} f_{LRF}(p) \\ 0 \end{bmatrix} \quad (4.15)$$

where $f_{LRF} : \mathfrak{R}^{2n} \rightarrow \mathfrak{R}^{2n-2}$ is smooth almost everywhere including a neighbourhood of the desired formation. For a coleader formation, equations (4.12) and (4.13) represent the dynamics of the autonomous closed-loop system, which may be written in the form

$$\dot{p} = f_C(p) \quad (4.16)$$

where $f_C : \mathfrak{R}^{2n} \rightarrow \mathfrak{R}^{2n}$ is smooth almost everywhere including a neighbourhood of the desired formation.

There is a smooth *manifold* of equilibria for (4.15) and (4.16) given by

$$\Psi = \{p \in \mathfrak{R}^{2n} | p = r^{-1}(d)\} \quad (4.17)$$

corresponding to formations where all distance constraints are satisfied. The manifold Ψ is a three-dimensional manifold because a formation with correct distances has three degrees of freedom associated with the planar Euclidean motions (two for translation and one for rotation). Given these degrees of freedom, it is evident that Ψ is not compact. For LRF formations, we can define a reduced-order system by fixing the position of the leader and obtain a compact equilibrium manifold.

4.4.2 Linearized Equations

We represent the position of the formation as $p(t) = \delta p(t) + \bar{p}$, where \bar{p} is any equilibrium position with desired shape close to the perturbed formation, and the displacements $\delta p(t)$ are assumed to be small. In particular, for agent i we have $p_i(t) = \delta p_i(t) + \bar{p}_i$. Let $p_i(t) = [x_i(t), y_i(t)]^T$, $\bar{p}_i = [\bar{x}_i, \bar{y}_i]^T$, and $\delta p_i(t) = [\delta x_i(t), \delta y_i(t)]^T$ in a global coordinate system to be defined later.

From [83], the linear part for the ordinary followers is given by

$$\begin{bmatrix} \dot{\delta x}_i \\ \dot{\delta y}_i \end{bmatrix} = K_i R_{ei}^{-1} R_{ij,ik} \begin{bmatrix} \delta x_i \\ \delta y_i \\ \delta x_j \\ \delta y_j \\ \delta x_k \\ \delta y_k \end{bmatrix} \quad (4.18)$$

where

$$R_{ei} = \begin{bmatrix} (\bar{p}_j - \bar{p}_i)^T \\ (\bar{p}_k - \bar{p}_i)^T \end{bmatrix}$$

and

$$R_{ij,ik} = \begin{bmatrix} (\bar{p}_i - \bar{p}_j)^T & (\bar{p}_j - \bar{p}_i)^T & 0 \\ (\bar{p}_i - \bar{p}_k)^T & 0 & (\bar{p}_k - \bar{p}_i)^T \end{bmatrix}.$$

The matrix R_{ei} is nonsingular because the equilibrium positions of i, j, k are not collinear (collinearity would violate minimal rigidity). Similarly, the linearized equation for the remote follower ($i = n - 1$) or the coleaders ($i = n - 2, n - 1, n$) is given by

$$\begin{bmatrix} \dot{\delta x}_i \\ \dot{\delta y}_i \end{bmatrix} = K_i R_{ei}^{-1} R_{ij(i),00} \begin{bmatrix} \delta x_i \\ \delta y_i \\ \delta x_{j(i)} \\ \delta y_{j(i)} \end{bmatrix} \quad (4.19)$$

where K_i is a 2×2 gain matrix,

$$R_{ei} = \begin{bmatrix} \bar{x}_{j(i)} - \bar{x}_i & \bar{y}_{j(i)} - \bar{y}_i \\ \bar{y}_i - \bar{y}_{j(i)} & \bar{x}_{j(i)} - \bar{x}_i \end{bmatrix}$$

and

$$R_{ij(i),00} = \begin{bmatrix} (\bar{p}_i - \bar{p}_{j(i)})^T & (\bar{p}_{j(i)} - \bar{p}_i)^T \\ 0 & 0 \end{bmatrix}.$$

For a LRF formation, the leader equations are of course

$$\begin{bmatrix} \dot{\delta x}_n \\ \dot{\delta y}_n \end{bmatrix} = 0. \quad (4.20)$$

Putting the equations together, we have for LRF

$$\dot{\delta p} = K R_e^{-1} \begin{bmatrix} R \\ 0 \end{bmatrix} \delta p \quad (4.21)$$

and we have for coleaders

$$\dot{\delta p} = K R_e^{-1} \begin{bmatrix} R_{1,n-3} \\ r_{n-2} \\ 0 \\ r_{n-1} \\ 0 \\ r_n \\ 0 \end{bmatrix} \delta p \quad (4.22)$$

where $K = \text{diag}[K_1, \dots, K_{n-1}, 0]$ with 2×2 K_i to be specified, $R_e = \text{diag}[R_{e1}, \dots, R_{e,n-1}, I_2]$ with each R_{ei} being a 2×2 submatrix of the rigidity matrix $R \in \mathfrak{R}^{2n-3 \times 2n}$. For coleaders $[R_{1,n-3}^T, r_{n-2}^T, r_{n-1}^T, r_n^T]^T \in \mathfrak{R}^{2n-3 \times 2n}$ is the rigidity matrix.

4.4.3 A Reduced-Order System for LRF Formations

For LRF formations, we define a reduced-order system by neglecting the stationary leader dynamics since $\dot{p}_n(t) = 0$. Let the global coordinate basis have the leader at the origin and let the x -axis be an arbitrary direction. Let $z = [p_1, \dots, p_{n-1}]^T \in \mathfrak{R}^{2n-2}$, $\bar{z} = [\bar{p}_1, \dots, \bar{p}_{n-1}]$, and $z = \delta z + \bar{z}$ where δz is assumed to be small. The reduced-order nonlinear system may then be written in the form

$$\dot{z} = \bar{f}(z). \quad (4.23)$$

The rigidity function associated with (4.23) is $r_z(z) = [\dots, \|z_j - z_k\|^2, \dots]^T$ where the i th entry of r_z corresponds to an edge $e_i \in E$ connecting two vertices j and k . If a vertex l is connected to the leader, then the corresponding entry in r_z is $\|z_l\|^2$. The equilibrium manifold associated with (4.23) is given by

$$\Psi_z = \{z \in \mathfrak{R}^{2n-2} | z = r_z^{-1}(d)\}. \quad (4.24)$$

Ψ_z is a one-dimensional manifold that can be characterized by a rotation around the leader since the the position of the leader is fixed. Therefore, since Ψ_z is a closed and bounded subset of Euclidean space, it is compact.

Now, expanding in a Taylor series about the equilibrium position, we

can rewrite (4.23) near the equilibrium position in the form

$$\dot{\delta z} = J_{\bar{f}}(\bar{z})\delta z + g(\delta z) \quad (4.25)$$

where the first term represents the reduced-order linear system and the second term represents the nonlinear part of order two or higher. The reduced-order linear system may be written in the form

$$\dot{\delta z} = \tilde{K}\tilde{R}_e^{-1} \begin{bmatrix} \tilde{R} \\ 0 \end{bmatrix} \delta z \quad (4.26)$$

where $\tilde{K} = \text{diag}[K_1, \dots, K_{n-1}]$, $\tilde{R}_e = \text{diag}[R_{e1}, \dots, R_{e,n-1}]$, and \tilde{R} is the submatrix of the rigidity matrix with the last two columns associated with the leader removed.

Observe that the Jacobian $J_{\bar{f}}(\bar{z})$ is rank deficient by one because of the row of zeros below the rigidity matrix. Thus one of its eigenvalues is zero. Thus, the equilibrium position is nonhyperbolic, and we can apply center manifold theory as developed in Section 4.3 to try to determine local stability of the equilibrium position. Since $J_{\bar{f}}(\bar{z})$ has one zero eigenvalue, there exists an invertible matrix Q such that

$$QJ_{\bar{f}}(\bar{z})Q^{-1} = \begin{bmatrix} 0 & 0 \\ 0 & A_s \end{bmatrix}. \quad (4.27)$$

where $A_s \in \mathfrak{R}^{2n-3 \times 2n-3}$ is a nonsingular matrix. Let $[\theta, \rho]^T = Q\delta z$ where $\theta \in \mathfrak{R}$ and $\rho \in \mathfrak{R}^{2n-3}$. Then (4.25) can be written in the form

$$\begin{aligned} \dot{\theta} &= g_1(\theta, \rho) \\ \dot{\rho} &= A_s\rho + g_2(\theta, \rho) \end{aligned} \quad (4.28)$$

where g_1 is the first entry of $Qg(Q^{-1}[\theta, \rho]^T)$ and satisfies $g_1(0, 0) = 0$ and $J_{g_1}(0, 0) = 0$, and g_2 is the last $2n - 3$ entries of $Qg(Q^{-1}[\theta, \rho]^T)$ and satisfies $g_2(0, 0) = 0$ and $J_{g_2}(0, 0) = 0$. This is in the normal form for center manifold theory.

To apply Theorem 4.3.1 we simply need the matrix A_s to be Hurwitz. Here, due to cycles in the graph presenting the possibility of instability, A_s must be *made* Hurwitz by a suitable choice of the gain matrices K_1, \dots, K_{n-1} . It is not however obvious that this can be done, or how to do it.

4.4.4 Full-Order System for Coleader Formations

Expanding in a Taylor series about an equilibrium position, we can express (4.16) in the form

$$\dot{\delta p} = J_f(\bar{p})\delta p + g_C(\delta p) \quad (4.29)$$

where the first term represents the linearized system given by (4.22) and the second term represents the nonlinear part of order two or higher. The Jacobian $J_f(\bar{p})$ is rank deficient by three because of the three rows of zeros; consequently, three of its eigenvalues are zero. Thus the equilibrium position is nonhyperbolic. Since $J_f(\bar{p})$ has three zero eigenvalues, there exists an invertible matrix Q_C such that

$$Q_C J_f(\bar{p}) Q_C^{-1} = \begin{bmatrix} 0 & 0 \\ 0 & A_{sC} \end{bmatrix}. \quad (4.30)$$

where $A_{sC} \in \mathfrak{R}^{2n-3 \times 2n-3}$ is a nonsingular matrix. Let $[\theta_C, \rho_C]^T = Q_C \delta p$ where $\theta_C \in \mathfrak{R}^3$ and $\rho_C \in \mathfrak{R}^{2n-3}$. Then (4.29) can be expressed in the form

$$\begin{aligned}\dot{\theta}_C &= g_{1C}(\theta_C, \rho_C) \\ \dot{\rho}_C &= A_{sC}\rho + g_{2C}(\theta_C, \rho_C)\end{aligned}\tag{4.31}$$

where g_{1C} comprises the first three entries of $Q_C g_C(Q_C^{-1}[\theta_C, \rho_C]^T)$ and satisfies $g_{1C}(0, 0) = 0$ and $J_{g_{1C}}(0, 0) = 0$, and g_{2C} comprises the last $2n - 3$ entries of $Q_C g_C(Q_C^{-1}[\theta_C, \rho_C]^T)$ and satisfies $g_{2C}(0, 0) = 0$ and $J_{g_{2C}}(0, 0) = 0$. This is in the normal form for center manifold theory.

Again, to apply Theorem 4.3.1 we simply need the matrix A_{sC} to be Hurwitz, and due to cycles in the graph presenting the possibility of instability, A_{sC} must be *made* Hurwitz by a suitable choice of the gain matrices K_1, \dots, K_n . Showing that such a choice of gains is indeed possible for both LRF and coleader formations is the topic of the next section.

4.5 Choosing Gains and the Principal Minor Condition

In this section we show that it is possible to choose the gain matrices for each agent such that all nonzero eigenvalues of the linearized system have negative real parts. This is the case if a certain submatrix of the rigidity matrix has all leading principal minors nonzero. That this condition is satisfied by all LRF and coleader formations is shown in the following. The arguments are similar but not identical to those of [83].

4.5.1 LRF Formations

Let the gain matrices K_1, \dots, K_{n-1} be chosen as follows:

$$K_i = \Lambda_i R_{e,i}, \quad i = 1, \dots, n-1 \quad (4.32)$$

where Λ_i is a diagonal matrix. Then we have

$$J_{\bar{f}}(\bar{z}) = \Lambda \begin{bmatrix} \tilde{R} \\ 0 \end{bmatrix} \quad (4.33)$$

where $\Lambda \in \mathfrak{R}^{2n-2 \times 2n-2}$ is a diagonal matrix where the diagonal entries can be chosen independently. The linearized system then has the following form

$$\dot{\delta z} = \Lambda \begin{bmatrix} \hat{R} & r_{12} \\ 0 & 0 \end{bmatrix} \delta z = J_{\bar{f}}(\bar{z}) \delta z \quad (4.34)$$

where $\Lambda \in \mathfrak{R}^{2n-2 \times 2n-2}$ is a diagonal matrix whose diagonal entries can be chosen independently and $\hat{R} \in \mathfrak{R}^{2n-3 \times 2n-3}$ is the rigidity matrix R with the last three columns removed. We have the following result from [83].

Theorem 4.5.1 ([83]). *Suppose \hat{R} is a nonsingular matrix with every leading principal minor nonzero and let $\Lambda = \text{diag}(\Lambda_1, \lambda_2)$ with $\Lambda_1 \in \mathfrak{R}^{2n-3 \times 2n-3}$ diagonal and $\lambda_2 \in \mathfrak{R}$. Then there exists a diagonal matrix Λ_1 such that the real parts of all nonzero eigenvalues of the linearized system are negative.*

Thus, $2n - 3$ eigenvalues of $J_{\bar{f}}(z)$ have negative real part and clearly the remaining eigenvalue is zero due to the rank deficiency of $J_{\bar{f}}(z)$. To make use of Theorem 4.5.1, we now need to show that \hat{R} satisfies the principal minor condition for LRF formations. Let $V' = \{v_1, \dots, v_{n-2}\}$ represent the set of ordinary followers, and let agents v_{n-1} and v_n correspond to the remote follower and leader, respectively.

Theorem 4.5.2. *Consider any minimally persistent LRF formation $F(G, p)$ of n agents at generic positions in the plane. Then there exists an ordering of the vertices of F and an ordering of the pair of outgoing edges for each vertex such that all leading principal minors of the associated \hat{R} are generically nonzero.*

The proof is nearly identical to the proof in [83]. We note the following partition of \hat{R} , which contrasts with the LFF partition in [83]:

$$\hat{R} = \begin{bmatrix} R(V') & \hat{r}_{12} \\ \hat{r}_{21}^T & \bar{x}_{n-1} - \bar{x}_l \end{bmatrix}. \quad (4.35)$$

$R(V')$ is the principal submatrix of \hat{R} obtained by retaining columns corresponding to the elements of V' . The vector \hat{r}_{21}^T has nonzero entries in the columns associated with v_l and is zero elsewhere. The vector \hat{r}_{12} has nonzero entries in the rows associated to edges that are pointing to the remote follower (there may be one or many nonzero entries), and is zero elsewhere. Additionally, consider a subset of ordinary follower vertices $V_1 \subseteq V'$ and define $R(V_1)$ as the principal submatrix of \hat{R} obtained by retaining columns corresponding to the elements of V_1 . We have the following result, which is stated in [83] for LFF formations and extends to LRF formations with identical proof.

Lemma 4.5.3. *For any minimally persistent LRF formation, \hat{R} is generically nonsingular and $R(V_1)$ is generically nonsingular for every $V_1 \subseteq V'$.*

Remark. The proof of Lemma 4.5.3 for the LFF case in [83] is stated for $V_1 \subset V'$ and trivially extends to the case for $V_1 \subseteq V'$.

Lemma 4.5.3 establishes that \hat{R} is generically nonsingular and that all even order principal minors are nonzero. Finally, the proof that all odd order principal minors are also nonzero relies on an appropriate ordering of edges and is identical to the proof in [83]. \square

This result shows that one can choose the diagonal matrix Λ such that the real parts of all nonzero eigenvalues of the reduced-order linearized system (4.26) are negative (and accordingly the matrix A_s in (4.28) is Hurwitz). The stabilizing gains are designed for a particular equilibrium point in the equilibrium manifold Ψ_z . It is important to note here that the control gains proposed in (4.32) may not be stabilizing for all other points in Ψ_z . Theorem 4.3.1 can be directly applied to show that for each $\bar{z} \in \Psi_z$, there is a neighbourhood $\Omega(\bar{z})$ of \bar{z} such that for any initial formation position $z(0) \in \Omega(\bar{z})$ there is a point $z^* \in \Psi$ such that $\lim_{t \rightarrow \infty} z(t) = z^*$ at an exponential rate, i.e. the formation converges locally exponentially to the desired shape.

4.5.2 Coleader Formations

Let the gain matrices K_1, \dots, K_n be chosen as follows:

$$K_i = \Lambda_i R_{e,i}, \quad i = 1, \dots, n \quad (4.36)$$

where the Λ_i are diagonal matrices. Reorder the coleader coordinates as

$$q = [x_1, y_1, \dots, x_{n-3}, y_{n-3}, x_{n-2}, y_{n-2}, x_{n-1}, y_{n-1}, x_n]^T.$$

An equilibrium position \bar{q} is defined from \bar{p} in the same manner as q is defined from p . Then the linearized system has the form

$$\dot{\delta q} = \Lambda \begin{bmatrix} \hat{R}_C & R_{12} \\ 0 & 0 \end{bmatrix} \delta q = J_q(\bar{q}) \delta q \quad (4.37)$$

where $\Lambda \in \mathfrak{R}^{2n \times 2n}$ is a diagonal matrix whose diagonal entries can be chosen independently and $\hat{R}_C \in \mathfrak{R}^{2n-3 \times 2n-3}$ is a submatrix of the rigidity matrix R that we will now define. Recall that R has two columns associated with each agent: one comprised of x -coordinates and one of y -coordinates. The matrix \hat{R}_C is obtained by removing the three columns from the rigidity matrix R as follows: one associated with each coleader and not all of x or y -type (i.e. one must remove two x -type and one y -type or vice versa). Theorem 4.5.1 extends to the coleader case; in particular, if \hat{R}_C is nonsingular with every leading principal minor nonzero, then Λ can be chosen such that all nonzero eigenvalues of the linearized system have negative real parts. Exactly three eigenvalues are necessarily zero. Again, to make use of this fact we now need to show that \hat{R}_C satisfies the principal minor condition for all coleader formations. Let $V' = \{v_1, \dots, v_{n-3}\}$ represent the set of ordinary followers, and let agents v_{n-2} , v_{n-1} , and v_n correspond to the coleaders. We have the following result:

Theorem 4.5.4. *Consider any minimally persistent coleader formation $F(G, p)$ of n agents at generic positions in the plane. Then there exists an ordering of the vertices of F and an ordering of the pair of outgoing edges for each vertex such that all leading principal minors of the associated \hat{R}_C are generically nonzero.*

We note the following structure of $\hat{R}_C \in \mathfrak{R}^{2n-3 \times 2n-3}$

$$\hat{R}_C = \begin{bmatrix} R(V') & \hat{R}_{12} \\ \hat{R}_{21} & \hat{R}_{22} \end{bmatrix}. \quad (4.38)$$

$R(V') \in \mathfrak{R}^{2n-6 \times 2n-6}$ is defined as before. Also, consider a subset of ordinary follower vertices $V_1 \subseteq V'$ and define $R(V_1)$ as before. Again, we have the following result from [83], which is stated for LFF formations and also extends to coleader formations with identical proof.

Lemma 4.5.5. *For any minimally persistent coleader formation, \hat{R}_C is generically nonsingular, and $R(V_1)$ is generically nonsingular for every $V_1 \subseteq V'$.*

Lemma 4.5.5 establishes that the largest leading principal minor is generically nonzero and that all even order leading principal minors up to size $2n - 6$ are generically nonzero. The proof that all odd order leading principal minors up to size $2n - 7$ are also generically nonzero relies on an appropriate ordering of edges and is identical to the proof in [83]. It now remains to show that the second and third largest leading principal minors (of size $2n - 5$ and $2n - 4$) are generically nonzero. We have the following two results that treat separately the case where the coleaders are connected and the case where the coleaders are not connected.

Lemma 4.5.6. *Suppose at most one coleader has its outgoing edge to V' , the set of ordinary followers. Then the second and third largest leading principal minors of \hat{R}_C are generically nonzero.*

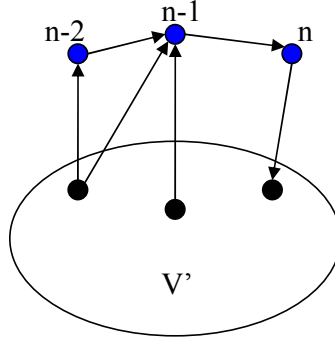


Figure 4.1: Coleader formation with only one coleader having its outgoing edge to the set of ordinary followers V' . There may be other edges from V' to the coleaders.

Proof. If at most one coleader, say that labeled n , has its outgoing edge to V' , then another coleader, say that labeled $n - 1$, has its outgoing edge to n , and the remaining coleader, labeled $n - 2$, has its outgoing edge to either $n - 1$ or n (suppose without loss of generality it is to $n - 1$). This situation is illustrated in Figure 4.1. Then the second and third largest leading principal submatrices of \hat{R}_C have the structure

$$M_{2n-5} = \begin{bmatrix} R(V') & \times \\ 0 & x_{n-2} - x_{n-1} \end{bmatrix}$$

$$M_{2n-4} = \begin{bmatrix} M_{2n-5} & \times \\ 0 & x_{n-1} - x_n \end{bmatrix}$$

where \times is a “don’t care” vector (only v_n may have an edge to V'). Since $R(V')$ is generically nonsingular, then M_{2n-5} is generically nonsingular, which then implies that M_{2n-4} is generically nonsingular. \square

Before considering the case where the coleaders are not connected, we shall need the following result.

Lemma 4.5.7. *Let $G(V, E)$ be the graph of a minimally persistent coleader formation with n agents and denote the coleaders $n - 2$, $n - 1$, and n . Suppose we obtain a new graph $G_2(V_2, E_2)$ as follows. Introduce two new agents labeled $n + 1$ and $n + 2$. Suppose that $n + 1$ has only one outgoing edge and that to $n + 2$; $n + 2$ has no outgoing edge; $n - 2$ (which was a coleader) has an additional outgoing edge to $n + 1$, $n - 1$ an additional edge to $n + 2$ and n an additional edge to either $n + 1$ or $n + 2$. Then G_2 is minimally persistent with LFF structure, with $n + 2$ the leader and $n + 1$ the first follower.*

Proof. First, we show that the underlying undirected graph G_2 is minimally rigid. Since G is minimally persistent, the underlying undirected graph is minimally rigid and satisfies the conditions of Theorem 2.2.3 with $|E| = 2|V| - 3$. To obtain G_2 , we have added to G two new vertices and four new edges; thus, $|E_2| = 2|V_2| - 3$ and so G_2 satisfies the condition of Theorem 2.2.3 for minimum edge count. Further, it is easy to check that no induced subgraph of G_2 involving vertices $n + 1$ and $n + 2$ violates the distribution condition for rigidity of Theorem 2.2.1. Thus, the underlying directed graph of G_2 is minimally rigid.

Next, since G is minimally persistent with coleader structure, the coleaders each have exactly one outgoing edge, and all remaining vertices have exactly two outgoing edges. To obtain G_2 we have added one outgoing edge from each coleader and so these vertices now have exactly two outgoing edges. Vertex $n + 1$ has exactly one outgoing edge to n , and n has no outgoing edges. Thus,

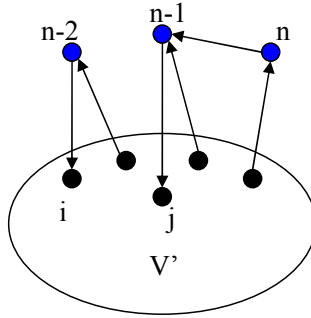


Figure 4.2: Coleader formation with two coleaders having outgoing edges to the set of ordinary followers V' . There may be other edges from V' to the coleaders.

G_2 is minimally persistent by Theorem 2.2.3, and it has LFF structure with $n + 2$ the leader and $n + 1$ the first follower. \square

Now we have the following result where the coleaders are not connected.

Lemma 4.5.8. *Suppose at least two coleaders have their outgoing edges to V' , the set of ordinary followers. Then the second and third largest leading principal minors of \hat{R}_C are generically nonzero.*

Proof. Assume that coleaders labeled $n - 2$ and $n - 1$ have outgoing edges to vertices i and j , respectively, both in V' . This situation is illustrated in Figure 4.2. Observe that the hypothesis permits $i = j$. The argument below applies regardless of whether $i = j$ and regardless of whether the sole outgoing edge of n is to an element of V' . Obtain a new LFF graph as described in Lemma 4.5.7 by introducing two *artificial* agents labeled $n + 1$ and $n + 2$. Call

this new graph $G_{LFF}(V_2, E_2)$. Consider the matrices below where B_l is the l -th order principal submatrix of the matrix obtained by removing the three last columns of the rigidity matrix of the artificial graph of G_{LFF} , where the precise values of a_i and b_i are immaterial to the argument to be presented..

$$\begin{aligned}
B_{2n-5} &= \begin{bmatrix} R(V') & a_1 \\ b_1 & x_{n-2} - x_i \end{bmatrix} \\
B_{2n-4} &= \begin{bmatrix} R(V') & a_1 & a_2 \\ b_1 & x_{n-2} - x_i & y_{n-2} - y_i \\ 0 & x_{n-2} - x_{n+1} & x_{n-2} - x_{n+1} \end{bmatrix} \\
B_{2n-3} &= \begin{bmatrix} R(V') & a_1 & a_2 & a_3 \\ b_1 & x_{n-2} - x_i & y_{n-2} - y_i & 0 \\ 0 & x_{n-2} - x_{n+1} & x_{n-2} - x_{n+1} & 0 \\ b_2 & 0 & 0 & x_{n-1} - x_j \end{bmatrix} \\
B_{2n-2} &= \begin{bmatrix} R(V') & a_1 & a_2 & a_3 & a_4 \\ b_1 & x_{n-2} - x_i & y_{n-2} - y_i & 0 & 0 \\ 0 & x_{n-2} - x_{n+1} & x_{n-2} - x_{n+1} & 0 & 0 \\ b_2 & 0 & 0 & x_{n-1} - x_j & y_{n-1} - y_j \\ 0 & 0 & 0 & x_{n-1} - x_{n+2} & y_{n-1} - y_{n+2} \end{bmatrix}
\end{aligned}$$

We note that all the even-dimensional submatrices above are generically non-singular, since they are the even-dimensional leading principal submatrices of a LFF structure (see [83]).

The third largest leading principal submatrix of \hat{R}_C is given by $M_{2n-5} = B_{2n-5}$. Suppose B_{2n-5} is not generically nonsingular. Then it is singular everywhere. Then because of the underlying symmetry of the x and y columns, the same would be true of the matrix

$$\begin{bmatrix} R(V') & a_2 \\ b_1 & y_{n-2} - y_i \end{bmatrix}.$$

But this implies that B_{2n-4} is singular, which establishes a contradiction.

Therefore, M_{2n-5} is generically nonsingular.

The second largest leading principal submatrix of \hat{R}_C is

$$M_{2n-4} = \begin{bmatrix} R(V') & a_1 & a_2 \\ b_1 & x_{n-2} - x_i & 0 \\ b_2 & 0 & x_{n-1} - x_j \end{bmatrix}.$$

We now argue that this matrix is generically nonsingular. Since B_{2n-2} is generically nonsingular, we assert the generic nonsingularity of B_{2n-3} , which implies the generic nonsingularity of

$$X = \begin{bmatrix} R(V') & a_1 & a_2 & a_3 \\ b_1 & x_{n-2} - x_i & y_{n-2} - y_i & 0 \\ b_2 & 0 & 0 & x_{n-1} - x_j \\ 0 & x_{n-2} - x_{n+1} & x_{n-2} - x_{n+1} & 0 \end{bmatrix}.$$

Indeed, suppose B_{2n-3} is singular for all positions. Then the symmetry of the x and y coordinates implies that the matrix obtained by replacing the last column of B_{2n-3} , by the first four elements of the last column of B_{2n-2} must also be singular for all positions. Consequently B_{2n-2} must be singular, establishing a contradiction. Thus, B_{2n-3} is generically nonsingular and so is X .

Now we assert that M_{2n-4} is generically nonsingular. To establish a contradiction suppose M_{2n-4} is singular everywhere. Then again, the matrix obtained by replacing the second column of M_{2n-4} by the first three elements of the third column of X must be singular everywhere. Thus X is singular. The contradiction proves the generic nonsingularity of M_{2n-4} . \square

Thus, all leading principal minors of \hat{R}_C are generically nonzero for all coleader formations. Therefore, again one can choose the diagonal matrix Λ such that the real parts of all nonzero eigenvalues of the linearized system (4.37) are negative (and accordingly the matrix A_{sC} in (4.31) is Hurwitz). The stabilizing gains are designed for a particular equilibrium point in the equilibrium manifold Ψ . It is important to note here that the control gains proposed in (4.36) may not be stabilizing for all other points in Ψ . Theorem 4.3.1 can be directly applied to show that for each $\bar{p} \in \Psi$, there is a neighbourhood $\Omega(\bar{p})$ of \bar{p} such that for any initial formation position $p(0) \in \Omega(\bar{p})$ there is a point $p^* \in \Psi$ such that $\lim_{t \rightarrow \infty} p(t) = p^*$ at an exponential rate, i.e. the formation converges locally exponentially to the desired shape.

Remark. There is an important distinction to be made between decentralized *design* and decentralized *implementation*. The control laws in this chapter are based on minimally persistent information architectures, and selecting stabilizing gains requires a suitable ordering of the vertices and edges. Therefore, the *design* of our control laws is inherently centralized. However, persistent information architectures provide a basis from which we can design control laws with decentralized *implementation*. Once the design is established, our control laws require only local information.

4.6 Simulations

4.6.1 LRF Formations

In this section, we demonstrate the performance of our algorithm via simulation. Figure 4.3 shows a LRF formation in the plane where agents 1 and 2 are ordinary followers, agent 3 is the remote follower, and agent 4 is the leader. Suppose the agents are in the desired formation shape in the position $\bar{p} = [0.3123, -0.1574, 0.7359, 0.5710, -0.0609, 0.6901, 0, 0]$. We note that if the gain matrices are all chosen to be identity, the nonzero eigenvalues of the linearized system are $\{-1.5363 \pm 0.9289i, 0.0726, -1, -1\}$, which implies instability. Suppose the gain matrices are chosen with the structure given by (4.32) where the diagonal multipliers are $\Lambda_1 = \text{diag}[-2, 2]$, $\Lambda_2 = \text{diag}[-2, -1]$, and $\Lambda_3 = \text{diag}[2, 0.5]$. Then the nonzero eigenvalues of the linearized system are given by $\{-1.9521 \pm 0.3196i, -0.2521 \pm 0.3886i, -0.7532\}$, and the desired formation shape is stable via the analysis in the previous sections. Figure 4.4 shows the agent trajectories in the plane under the formation shape maintenance control laws. The desired formation shape is restored, though not to the initial unperturbed formation. Figure 4.5 shows that the interagent distance errors all converge to zero. Simulations for large perturbations are explored for coleader formations.

4.6.2 Coleader Formations

Figure 4.6 shows a coleader formation in the plane where agent 1 is an ordinary follower and agents 2, 3, and 4 are coleaders. Suppose the agents are

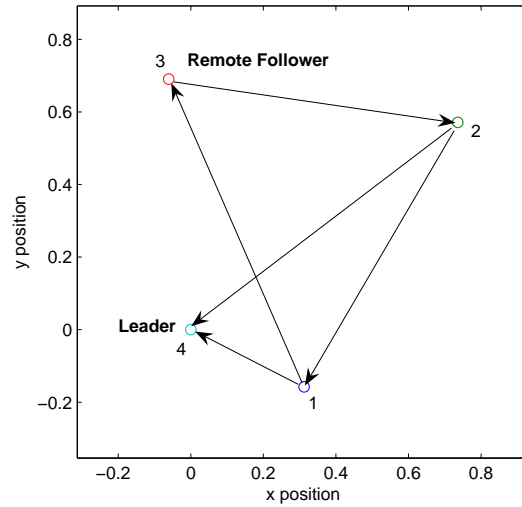


Figure 4.3: LRF formation in unstable agent positions for identity gain.

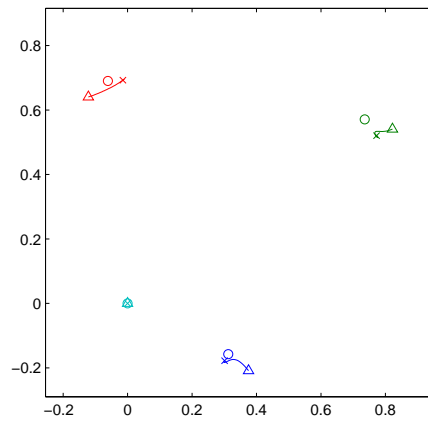


Figure 4.4: Agent trajectories in the plane: circles represent the initial desired formation shape, triangles represent the perturbed agent positions, and X's represent the final agents positions under the formation shape maintenance control laws. The desired shape has been restored. The leader does not move.

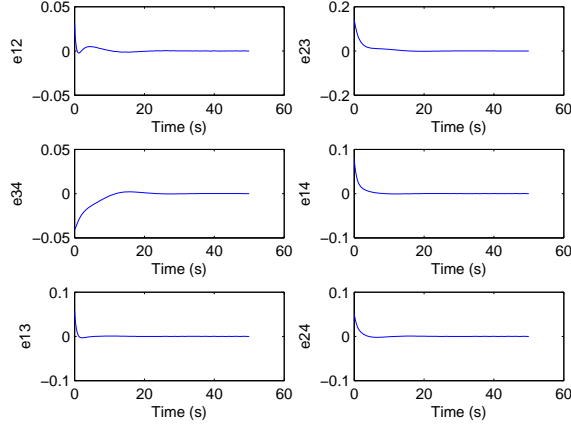


Figure 4.5: The interagent distance errors, defined as $e_{ij} = \|p_i - p_j\| - d_{ij}$, all converge to zero, thus recovering the desired formation shape.

in the desired formation shape in the position

$$\bar{p} = [0.7036, 0.485, 0.1146, 0.6649, 0.3654, 0.140, 0.5668, 0.823].$$

If the gain matrices are all chosen to be identity, the nonzero eigenvalues of the linearized system are $\{-1.2339 \pm 0.8376i, -1.5356, -1, 0.0034\}$, which implies instability. Suppose the gain matrices are chosen with the structure given by (4.36) where the diagonal multipliers are $\Lambda_1 = \text{diag}[-1.3, -0.9]$, $\Lambda_2 = \text{diag}[0.5, 0.75]$, $\Lambda_3 = \text{diag}[1.2, 0.35]$, and $\Lambda_4 = \text{diag}[-2.7, -0.25]$. Then the nonzero eigenvalues of the linearized system are given by $\{-0.3655 \pm 0.0933i, -0.5719, -0.9378, -1.0712\}$, and the desired formation shape is stable via the analysis in the previous sections. Figure 4.7 shows the agent trajectories in the plane under the formation shape maintenance control laws. The desired formation shape is restored, though the final formation is translated

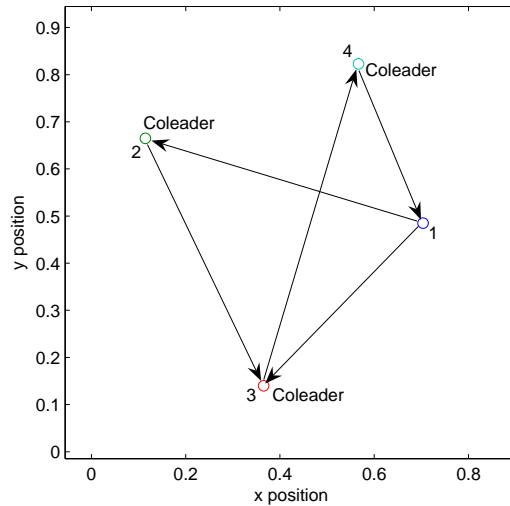


Figure 4.6: Coleader formation in the plane in unstable agent positions for identity gain.

and rotated from the original unperturbed formation. Figure 4.8 shows that the interagent distance errors all converge to zero.

The stability result is local; thus, convergence is only guaranteed for formations that are initially close enough to the desired shape. The following simulations investigate potential outcomes for larger perturbations from the desired shape. Figure 4.9 shows convergence to the desired shape despite initial perturbations as large as 50% of the desired interagent distance, which indicates a sizable region of attraction. Figure 4.10 shows the corresponding interagent distance errors converging to zero. Another possible outcome is shown in Figure 4.11 where the agents converge to a formation that is *equivalent*, but not *congruent*, to the desired formation. In Figure 4.12 all interagent

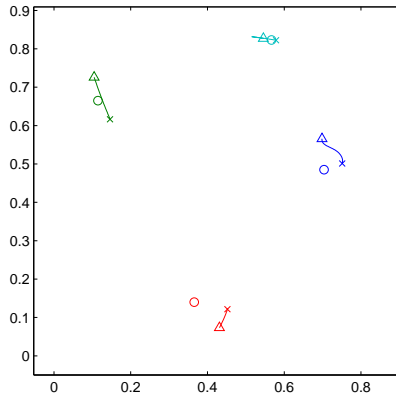


Figure 4.7: Agent trajectories in the plane: circles represent the initial desired formation shape, triangles represent the perturbed agent positions, and X's represent the final agents positions under the formation shape maintenance control laws. The desired shape has been restored, though the final formation is translated and rotated from the original unperturbed formation.

distance errors corresponding to an edge in the graph converge to zero, whereas the only interagent distance error that does not correspond to an edge, viz. e_{24} , converges to a non-zero value. The position of agent 2 (green) has been reflected about the line connecting agents 1 and 3 (blue and red). Despite the fact that the linearized system is locally stable, there remains a possibility of instability given sufficiently large initial perturbations, as illustrated in the agent trajectories in Figure 4.13 and the interagent distance errors in Figure 4.14.

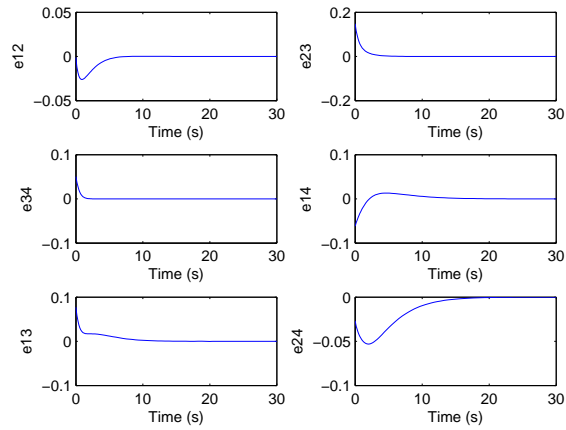


Figure 4.8: The interagent distance errors all converge to zero, thus recovering the desired formation shape. That e_{24} , which does not correspond to an edge of the formation graph, goes to zero is due to the underlying rigidity and the convergence of the other e_{ij} to zero.

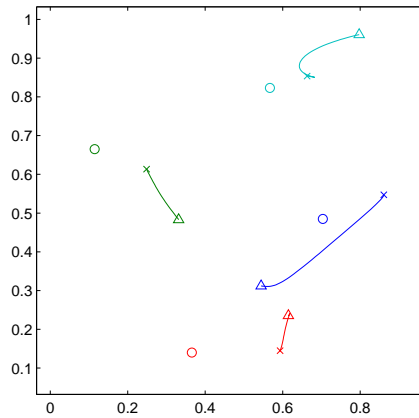


Figure 4.9: Agent trajectories after a larger perturbations: the desired shape has been restored, though the final formation is translated and rotated from the original unperturbed formation. The circles, triangles and X's are as for Figure 7.

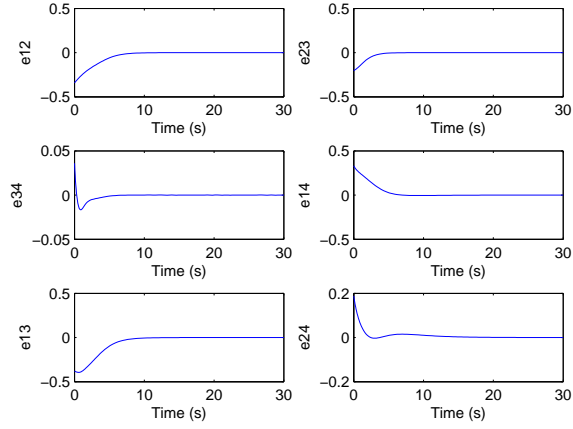


Figure 4.10: The interagent distance errors all converge to zero, thus recovering the desired formation shape.

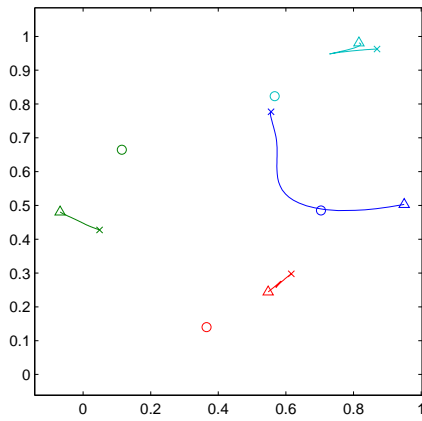


Figure 4.11: Agent trajectories in the plane after large perturbations: the formation converges to an equivalent, but not congruent, shape.

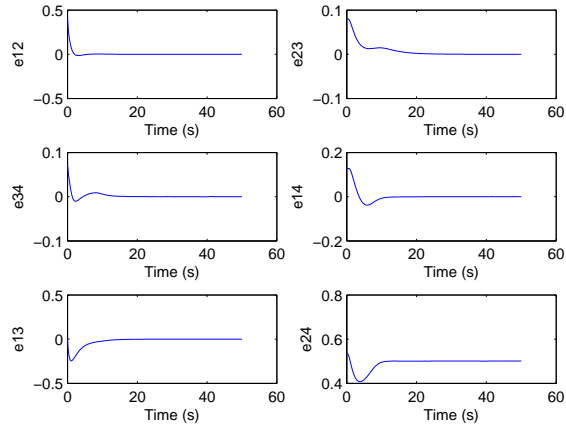


Figure 4.12: All interagent distance errors except one converge to zero.

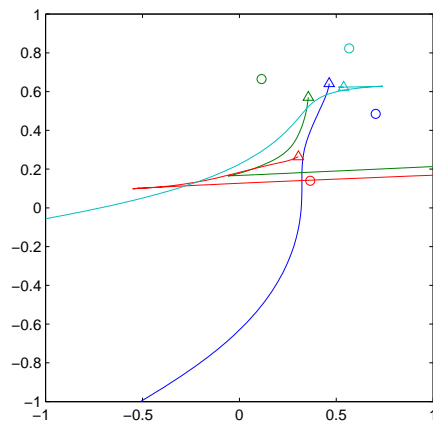


Figure 4.13: Agent trajectories in the plane after larger perturbations: instability.

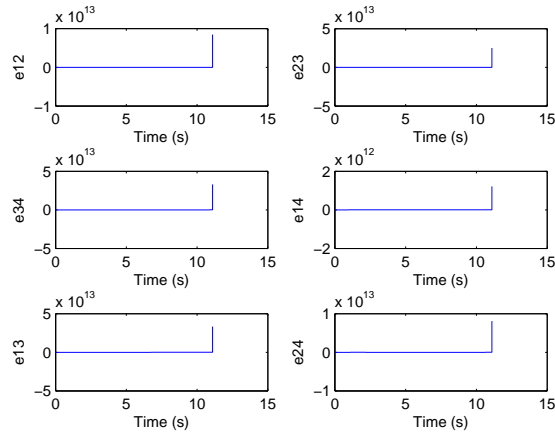


Figure 4.14: The interagent distance errors all blow up.

4.7 Concluding Remarks

This chapter has solved a n -agent formation shape maintenance problem for minimally persistent leader-remote-follower and coleader formations. We presented decentralized nonlinear control laws that restore the desired formation shape in the presence of small perturbations from the desired shape. The nonlinear system has a manifold of equilibria, which implies that the linearized system is nonhyperbolic. We applied center manifold theory to show local exponential stability of the equilibrium formation with desired shape. We have also shown that a principal minor condition holds for all LRF and coleader formations, which allows a choice of stabilizing gain matrices. Finally, we demonstrated our results through numerical simulation.

The stability results in this chapter are local in that convergence to the desired shape is only guaranteed under sufficiently small perturbations

from the desired shape. Global stability, which guarantees convergence to the desired shape for any initial condition, is a significant challenge in rigidity-based formation control. The next chapter builds theory for the global stability of a four-agent formation and identifies open research questions in this area.

Chapter 5

Formation Shape Control: Global Asymptotic Stability of a Four-Agent Formation

5.1 Introduction

Global stability, where a desired formation shape is produced from any initial configuration, remains a challenging open problem in rigidity-based formation shape control problems. This is largely due to the inherent nonlinearity of these problems and the potential existence of additional equilibrium shapes. Nonlinear systems do not always admit closed form analytical solutions, and, in order to show that one point in a multiple equilibrium point system is globally stable, all other equilibrium points must be shown to be unstable. The global stability properties in nonlinear systems are difficult to characterize.

Almost¹ global stability is demonstrated for a directed, cyclic, three-agent formation in [1] and for a directed, acyclic three-agent formation in [13, 14]. It is noted in [19] that these results extend easily to the undirected three-agent case. In [12], almost² global stability is demonstrated for directed,

¹The formations converge to a desired triangular shape from any *non-collinear* initial configuration, so what is demonstrated is actually *almost* global stability since the set of collinear configurations is thin (Lebesgue measure zero).

²Again, convergence is shown from all initial configurations outside of a thin set.

acyclic, n -agent formations. In [38], Krick et al study an undirected n -agent rigidity-based formation control problem. They prove for undirected rigid formations that the desired formation shape is *locally* asymptotically stable under a gradient control law if the information architecture is rigid. An interesting simulation from [38] relating to global stability properties involves a four-agent formation with a complete graph information architecture (i.e. all interagent distances are actively controlled). The formation appears to converge to an incorrect shape, with interagent distances not all the same as those in the desired shape, and the paper concluded that the desired shape is not globally asymptotically stable. The complete graph architecture on four agents is of particular interest because it is the only globally rigid graph on four agents; thus, it is the only graph in which the distances specify a *unique* shape.

This chapter elaborates on this example from [38]. Section 5.2 presents the equations of motion for the four-agent formation shape control problem and shows that the observed incorrect equilibrium formation shape from [38] is in fact an unstable saddle. We provide an easily checkable condition for local instability of an equilibrium shape and use this condition to show that the *class* of rectangular incorrect shapes identified in [38] is unstable. Section 5.3 shows how to compute a desired equilibrium shape from a supposed incorrect equilibrium shape. Section 5.4 gives concluding remarks.

5.2 Equations of Motion and Examples

In this section, we present equations of motion for the four-agent formation shape control problem in the plane. We then examine the example from [38] that illustrates existence of an incorrect equilibrium formation shape and show that this shape is an unstable saddle.

5.2.1 Equations of Motion

Let $p = [p_1, p_2, p_3, p_4]^T \in \mathfrak{R}^8$ be a vector of the four agent positions in the plane. Following [38], we use a single integrator agent model to describe the motion of each agent

$$\dot{p}_i = u_i$$

where u_i is the control input to be specified. Let $\bar{d} = [\bar{d}_{12}, \bar{d}_{13}, \bar{d}_{14}, \bar{d}_{23}, \bar{d}_{24}, \bar{d}_{34}]^T$ be a vector of desired interagent distances that define the formation shape and are to be actively controlled. We assume that the entries of \bar{d} correspond to a realizable shape. Let $d(p) = [d_{12}(p), d_{13}(p), d_{14}(p), d_{23}(p), d_{24}(p), d_{34}(p)]^T$ denote instantaneous interagent distances. The rigidity function is given by

$$r(p) = d^2(p) = [\|p_1 - p_2\|^2, \|p_1 - p_3\|^2, \|p_1 - p_4\|^2, \\ \|p_2 - p_3\|^2, \|p_2 - p_4\|^2, \|p_3 - p_4\|^2]^T$$

We define the the error function

$$e(p) = d^2(p) - \bar{d}^2 \\ = [e_{12}, e_{13}, e_{14}, e_{23}, e_{24}, e_{34}]^T \quad (5.1)$$

The desired formation shape is a three-dimensional manifold in \mathfrak{R}^8 given by

$$P_d = \{p \in \mathfrak{R}^8 | d^2(p) = \bar{d}^2\} \quad (5.2)$$

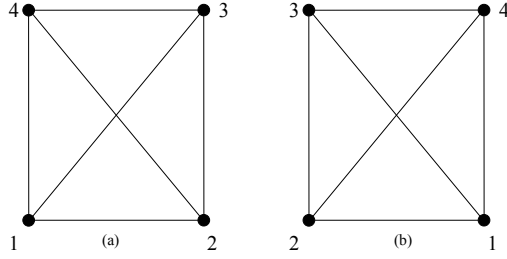


Figure 5.1: A desired formation configuration and its reflection in the plane both satisfy the same prescribed interagent distance constraints.

which is non-empty for a realizable \bar{d} . Note the following symmetry for any planar formation: two distinct formation orientations both correspond to a correct formation shape: one orientation and its reflection in the plane, as illustrated in Figure 5.1.

Now consider the potential function

$$\begin{aligned} V(p) &= \frac{1}{2} \|e(p)\|^2 \\ &= \frac{1}{2} (e_{12}^2 + e_{13}^2 + e_{14}^2 + e_{23}^2 + e_{24}^2 + e_{34}^2). \end{aligned}$$

The function quantifies the total interagent distance error between the current formation and the desired formation \bar{d} . Note that $V \geq 0$ and $V = 0$ if and only if $e(p) = 0$, that is if and only if the formation is in the desired shape. Thus, V is a suitable potential function from which to derive a gradient control law. Accordingly, let the control input be given by

$$u = -\nabla V(p)^T. \quad (5.3)$$

Then the closed-loop system is given by

$$\begin{aligned}\dot{p} &= -\nabla V(p)^T \\ &= -[J_r(p)]^T e(p)\end{aligned}\tag{5.4}$$

where $J_r(p)$ is the Jacobian of the rigidity function $r(p)$ (also known as the *rigidity matrix*). This can be expressed in the following form

$$\dot{p} = -(E(p) \otimes I_2)p\tag{5.5}$$

where the matrix $E(p)$ is given by

$$E(p) = \begin{bmatrix} e_{12} + e_{13} + e_{14} & -e_{12} & -e_{13} & -e_{14} \\ -e_{12} & e_{12} + e_{23} + e_{24} & -e_{23} & -e_{24} \\ -e_{13} & -e_{23} & e_{13} + e_{23} + e_{34} & -e_{34} \\ -e_{14} & -e_{24} & -e_{34} & e_{14} + e_{24} + e_{34} \end{bmatrix}\tag{5.6}$$

where \otimes is the Kronecker product. Agent-wise, the equations of motion are

$$\begin{aligned}\dot{p}_1 &= e_{12}(p_2 - p_1) + e_{13}(p_3 - p_1) + e_{14}(p_4 - p_1) \\ \dot{p}_2 &= e_{12}(p_1 - p_2) + e_{23}(p_3 - p_2) + e_{24}(p_4 - p_2) \\ \dot{p}_3 &= e_{13}(p_1 - p_3) + e_{23}(p_2 - p_3) + e_{34}(p_4 - p_3) \\ \dot{p}_4 &= e_{14}(p_1 - p_4) + e_{24}(p_2 - p_4) + e_{34}(p_3 - p_4)\end{aligned}\tag{5.7}$$

Note that the development above is identical if the formation evolves in three dimensions, with the p_i becoming 3-vectors.

A standard argument appealing to LaSalle's Invariance Principle establishes that from any initial configuration, the system trajectories tend to an equilibrium in which $(E(p) \otimes I_2)p = 0$. The equilibrium points of the closed-loop system (7.18) are the same as the critical points of the potential function

V . The Jacobian of the right side of (7.18), which we denote as $J_f(p)$, is the same as the negative of the Hessian of V , which we denote as $H_V(p)$. These are given by

$$H_V(p) = 2J_r(p)^T J_r(p) + E(p) \otimes I_2 = -J_f(p). \quad (5.8)$$

Therefore, a study of the stability of the equilibrium points of (7.18) amounts to a study of the nature of the critical points of V : minima are locally stable and maxima and saddle points are locally unstable. Note that the stability of an equilibrium point is independent of rotation and translation of the formation shape; only relative positions matter.

Since we actively control every interagent distance, the information architecture is the complete graph K_4 . It turns out that there are formation positions p^* for which $e(p^*) \neq 0$ (i.e. $d^2(p^*) \neq \bar{d}^2$ and so $p^* \notin P_d$) and $(E(p^*) \otimes I_2)p^* = 0$. Such a position is called an *incorrect equilibrium shape*.

5.2.2 Krick Example

In [38], Krick et al prove for an n -agent formation that under the gradient control law (5.3), the desired formation is locally asymptotically stable (in the sense that for $\|e(p(0))\|$ sufficiently small, $\|e(p(t))\| \rightarrow 0$ as $t \rightarrow \infty$) if the underlying information architecture is rigid.

The paper also shows a four-agent example with K_4 information architecture in which the formation appears to converge to an incorrect equilibrium shape. The example is as follows. Suppose the desired formation is a

1×2 rectangle given by $\bar{d}^2 = [1, 5, 4, 4, 5, 1]^T$. It is easy to verify that when we use the desired distances specified by \bar{d} , any formation with distance set $d^{*2} = [\frac{11}{3}, \frac{7}{3}, \frac{4}{3}, \frac{4}{3}, \frac{7}{3}, \frac{11}{3}]^T$ is an incorrect equilibrium shape. The incorrect equilibrium is a “twisted rectangle” with the term twisted referring to a change in agent ordering, as illustrated in the middle formation of Figure 5.2 (it turns out there is a further incorrect equilibrium shape, which we discuss later). Krick et al concluded that the desired shape is not globally attractive since the control law appears to cause convergence to an incorrect equilibrium shape. However, the convergence is only apparent, occurring along the ridge of a saddle. The eigenvalues of the negative of the Hessian evaluated at the incorrect shape (i.e. $\text{eig}[J_f(p^*)] = \text{eig}[-H_V(p^*)]$ where p^* satisfies $d^2(p^*) = \bar{d}^2$) are $\{0, 0, 0, -22.78, -14.67, -6.56, 1.33, 5.33\}$. Since there are both positive and negative eigenvalues, then the incorrect equilibrium shape is in fact a saddle and is therefore unstable.

The question becomes: given an arbitrary (realizable) desired shape, are there any attractive incorrect equilibrium shapes? In other words, is there any $p^* \in \mathfrak{R}^8$ with $e(p^*) \neq 0$ and $(E(p^*) \otimes I_2)p^* = 0$ for which $p^T H_V(p^*)p \geq 0 \forall p \in \mathfrak{R}^8$? For arbitrary desired shapes, this question remains open. The next section considers the special case of rectangular desired shapes.

5.3 Rectangular Formations

For rectangular desired formations of arbitrary size, we can calculate two possible rectangular incorrect equilibrium shapes which manifest as

“twisted rectangles” with a change in agent ordering. We shall show that the incorrect equilibrium shapes are unstable saddles.

Suppose that the desired formation is an $a \times b$ rectangle given by $\bar{d}^2 = [a^2, a^2 + b^2, b^2, b^2, a^2 + b^2, a^2]^T$ with agents 1,2,3,4 in counterclockwise order. Suppose there is a rectangular incorrect equilibrium shape p_1^* with agents 1,3,2,4 in counterclockwise order with $d_{13}(p^*) = d_{24}(p^*) = a_1^*$ and $d_{23}(p^*) = d_{14}(p^*) = b_1^*$. Evaluating each component in the equilibrium condition for agent 1 in (5.7) yields the following two relationships

$$\begin{aligned} a_1^{*2} &= a^2 + \frac{1}{3}b^2 \\ b_1^{*2} &= \frac{1}{3}b^2 \end{aligned} \tag{5.9}$$

Thus, any twisted rectangle with interagent distances given by

$$d_1^{*2} = \left[a^2 + \frac{2}{3}b^2, a^2 + \frac{1}{3}b^2, \frac{1}{3}b^2, \frac{1}{3}b^2, a^2 + \frac{1}{3}b^2, a^2 + \frac{2}{3}b^2 \right]^T$$

is an incorrect equilibrium shape. Now suppose there is a different rectangular incorrect equilibrium shape p_2^* with agents 1,3,4,2 in counterclockwise order with $d_{13}(p^*) = d_{24}(p^*) = a_2^*$ and $d_{12}(p^*) = d_{34}(p^*) = b_2^*$. A similar argument yields

$$\begin{aligned} a_2^{*2} &= \frac{1}{3}a^2 + b^2 \\ b_2^{*2} &= \frac{1}{3}a^2 \end{aligned} \tag{5.10}$$

and shows that the twisted rectangle with interagent distances given by

$$d_2^{*2} = \left[\frac{1}{3}a^2, \frac{1}{3}a^2 + b^2, \frac{2}{3}a^2 + b^2, \frac{2}{3}a^2 + b^2, \frac{1}{3}a^2 + b^2, \frac{1}{3}a^2 \right]^T$$

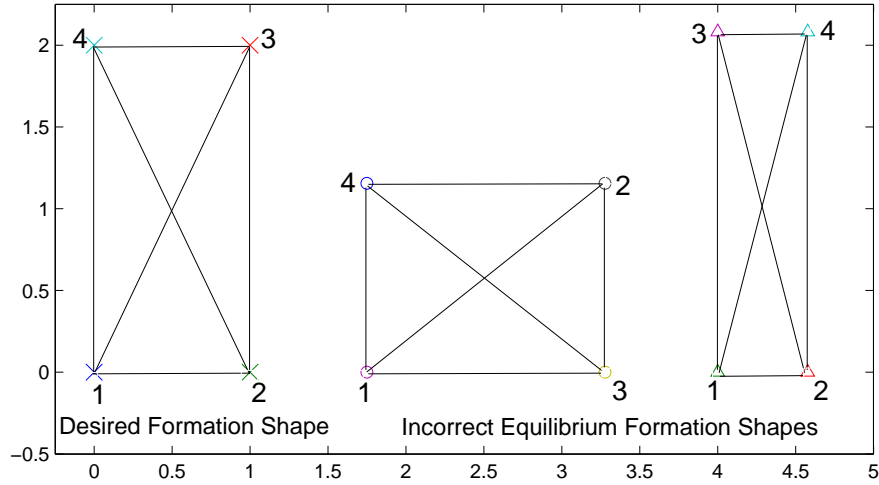


Figure 5.2: The desired formation is rectangular and there are two possible “twisted rectangles” that are incorrect equilibrium shapes. Note that each formation has two different pairs of agents on the diagonals of the rectangle: (a) 13 and 24, (b) 12 and 34, and (c) 14 and 23.

is also an incorrect equilibrium shape. The desired and both twisted equilibrium shapes are illustrated in Figure 5.2 for the Krick example where $a = 1$ and $b = 2$.

We now show that both of these incorrect equilibrium shapes are unstable via direction calculation on the Hessian. Consider the first incorrect equilibrium shape p_1^* . The Hessian evaluated at p_1^* can be easily calculated given \bar{d} and d_1^{*2} (for example, with agent 1 at the origin and agent 3 on the x -axis). The eigenvalues of the 4×4 leading principal submatrix can be cal-

culated analytically and are given by

$$\text{eig}(H(1 : 4, 1 : 4)) = \begin{bmatrix} -\frac{2}{3}b^2 \\ 2a^2 - \frac{2}{3}b^2 \\ 3a^2 + 2b^2 - \sqrt{9a^4 + \frac{8}{3}a^2b^2 + \frac{8}{9}b^4} \\ 3a^2 + 2b^2 + \sqrt{9a^4 + \frac{8}{3}a^2b^2 + \frac{8}{9}b^4} \end{bmatrix} \quad (5.11)$$

Since this leading principal submatrix has both positive and negative values, the Hessian is not sign semidefinite. Therefore, the closed-loop system (7.18) is an unstable saddle at p_1^* . The same argument shows the instability of the closed-loop system at p_2^* .

We cannot say whether or not the desired shape given by \bar{d} is globally stable or not because we do not know if the incorrect equilibrium shapes given by d_1^* and d_2^* are the only ones associated with \bar{d} . The set of algebraic equilibrium equations obtained by setting (5.7) to zero are nonlinear and difficult to solve for a K_4 information architecture.

5.4 Computing a Desired Equilibrium Shape from an Incorrect Equilibrium Shape

This section describes how one can compute a desired equilibrium given a supposed incorrect equilibrium shape. Take an arbitrary generic $p^* \in \mathfrak{R}^8$ and suppose it is an incorrect equilibrium shape with interagent distances $d_{ij}^*(p^*)$ corresponding to some desired shape with distances \bar{d}_{ij} . Recall that $e_{ij}(p^*) = d_{ij}^{*2}(p^*) - \bar{d}_{ij}^2$. It follows from (5.4) that the error vector $e(p^*)$ lies in the left null space of the rigidity matrix $J_r(p^*)$ (since p^* is an equilibrium point). The left null space of the rigidity matrix $J_r(p^*) \in \mathfrak{R}^{8 \times 6}$ is one-dimensional

since $\text{rank}[J_r(p^*)] = 5$ from Theorem 2.2.2 in Chapter 2. Thus, $e(p^*)$ can always be computed up to a scaling constant:

$$e(p^*) = d_{ij}^{*2}(p^*) - \bar{d}_{ij}^2 = \lambda \tilde{e} \quad (5.12)$$

where \tilde{e} is any left null vector of $J_r(p^*)$ and $\lambda \in \Re$ is a constant.

The scaling constant λ can be determined through the *Cayley-Menger determinant*, which is widely used in distance geometry [11]. The *Cayley-Menger matrix* of a set of n points $\{p_1, \dots, p_n\}$, with $p_i \in \Re^m$, is defined as

$$M(p_1, \dots, p_n) = \begin{bmatrix} 0 & \|p_1 - p_2\|^2 & \cdots & \|p_1 - p_n\|^2 & 1 \\ \|p_1 - p_2\|^2 & 0 & \cdots & \|p_2 - p_n\|^2 & 1 \\ \vdots & \vdots & \ddots & \vdots & \vdots \\ \|p_1 - p_n\|^2 & \|p_2 - p_n\|^2 & \cdots & 0 & 1 \\ 1 & 1 & \cdots & 1 & 0 \end{bmatrix} \quad (5.13)$$

The determinant of the Cayley-Menger matrix M gives an expression for the hyper-volume of a simplex³ in terms of the edge lengths. For our four-agent formation, this gives the volume of the tetrahedron defined by the four agent positions. And since our formation evolves in the plane, this volume must be zero, so the Cayley-Menger determinant is zero.

Now consider the Cayley-Menger determinant at the desired equilib-

³A simplex of n points is the smallest $n - 1$ dimensional convex hull that contains the points.

rium. We have

$$\begin{aligned}
\det(M) &= \begin{vmatrix} 0 & \bar{d}_{12}^2 & \bar{d}_{13}^2 & \bar{d}_{14}^2 & 1 \\ \bar{d}_{12}^2 & 0 & \bar{d}_{23}^2 & \bar{d}_{24}^2 & 1 \\ \bar{d}_{13}^2 & \bar{d}_{23}^2 & 0 & \bar{d}_{34}^2 & 1 \\ \bar{d}_{14}^2 & \bar{d}_{24}^2 & \bar{d}_{34}^2 & 0 & 1 \\ 1 & 1 & 1 & 1 & 0 \end{vmatrix} \\
&= \begin{vmatrix} 0 & d_{12}^{*2}(p^*) - \lambda\tilde{e}_{12} & d_{13}^{*2}(p^*) - \lambda\tilde{e}_{13} & d_{14}^{*2}(p^*) - \lambda\tilde{e}_{14} & 1 \\ d_{12}^{*2}(p^*) - \lambda\tilde{e}_{12} & 0 & d_{23}^{*2}(p^*) - \lambda\tilde{e}_{23} & d_{24}^{*2}(p^*) - \lambda\tilde{e}_{24} & 1 \\ d_{13}^{*2}(p^*) - \lambda\tilde{e}_{13} & d_{23}^{*2}(p^*) - \lambda\tilde{e}_{23} & 0 & d_{34}^{*2}(p^*) - \lambda\tilde{e}_{34} & 1 \\ d_{14}^{*2}(p^*) - \lambda\tilde{e}_{14} & d_{24}^{*2}(p^*) - \lambda\tilde{e}_{24} & d_{34}^{*2}(p^*) - \lambda\tilde{e}_{34} & 0 & 1 \\ 1 & 1 & 1 & 1 & 0 \end{vmatrix} \\
&\hspace{20em} (5.14)
\end{aligned}$$

Setting $\det(M)$ to zero yields a third-order polynomial in λ . Since the Cayley-Menger determinant must also be zero at the incorrect equilibrium, then $\lambda = 0$ is always a solution. Thus, there are at most two possible desired equilibrium shapes corresponding to the incorrect equilibrium shape. However, there are a few circumstances in which the non-zero solutions for λ do not result in an actual desired equilibrium. These circumstances are listed as follows, with an indication of whether they have been observed in simulations in which a random incorrect equilibrium is generated and the associated desired equilibrium is calculated:

- If the non-zero solutions for λ are complex, then there is no desired equilibrium. This has not been observed in simulations
- Real solutions for λ give real solutions for the \bar{d}_{ij}^2 via (5.12), but if these are negative, then there is no desired equilibrium. This has been observed in simulations.

- Real solutions for the \bar{d}_{ij} must satisfy certain triangle inequalities; if not, there is no desired equilibrium. This has not been observed in simulations.

Simulations, in which incorrect equilibrium shapes are generated randomly and potential corresponding desired equilibrium shapes are computed, indicate that there is almost always only one desired equilibrium shape corresponding to a supposed incorrect equilibrium shape, and that the incorrect equilibrium shape is an unstable saddle. Interestingly, note that for a square incorrect equilibrium shape (i.e. $a^{*2} = b^{*2}$), neither (5.9) nor (5.10) give a corresponding non-degenerate desired equilibrium shape.

5.5 Concluding Remarks

This chapter has studied a four-agent formation shape control problem using gradient-based interagent distance control laws with relative position measurements. When the information architecture is a complete graph, we showed that there may exist incorrect equilibrium shapes and proved that a class of rectangular incorrect shapes are unstable. We also showed how to compute a desired equilibrium shape from a supposed incorrect equilibrium shape. The most significant remaining open question is: can there ever exist an attractive incorrect equilibrium shape given some desired shape?

The previous three chapters have demonstrated that rigid and persistent information architectures play a crucial role in solving certain formation

shape control problems. They provide insight into the problem of realizing the advantage of improved sensing capability in autonomous vehicle formations, which crucially depends on maintaining the formation in a prescribed shape. The next chapter returns to another strong motivation for autonomous vehicle formations: ensuring that a formation can control its shape in the event of the failure of a single agent. To provide robustness to agent loss, we must *design* information architectures to recover or preserve desirable properties.

Chapter 6

Addressing Agent Loss in Vehicle Formations and Sensor Networks

6.1 Introduction

A primary motivation for using large-scale vehicle formations and sensor networks is their potential robustness to loss of a single agent or a small number of agents. This chapter addresses agent loss in planar formations via two separate approaches: (1) perform a “self-repair” operation in the event of agent loss to recover rigidity or global rigidity, or (2) introduce robustness into the information architecture *a priori* such that agent loss does not destroy rigidity or global rigidity. Information architectures with these properties would allow formation shape control or self-localization tasks to be performed in the event of loss of any single agent. The “self-repair” approach is *reactive* in that the formation reacts to an agent loss event. The robustness approach is *proactive* in that redundancy is built into the formation *a priori* in anticipation of an agent loss event.

The “self-repair” approach is an instance of the *closing ranks problem*. Previous work by Eren et al [20] demonstrated a solution to the closing ranks problem that cannot always be implemented using only local information. We

contribute decentralized sub-optimal solutions to the closing ranks problem, providing algorithms to recover both rigidity and global rigidity. The solutions are sub-optimal in that they potentially add more links than required by a minimal solution, but only up to twice as many. However, this trade-off allows decentralized implementation, highlighting the need to sacrifice a measure of optimality when faced with constraints.

The robustness approach requires graphs with the property that rigidity or global rigidity is preserved after removing any single vertex, which we call *2-vertex-rigidity*¹ or *2-vertex-global-rigidity*, respectively. In [67], Servatius identified some subtle graph theoretic features that make obtaining a complete theoretic characterization of these properties difficult. She characterized a particular class of *2-vertex-rigid* graphs, which we call *strongly minimal* and posed an open question about other types of 2-vertex-rigid graphs. We answer this open question by developing a separate class of *2-vertex-rigidity*, which we call *weakly minimal*. We also characterize a class of 2-vertex-globally-rigid graphs called *strongly minimal 2-vertex-global-rigidity*.

The self repair approach is described in Section 6.2, where we review the closing ranks problem and discuss previous solutions. We then present our new decentralized solutions, recovers rigidity or global rigidity in the information architecture. In Section 6.3, we discuss implementation and illustrates our results with algorithms and examples. Section 6.4 describes the robustness

¹We use the term *2-vertex-rigidity*, rather than *1-vertex-rigidity* because these definitions are analogous to the standard definitions for graph connectivity.

approach for rigid graphs. We review the work of Servatius [67] and Yu and Anderson [82] on redundant rigidity concepts and develop *weakly minimal 2-vertex-rigidity*. Section 6.5 describes the robustness approach for globally rigid graphs. We characterize a class of redundantly globally rigid graphs called *strongly minimal 2-vertex-global-rigidity*. Finally, Section 6.6 provides concluding remarks.

6.2 The Self-Repair Approach

This section describes the “self-repair” approach for addressing agent loss. We describe the *closing ranks problem* and show that while previous results permit local repair of the information architecture involving only neighbours of the lost agent, the repair cannot always be implemented using only local information. We then introduce new results that can be implemented in a decentralized way, using only local information. The new results permit decentralized recovery of both rigidity and global rigidity for formations and sensor networks in two dimensions.

6.2.1 The Closing Ranks Problem

The *closing ranks problem* is the problem of determining new sensing/communication links in the event of an agent loss to recover rigidity or global rigidity [20]. Consider a rigid (globally rigid) graph $G(V, E)$ which is the underlying graph of a formation in real d -dimensional space. Let v_i denote a vertex in V , and let E_i denote the set of edges incident to v_i . Now

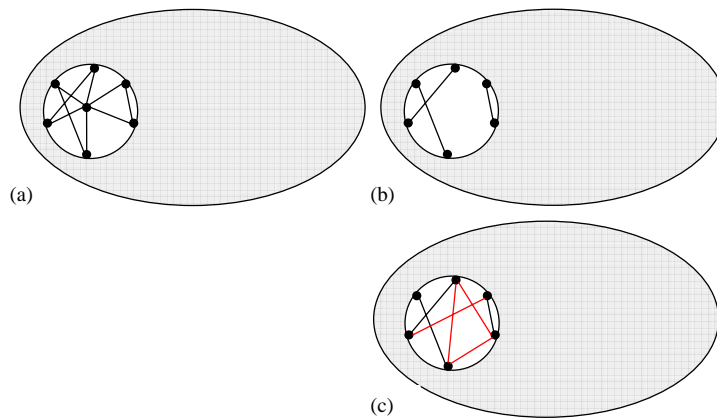


Figure 6.1: Illustration of Closing Ranks: (a) original rigid formation (b) a vertex and incident edges are removed (c) the minimum number of new edges are added to regain rigidity. It is sufficient to add edges to neighbours of the lost vertex.

suppose that v_i and E_i are removed from G and denote the resulting graph $G^*(V^*, E^*)$, where $V^* = V \setminus v_i$ and $E^* = E \setminus E_i$. The closing ranks problem is to determine the new edges E_{new} to add to G^* such that the resulting graph $G'(V^*, E^* \cup E_{new})$ is rigid (globally rigid). We call a solution a *rigid cover* (*globally rigid cover*). A *minimal cover* is one where $|E_{new}|$ is minimum. A minimal cover for a closing ranks problem is illustrated in Figure 6.1.

We desire the cover to be decentralized, which encompasses two properties: (1) local repair involving only neighbours of the lost agent, and (2) designing the repair, i.e. determining which agent pairs acquire an edge between them, using only local information. Local repair is provided by the following result from [73]:

Theorem 6.2.1. *Let G be a minimally rigid graph with a vertex v_i of degree*

k. Then there exists at least one set of $k - 2$ edges among the neighbours of v_i such that a minimally rigid graph is obtained by removing v_i and its incident edges and adding the set of $k - 2$ edges.

Thus, it is sufficient to add edges only between neighbours of the lost agent to recover rigidity. However, the difficulty in applying this theorem is to select the $k - 2$ edges. If though we drop the requirement for minimality, one straightforward solution to the closing ranks problem is a *complete cover*: simply add every possible edge between neighbours of the lost vertex. Thus, if a vertex of degree k is lost, then $k(k - 1)$ edges are added ($O(k^2)$). This may be significantly more than the necessary $k - 2$ edges for vertices of large degree.

It turns out that the minimal cover cannot always be implemented using only local information. The systematic method presented in [20] to determine a minimal cover may involve decomposing the entire graph, which uses an inherently global perspective. Indeed, when adding only the minimal number of required edges, one must ensure that each added edge is independent. To identify whether a proposed new edge will be independent or not, one must check whether or not there is a minimally rigid subgraph containing the two vertices on which the proposed new edge will be incident. A simple observation shows that generally such a minimally rigid subgraph may be arbitrarily large, and thus looking for it is not a procedure that involves just local operations; given a minimally rigid subgraph on three or more vertices, the edge splitting operation may always be used to increase indefinitely the size of the minimally

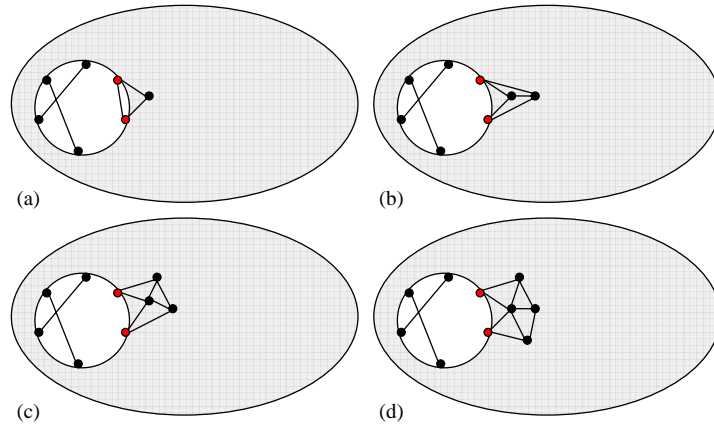


Figure 6.2: Edge splitting creates edge dependency between the highlighted vertices. Repeatedly applying edge splitting increases the size of the dependent subgraph.

rigid subgraph. This is illustrated in Figure 6.2. Further, when checking for edge independence, there is no way to know a priori which subgraph to check, and consequently, one may end up checking the entire graph.

For large formations, it is crucial to be able to implement a closing ranks solution in a decentralized way. There is an inherent conflict between the desire to add a minimum number of new edges and the constraint of using only local information. Thus, we will seek a decentralized cover that is sub-optimal in the sense that we may have to add more than the minimum number of required new edges.

6.2.2 Decentralized Rigidity Recovery

We have seen from Theorem 6.2.1 that there exists a rigid cover among neighbours of the lost vertex. We now present a substitution principle for rigid graphs, originally introduced in [78].

Theorem 6.2.2 ([78]). *Given a rigid graph $G(V, E)$ in d -dimensional space, if for any vertex subset V' the induced subgraph $G'(V', E')$ is replaced with a minimally rigid graph $\bar{G}(V', \bar{E})$ on those vertices (V'), then the modified graph $\tilde{G}(V, \tilde{E})$ where $\tilde{E} = (E \setminus E') \cup \bar{E}$ is also a rigid graph in d -dimensional space.*

Here, G corresponds to a graph that has lost a vertex and has been repaired via the method from [20], and V' corresponds to the former neighbours of the lost vertex. Theorem 6.2.2 shows that implementing a minimally rigid subgraph, which we refer to as a *minimally rigid patch* (\bar{G} in the theorem), on the former neighbours of a lost vertex will recover rigidity. It is not necessary to first make the repair via the method from [20]; one can immediately implement the minimally rigid patch. The requirement of a minimally rigid patch is only to reduce the number of new edges added; the theorem is equally valid with a rigid patch. Effectively, every minimally rigid patch contains at least one cover which recovers rigidity. Note that the theorem is valid in any dimension. The following proposition provides a way to implement such a patch in 2 dimensions.

Proposition 6.2.3. *In 2 dimensions, the following “Double Patch” implemented on the neighbours of a lost vertex is a rigid cover for the closing ranks*

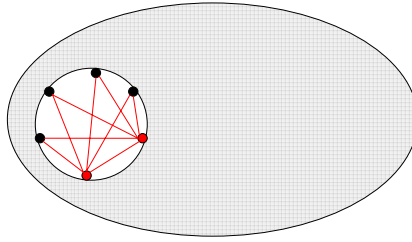


Figure 6.3: Illustration of the Double Patch: The two highlighted vertices serve as coordinators to which every other vertex is connected.

problem.

- **Double Patch:** Choose two vertices among the neighbours of the lost vertex to serve as “coordinators” and connect them with an edge. Then add edges between every other neighbour and the coordinators.

The Double Patch is illustrated in Figure 6.3. This process creates a particular minimally rigid graph on the neighbours of the lost vertex. We are stacking together triangles with a common base edge, which is a rigid structure. Equivalently, we start with a complete graph on the coordinators, and the remaining vertices are added via the vertex addition operation, which is a rigid structure. The choice of the two coordinators is arbitrary and the structure does not depend on the rest of the graph. Thus, the patch can be created using only local information.

When a vertex of degree k is lost, we are adding $2k - 3$ edges using the minimally rigid patch. Although we add more edges than with the minimal

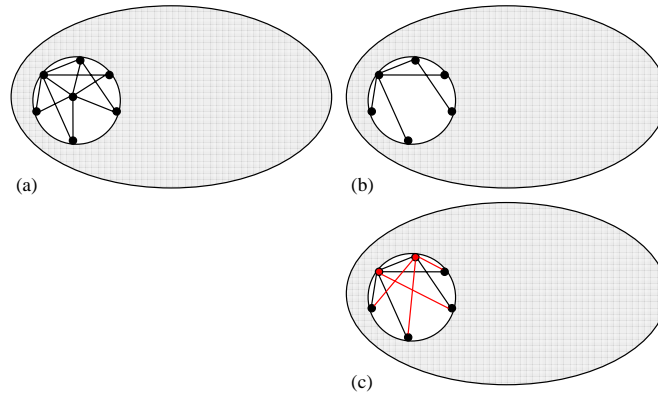


Figure 6.4: Utilizing existing cover edges with the Double Patch: (a) the lost vertex has degree 6, (b) edges exist among neighbours of the lost vertex, (c) coordinators for the Double Patch are chosen to utilize these existing edges, and 4 *new* edges are added - a minimal cover.

cover (where $k - 2$ edges are added), the number of added edges is still linear in the lost vertex degree, as opposed to quadratic for a complete cover.

By appropriate choice of coordinators, one could utilize existing edges among neighbours of the lost vertex, which we call *existing cover edges*, to minimize the number of *new* added edges. Simple counting arguments can be used to show that there could be up to $k - 1$ existing cover edges. In fact, there are certain scenarios in which one adds $2k - 3 - (k - 1) = k - 2$ new edges, utilizing the existing cover edges to obtain a minimal cover. This scenario is illustrated in Figure 6.4.

Remark. One might ask whether a “single patch” is sufficient to recover rigidity. That is, could one choose only one vertex among neighbours of the lost vertex as a coordinator? In this case, we add $k - 1$ edges - i.e. potentially only

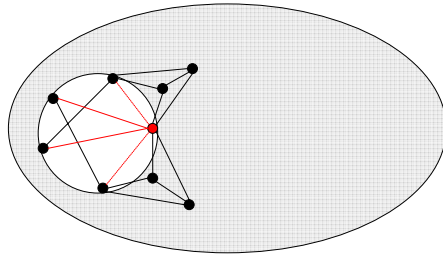


Figure 6.5: Single Patch Counterexample. The two dependent edges cause the single patch to fail.

one more edge than for a minimal cover. Simulations support the conjecture that there always exists at least one vertex among neighbours of the lost vertex on which a single patch works. In fact, one can show that in 2 dimensions there are two such vertices. However, we are again faced with the task of choosing the appropriate vertex; once again, local information will not suffice to effect the choice.

The counterexample in Figure 6.5 shows a case where a vertex with no existing cover edges fails using a single patch even though $k - 1$ new edges are added. Ultimately, the single patch repair approach fails to be decentralized for the same reason as the minimal cover - one must resort to possibly non-local checking of each new edge for dependency in order to choose the appropriate vertex.

6.2.3 Decentralized Global Rigidity Recovery

The ideas discussed above for recovering rigidity can also be applied to recovering global rigidity. The following theorem extends the substitution principle to globally rigid graphs.

Theorem 6.2.4. *Given a globally rigid graph $G(V, E)$ in d -dimensional space, if any subgraph $G'(V', E')$ is replaced with a globally rigid graph on those vertices (V'), then the modified graph is also a globally rigid graph in d -dimensional space.*

*Proof.*² Assume formation $F(G, p)$ is globally rigid, and $G'(p)$ is created by the substitution of a globally rigid formation $F'(p)$ for a sub-formation $F(p)$ in $G(p)$. By Theorem 6.2.2, $G'(p)$ is certainly rigid. If $G'(p)$ is not globally rigid, then there is a second realization, i.e. formation whose edge lengths equal those of $G'(p)$, $G'(q)$ which is not congruent. There is a pair of vertices (i, j) for which the corresponding inter-agent distance is different for $G'(p)$ and $G'(q)$. By assumption on F' , $F'(p)$ must be congruent to $F'(q)$. So i, j cannot both be in F' (or F). If we now replace $F'(q)$ with $F(q)$ (which will also be congruent to $F(p)$) then we will have $G(p)$ and $G(q)$ with all edge lengths the same, but not congruent. This contradicts the original assumption that $G(p)$ was globally rigid. \square

Theorem 6.2.4 shows that placing a globally rigid subgraph, which we refer to as a *globally rigid patch*, on neighbours of the lost vertex will recover

²Thanks to Professor Walter Whiteley for his help in contributing this proof.

global rigidity. Again, the theorem is valid in any dimension. Proposition 2 provides a way to implement such a patch in 2 dimensions.

Proposition 6.2.5. *In 2 dimensions, the following “Wheel Patch” implemented on the neighbours of a lost agent is a globally rigid cover for the closing ranks problem.*

- **Wheel Patch:** Choose one vertex among the neighbours of the lost agent to serve as “coordinator” and connect it with every other neighbour of the lost agent. Then create a cycle among the neighbours that excluding the coordinator.

The Wheel Patch is illustrated in Figure 6.6. This process creates a *wheel graph* on the neighbours of the lost agent, which is a particular minimally globally rigid graph. A *wheel graph* on n vertices is a graph that contains a single vertex (the “hub”) connected to all vertices of an $(n - 1)$ -cycle. The choice of hub or coordinator is arbitrary and the structure does not depend on the rest of the graph. Thus, the patch can be created using only local information. Again, the coordinator can be chosen to minimize the number of new edges added.

6.3 Implementation

This section describes implementation of our decentralized closing ranks solutions and illustrate with examples. An explicit discussion of underlying

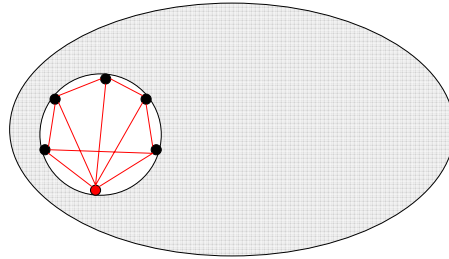


Figure 6.6: Illustration of the Wheel Patch: the highlighted vertex serves as the coordinator and connects to every other vertex in the cycle.

assumptions is worthwhile. First, we assume that neighbours of a lost agent recognize the loss immediately. That is, we are not dealing with the separate problem of determining whether agent loss has occurred. Agent loss could occur when an agent has been deployed for another task, or in the event of agent failure. There are in principle many different ways in which an agent could fail, from complete loss of an entire agent (e.g. a UAV crashes) to failure of a single sensor, actuator, or communication link. Of course, recognizing various failure modes is an important consideration for actual implementation, but here we use a “vaporize” agent failure model (that is, regard any failure as complete loss of agent) and assume neighbour agents immediately recognize the loss. Second, we assume that each agent has a unique ID. This is necessary so that the agents can distinguish amongst one another when determining which new links to add.

Each agent stores the following local information: a list of links for all neighbours and 2-hop neighbours. This information is local in the sense

that it is independent of the size of the formation or sensor network. Since all neighbours of a lost agent will be at most 2-hop neighbours of one another, they each can search the aforementioned list of links to form the subgraph involving all neighbours of the lost agent and existing cover edges. From this subgraph, each neighbour of the lost agent can choose coordinators and determine the new links to add in order to implement one of the patches discussed previously. This can be done in two ways: (1) choose coordinator(s) based on agent ID (e.g. agents with lowest two IDs are coordinators for the double patch), or (2) choose coordinator(s) to minimize number of links added. For the wheel patch, the cycle can also be created using agent ID. Then, the agents establish the appropriate links to recover rigidity or global rigidity. The process is captured in the following algorithms (using agent ID to choose coordinators and cycle order) and illustrated in Figures 6.7 and 6.8.

Remark. Establishing an link between two agents effectively requires the ability of each agent to *sense* IDs. Existence of a link between two agents means that the agents actively maintain the Euclidean distance constant via control of agent motion. As noted before, this requires sensing relative position. Any given agent will have multiple links to maintain and may also have other non-neighbour agents within its sensing range. For each particular link, each agent must be able to distinguish ID through sensing amongst other agents in its sensing range in order to adjust its distance to the appropriate agent.

```

if agent fails then
  for neighbours of lost agent do
    n = get(lost agent neighbours);
    coordinator1 = minID(n);
    coordinator2 = secondMinID(n);
    if I am a coordinator then
      establish links w/ all n;
    else
      establish links w/ coordinators;
    end
  end
end

```

Algorithm 1: Double Patch

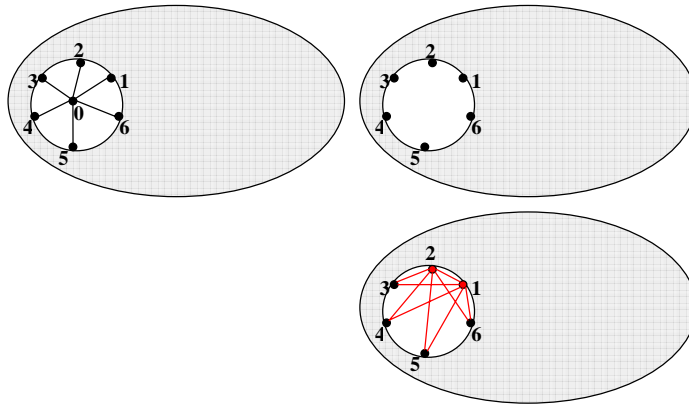


Figure 6.7: Double Patch: (a) rigid formation with agent IDs, (b) agent 0 fails, neighbours recognize the loss, (c) coordinators 1 and 2 are chosen via minimum agent ID and links established.

6.4 Redundant Information Architectures

This section describes the robustness approach to addressing agent loss. In particular, we investigate the structure of graphs in the plane with the property that rigidity is preserved when any single vertex and its incident

```

if agent fails then
  for neighbours of lost agent do
    n = get(lost agent neighbours);
    coordinator = minID(n);
    cycle = orderID(n\coordinator);
    m = getCycleNeighbours(cycle);
    if I am coordinator then
      establish links w/ all n;
    else
      establish links w/ coordinator & m;
    end
  end
end
end

```

Algorithm 2: Wheel Patch

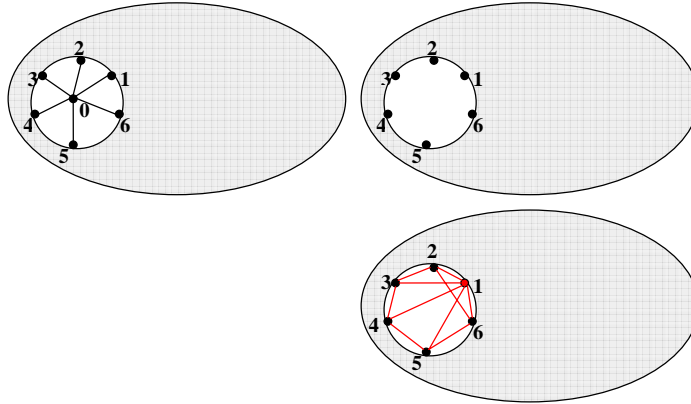


Figure 6.8: Wheel Patch: (a) globally rigid formation with agent IDs, (b) agent 0 fails, neighbours recognize the loss, (c) coordinator 1 is chosen via minimum agent ID, cycle formed via agent ID ordering, and links established.

edges are removed. Information architectures with this structure would allow vehicle formations to maintain formation shape even in the event of agent loss. We review general redundant rigidity definitions and concepts, and overview characterization of a particular class of *2-vertex-rigidity*, which we call *strongly minimal*, given by Servatius in [67]. We then present new developments of a

particular class of *2-vertex-rigidity*, which we call *weakly minimal*, making significant strides toward a complete characterization.

6.4.1 Redundant Rigidity Concepts

In [67], Servatius introduced the notions of *edge birigidity* and *vertex birigidity* of a graph. A graph is called *edge birigid* if it remains rigid after removing any edge. As discussed previously, this property is used to characterize global rigidity (it is simply called *redundant rigidity* in that context). A graph is called *vertex birigid* if the graph remains rigid after removing any vertex and its incident edges.

In [82], Yu and Anderson introduced the generalized terms *k-edge-rigidity* and *k-vertex-rigidity*. A graph is called *k-edge-rigid* if it remains rigid after removing any $k - 1$ edge(s). Similarly, a graph is called *k-vertex-rigid* if it remains rigid after removing any $k - 1$ vertices. (For consistency of the results, it is convenient to define any graph with fewer than 3 vertices in two dimensions as nonrigid.) This notation is analogous to the standard notation for connectivity: a graph is *k-edge-connected* (*k-vertex-connected*) if it remains connected after removing any $k - 1$ edges (vertices). Conventionally, the simplified term *k-connectivity* is used to refer to *k-vertex-connectivity*. In [82], Yu and Anderson characterize the relationship between *k-edge-rigidity* and *k-vertex-rigidity*, confirming the natural intuition that vertex-rigidity is a more demanding concept than edge-rigidity. They also explore redundant rigidity properties for special types of graphs, including the complete graph,

the wheel graph, and powers of a graph. We shall use the terminology of [82] and restrict our attention in this chapter to *2-vertex-rigidity*.

Remark. A graph is more vulnerable to loss of a vertex with large degree than a vertex with smaller degree because more edges are removed. For example, consider the wheel graph on n vertices, which consists of a single vertex (the “hub”) connected to every vertex in a $(n-1)$ -cycle. If any vertex in the cycle is removed, the graph remains rigid. However, if the hub is removed, the resulting graph is not rigid, and one must add $n-3$ new edges to recover rigidity. The hub is in a sense more important than the other vertices since the health of the formation is more vulnerable to its failure than to failure of any other vertex.

In [82], Yu and Anderson differentiate between *deterministic* and *statistical* metrics of redundant rigidity. For example, one might regard a wheel graph as nearly 2-vertex-rigid in a *statistical* sense. Loss of rigidity occurs when just one particular vertex (out of n) is removed. In an application where the concern is random failure, such as enemy attack on a random agent of a military UAV formation, we could say that the formation is statistically $\frac{n-1}{n}$ 2-vertex-rigid. However, in this chapter we focus on deterministic 2-vertex-rigidity.

6.4.2 Strongly Minimal 2-Vertex-Rigidity

It is natural to seek a characterization of *minimal 2-vertex rigidity* analogous to the way that a graph being rigid implies existence of a minimally rigid

subgraph. However, as we will show in the following, the concept of minimality in 2-vertex-rigid graphs gives rise to a subtlety that contrasts with minimality in rigid graphs. Given a rigid graph $G(V, E)$, minimality is characterized equivalently by either of the following statements: (1) G has the minimum possible number of edges ($|E| = 2|V| - 3$), and (2) removing any edge destroys rigidity. For 2-vertex-rigid graphs, an attempt to generalize these statements gives rise to two distinct types minimally 2-vertex-rigid graphs, which we call *strongly minimal* and *weakly minimal*:

- A 2-vertex-rigid graph is called *strongly minimal* if it has the minimum possible number of edges on a given number of vertices.
- A 2-vertex-rigid graph is called *weakly minimal* if it has more than the minimum possible number of edges on a given number of vertices, but has the property that removing any edge destroys 2-vertex-rigidity.

In [67], Servatius provides a characterization of strongly minimal 2-vertex-rigidity and gives an example that shows existence of a weakly minimal 2-vertex-rigid graph, which we now review.

We begin with the following result, which gives a lower bound on the number of edges in a 2-vertex-rigid graph in terms of the number of vertices.

Lemma 6.4.1. *If $G(V, E)$ is a 2-vertex-rigid graph on 5 or more vertices, then $|E| \geq 2|V| - 1$.*

Proof. Suppose $G(V, E)$ is a 2-vertex-rigid graph on 5 or more vertices with $|E| = 2|V| - 2$. The average degree in a graph on $|V|$ vertices with $|E| = 2|V| - 2$ is $4 - 4/|V|$. Thus, such a graph on 5 or more vertices has a vertex of degree at least 4. Removing such a vertex results in a graph $G'(V', E')$ where $|E'| = 2|V'| - 4$. Thus, G' cannot be rigid, which contradicts our original assumption that G was 2-vertex-rigid. \square

Servatius uses the concept of *excess* to distinguish between our terms strongly and weakly minimal. The *excess* of a rigid graph $G(V, E)$ in 2 dimensions is defined as $|E| - (2|V| - 3)$. A minimally rigid graph has excess zero (i.e. $|E| = 2|V| - 3$). A minimally globally rigid graph has excess one (i.e. $|E| = 2|V| - 2$). On 4 or fewer vertices, it is impossible to have $|E| \geq 2|V| - 1$, and a graph must be complete to be 2-vertex-rigid. A strongly minimal graph (on 5 or more vertices) has excess two while a weakly minimal graph has excess more than two.

The following two results from [67] give a complete characterization of the structure of strongly minimal 2-vertex-rigid graphs.

Theorem 6.4.2. *Let $G(V, E)$ be a strongly minimal 2-vertex-rigid graph on 5 or more vertices. Then G has exactly two vertices with degree 3 and the remaining have degree 4, which implies $|E| = 2|V| - 1$.*

Theorem 6.4.3. *A graph $G(V, E)$ is strongly minimal 2-vertex-rigid if and only if G has exactly two vertices of degree 3 and there is a partition of the edge set E*

$$E = E_1 \cup E_2 \cup \cdots \cup E_k$$

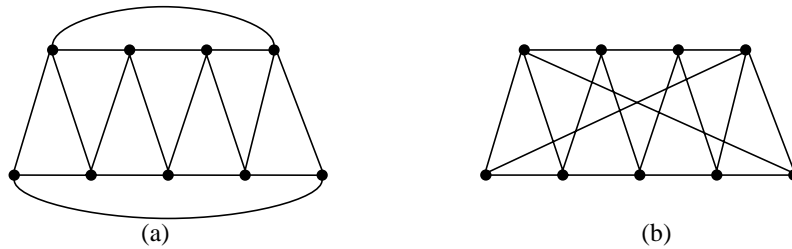


Figure 6.9: Examples of the two possible partitions of the edge set for strongly minimal 2-vertex-rigid graphs: (a) the degree three vertices are adjacent, and (b) the degree three vertices are non-adjacent.

such that the graph induced by $E \setminus E_i$ is minimally redundantly rigid for all i , and either

- E_1 and E_2 are the edges incident to the two non-adjacent vertices of degree 3, respectively, and E_i is a single edge for $3 \leq i \leq k$
- E_1 is the union of the edges incident to the two adjacent vertices of degree 3, and E_i is a single edge for $2 \leq i \leq k$.

This can be thought of as a Laman-type characterization, analogous to minimal rigidity: there must be a minimum number of edges ($|E| = 2|V| - 1$), and the edges must be properly distributed, as described in the theorem conditions. The two possible partitions of the edge set correspond to whether or not the two degree 3 vertices are adjacent.

Figure 6.9, originally from [67], shows examples of strongly minimal 2-vertex-rigid graphs with each type of partition. Note that triangles could be

“stacked” together in such a fashion to produce arbitrarily large 2-vertex-rigid graphs of excess two.

In fact, Servatius also provides a way to “grow” all strongly minimal 2-vertex-rigid graphs using an operation similar to the edge splitting operation discussed previously. This operation gives an increase of $|V|$ by 1 and an increase of $|E|$ by 2, and thus preserves the constraint $|E| = 2|V| - 1$. Thus, we have a complete characterization and a way to obtain all strongly minimal 2-vertex-rigid graphs.

6.4.3 Weakly Minimal 2-Vertex-Rigidity

Can one simply add edges to a strongly minimal 2-vertex-rigid graph to obtain every (non-minimal) 2-vertex-rigid graph (as can be done for rigid graphs)? The answer to this question is no. The example in Figure 6.10, originally shown in [67], shows existence of a weakly minimal 2-vertex-rigid graph, which contains more than the minimum possible number of edges yet has the property that removing any edge destroys 2-vertex-rigidity.

Proposition 6.4.4. *The graph $G(V, E)$ in Figure 6.10 is weakly minimal 2-vertex-rigid.*

Proof. Every vertex has degree 4; thus, $|E| = 2|V|$, which is excess three. Observe that the subgraphs induced by the left and right nine vertices (call them G_L and G_R) both have excess one. Removing any vertex in G results in a graph of excess one that has exactly one subgraph of excess one, which is rigid. Thus, the graph is 2-vertex-rigid. \square

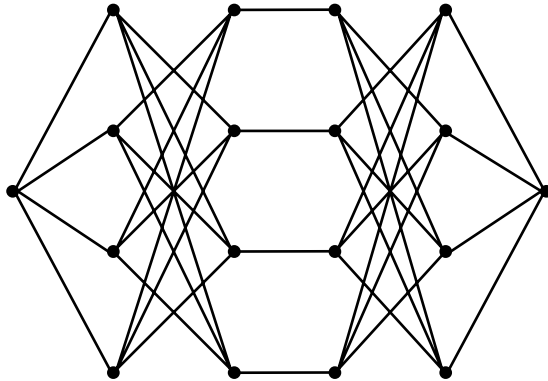


Figure 6.10: Example of a weakly minimal 2-vertex-rigid graph. The graph has an excess of three, but removing any edge destroys 2-vertex-rigidity. Thus, this graph cannot be obtained by adding an edge to a graph described by Theorem 6.4.3.

Now remove any edge outside of G_L ; call the new graph G' . Then remove any degree 4 vertex in $G' \setminus G_L$. The resulting graph, call it G'' , has an excess of zero with a subgraph of excess one (viz G_L), and so G'' is not rigid by Laman's theorem. Therefore, G' is not 2-vertex-rigid. Obviously, the same argument applies if we remove any edge outside of G_R . Hence, removing any edge in G destroys 2-vertex-rigidity, and thus G is weakly minimal 2-vertex-rigid.

This example points to a particular class of weakly minimal 2-vertex-rigid graphs that generally consist of two redundantly rigid subgraphs connected by four edges. The smallest such graph, presented here for the first time in Figure 6.11, consists of two complete graphs on four vertices con-

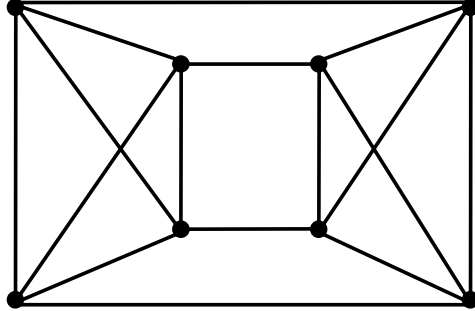


Figure 6.11: Smallest example of a weakly minimal 2-vertex-rigid graph in the class defined by the Servatius example.

nected by four edges. Further, we can use what is called the *X-replacement* operation, which is shown to preserve rigidity and redundant rigidity in [9], to “grow” arbitrarily large weakly minimal 2-vertex-rigid graphs. The operation is illustrated in Figure 6.12 and described below.

Definition 6.4.1. Given two non-adjacent edges ux and wy in a graph $G(V, E)$, an *X-replacement* adds a degree 4 vertex z to construct the graph $G'(V', E')$, where $V' = V \cup \{z\}$ and $E' = E \setminus \{ux, wy\} \cup \{uz, wz, xz, yz\}$.

Since the *X-replacement* preserves redundant rigidity, it can be applied successively to each redundantly rigid subgraph in Figure 6.11 (that is, each complete subgraph on four vertices) to create a class of weakly minimal 2-vertex-rigid graphs with excess three, which includes the Servatius example in Figure 6.10. Indeed, one can easily verify that the graph in Figure 6.11 can be obtained by repeatedly applying the reverse *X-replacement* operation on the

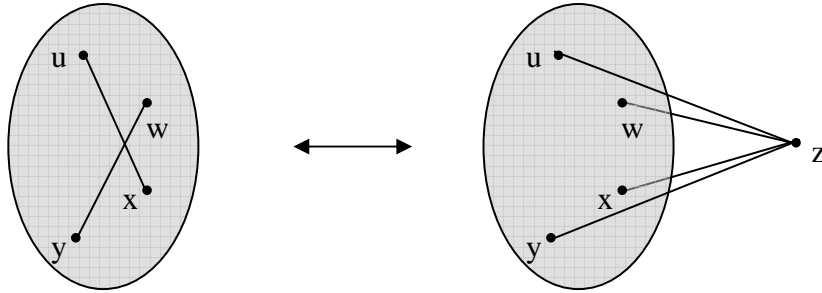


Figure 6.12: Representation of the X -replacement operation.

left and right subgraphs in Figure 6.10.

In [67], Servatius poses an open question regarding existence of other weakly minimal 2-vertex-rigid graphs with larger excess. We have discovered such a new class that can have arbitrarily large excess. The graph shown in Figure 6.13(a) illustrates an example with excess three, and the graph shown in Figure 6.13(b) illustrates an example with excess four obtained by applying what we call a *degree 3 vertex addition*. Let i, j , and k be three distinct vertices in a graph $G(V, E)$. A *degree 3 vertex addition* operation adds a vertex l and edges il, jl , and kl . This operation preserves weakly minimal 2-vertex-rigidity under certain conditions given in [67] and also increases the excess by one. By successively applying the operation as shown, one can obtain weakly minimal 2-vertex-rigid graphs with arbitrarily large excess.

Proposition 6.4.5. *The class of graphs illustrated in Figure 6.13 is weakly minimal 2-vertex-rigid.*

Proof. Let $G(V, E)$ be the graph in Figure 6.13(a). One can easily

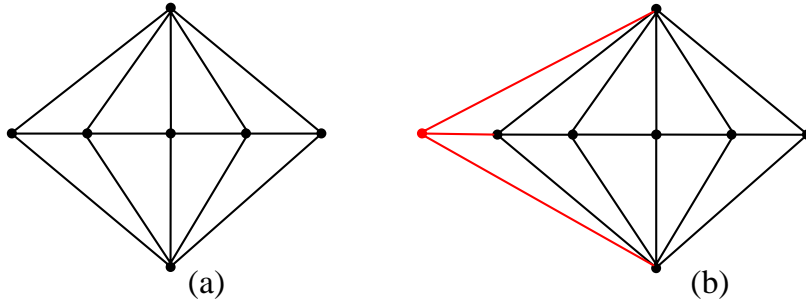


Figure 6.13: A new class of weakly minimal 2-vertex-rigidity: (a) a weakly minimal 2-vertex-rigid graph with excess three, (b) adding a degree 3 vertex to create a weakly minimal 2-vertex-rigid graph with excess four. By successively adding a degree 3 vertex to either end, one can obtain weakly minimal 2-vertex-rigid graphs with arbitrarily large excess.

verify that $|E| = 2|V|$ (excess three) and that removing any vertex from G results in a rigid graph; thus, G is 2-vertex-rigid. Now, remove any edge not incident to the top vertex, then remove the top vertex, resulting in a graph $G'(V', E')$. We have $|E'| = 2|V'| - 4$, which implies that G' is not rigid. The same argument holds when removing any edge not incident to the bottom vertex, then removing the bottom vertex. Thus, removing any edge in G destroys 2-vertex-rigidity, and therefore G is weakly minimal 2-vertex-rigid. The same analysis holds for the graph in Figure 6.13(b) and all other graphs in this class. \square

Clearly, the existence of weakly minimal 2-vertex-rigid graphs make a complete characterization of 2-vertex-rigidity rather subtle and difficult. We conclude this section with a conjecture that the *X-replacement* and *degree 3 vertex addition* operations are sufficient to “grow” *all* weakly minimal 2-

vertex-rigid graphs. We have already observed that these operations preserve weakly minimal 2-vertex-rigidity under certain conditions. For a complete characterization, we need to show that the reverse operations can always be applied to a weakly minimal 2-vertex-rigid graph.

Conjecture 1. *Let $G(V, E)$ be a weakly minimal 2-vertex-rigid graph with at least 9 vertices. Then there exists either (a) a degree 4 vertex on which a reverse X-replacement operation can be performed to obtain a weakly minimal 2-vertex-rigid graph, or (b) there exists a degree three vertex on which a reverse degree 3 vertex addition can be performed to obtain a weakly minimal 2-vertex-rigid graph.*

6.5 Strongly Minimal 2-Vertex-Global-Rigidity

In this section, we investigate the structure of graphs with the property that global rigidity is preserved when any single vertex and its incident edges are removed. Analogously, a graph is called *2-vertex-globally-rigid* if it remains globally rigid after removing any single vertex. Information architectures with this structure would allow self-localization in sensor networks to be performed even in the event of loss of any one. We provide a complete characterization of *strongly minimal 2-vertex-global-rigidity*.

We begin with the following result, which gives a lower bound on the number of edges necessary for 2-vertex-globally-rigidity.

Lemma 6.5.1. *If $G(V, E)$ is a 2-vertex-globally-rigid graph on 5 or more*

vertices, then $|E| \geq 2|V|$ (excess three or more).

Proof. Suppose $G(V, E)$ is a 2-vertex-globally-rigid graph on 5 or more vertices with $|E| = 2|V| - 1$. The average degree in a graph on $|V|$ vertices with $|E| = 2|V| - 1$ is $4 - 2/|V|$. Thus, such a graph on 5 or more vertices has a vertex of degree at least 4. Removing such a vertex results in a graph $G'(V', E')$ with $|E'| = 2|V'| - 3$, which cannot be redundantly rigid and therefore cannot be globally rigid. This contradicts our original assumption that G was 2-vertex-globally-rigid. \square

The following two results completely characterize the structure of strongly minimal 2-vertex-globally-rigid graphs.

Theorem 6.5.2. *Let $G(V, E)$ be a strongly minimal 2-vertex-globally-rigid on 5 or more vertices. Then we have the following:*

- $|E| = 2|V|$.
- Every vertex in G has degree 4.

Proof. For the first condition, removing an edge results in a graph of excess two, which is not 2-vertex-globally-rigid by Lemma 6.5.1. Further, Figure 6.14 shows a 2-vertex-globally rigid graph where $|E| = 2|V|$. For the second condition, since G is globally rigid, it contains no vertex of degree less than 3. Suppose v is a vertex of degree 3. Remove a neighbour of v . In the resulting graph, v has degree 2 and this graph is not globally rigid. Thus, there cannot be a vertex of degree 3.

Since $|E| = 2|V|$, then the average vertex degree is 4. Since there cannot be a vertex of degree 3 or fewer, then there cannot be any vertices of degree 5 or more. Thus, all vertices must have degree 4, which completes the proof. \square

Theorem 6.5.3. *A graph $G(V, E)$ is strongly minimal 2-vertex-globally-rigid if and only if the following conditions hold*

- $|E| = 2|V|$
- G is 4-connected
- G is redundantly strongly minimal 2-vertex-rigid (i.e. removing any edge results in a strongly minimal 2-vertex-rigid graph).

Proof. For sufficiency, suppose the conditions hold for a graph G . Note first that since G is 4-connected, a graph obtained by removing a vertex and its incident edges is 3-connected. Further, 4-connectivity implies that every vertex has degree at least 4, (see e.g. [29]), and since $|E| = 2|V|$ then every vertex has precisely degree 4. Now choose any vertex v in G and remove any edge incident to this vertex. The resulting graph is 2-vertex-rigid by the third condition. Remove another edge incident to v . Via the edge partition in Theorem 6.4.3, the resulting graph consists of v with degree 2 attached to a redundantly rigid graph. Now we can remove v and the resulting graph is redundantly rigid. By the second condition, it is also 3-vertex-connected and

therefore is globally rigid. The argument holds for any vertex v in G , which proves that G is 2-vertex-globally-rigid, and thus the conditions are sufficient.

The 4-connectivity of G is obviously necessary because G minus any vertex must be 3-connected. Further, $|E| = 2|V|$ is necessary because if $|E| < 2|V|$ then there is a vertex with degree 3, which implies that G is not 4-connected. Now we need to prove the necessity of the final condition. To obtain a contradiction, suppose G is a 2-vertex-globally-rigid graph with an edge e that when removed does not result in a 2-vertex-rigid graph. Remove such an edge e and call the resulting graph G' . This implies that there exists a vertex v in G' that when removed results in a non-rigid graph G'' . There are two cases: First, if e is incident to v , then effectively we have removed v from G to obtain a non-rigid graph G'' . Thus, G is not 2-vertex-globally-rigid, contradicting our assumption. Second, if e is not incident to v , then if G is 2-vertex-globally-rigid, we should be able to reinsert e into G'' to obtain a globally rigid graph. However, it is impossible to add a single edge to a non-rigid graph to make it redundantly rigid. This again contradicts our assumption, which proves the necessity of the final condition and completes the proof. \square

Theorem 6.5.3 is clearly analogous to the characterization of global rigidity given by Theorem 2.3.1. An example of a 2-vertex-globally-rigid graph is given in Figure 6.14. This example is a C^2 graph, which can be obtained starting with a cycle on n vertices and connecting 2-hop neighbours. One could also obtain a different 2-vertex-globally-rigid graph by starting with a cycle on n vertices and connecting 3-hop neighbours. The smallest strongly

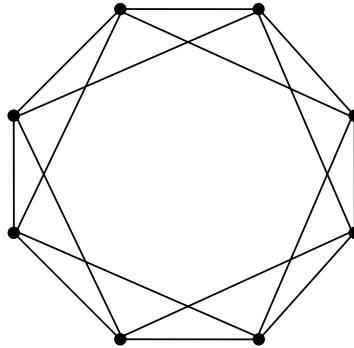


Figure 6.14: Example of a strongly minimal 2-vertex-globally-rigid graph described in Theorem 6.5.3.

minimal 2-vertex-globally-rigid graph is the complete graph on 5 vertices.

Operations to “grow” all strongly minimal 2-vertex-globally-rigid graphs and existence of weakly minimal 2-vertex-globally-rigid graphs remain open questions. In addition, note that generalizing Theorem 6.5.3 will require a complete characterization of 2-vertex-rigidity, again emphasizing the importance of resolving the difficulties discussed in the previous section.

6.6 Concluding Remarks

This chapter has addressed the problem of agent loss via two separate approaches. The first is to perform a “self-repair” operation in the event of agent loss to recover rigidity or global rigidity. The second is to build robustness into the information architecture *a priori* such that agent loss does not destroy rigidity or global rigidity.

The self-repair approach utilized in this chapter to address the problem of agent loss has allowed a decentralized solution of the closing ranks problem. This self-repair involves only neighbors of the lost agent and requires only local information that is independent of formation size. The results can be implemented to recover rigidity and global rigidity. This chapter has also approached the problem of agent loss by building robustness into the information architecture. This progressed the theory of *2-vertex-rigid* and *2-vertex-global-rigid* graphs. Information architectures with these properties would allow formation shape control or self-localization tasks to be performed even in the event of the loss of any single agent. We developed *weakly minimal 2-vertex-rigidity* and characterized *strongly minimal 2-vertex-global-rigidity*. The existence of weakly minimal 2-vertex-rigid graphs makes a complete characterization of 2-vertex-rigidity subtle and difficult, in comparison to rigidity. The existence of weakly minimal 2-vertex-global-rigidity remains an open question.

This dissertation has addressed rigidity-based formation shape control problems and the design of robust information architectures to recover or preserve rigidity or global rigidity in the event of agent loss. In formation shape control problems, the agents can be suitably modeled by points, neglecting the individual agent orientation, or attitude. However, the orientations of the agents in a formation are also crucial to realizing certain advantages. The next chapter considers a rigid body attitude synchronization problem, in which the objective is to design torque control laws to asymptotically synchronize the attitudes of a team of rigid bodies.

Chapter 7

Rigid Body Attitude Synchronization with Communication Time Delays

7.1 Introduction

A fundamental problem for autonomous vehicle formations, in addition to ensuring the precise control of formation shape, is ensuring the precise control of formation *orientation*, or *attitude*. This chapter addresses the problem of formation attitude synchronization by engaging with two discrete areas in the literature: synchronization/consensus problems, and the rigid body attitude synchronization problem.

The rigid body attitude synchronization problem is to design torque control laws to asymptotically synchronize the attitude of a team or rigid bodies. The agents communicate attitude information with one another, and this communication architecture is modeled as a graph. In synchronization/consensus problems, *spectral graph theory*, rather than rigid graph theory, yields the properties that relate to the stability of the synchronized configuration.

The synchronization/consensus problems addressed in this chapter have double integrator agent dynamics and time delays. Double integrators are appropriate for mechanical systems, which are generally controlled through

acceleration, while the effect of time delays on stability becomes an important consideration when agents communicate state information. Previous stability results in the literature are in need of generalization when there are double integrator dynamics and time delays. Recent progress has been made in [51, 68, 85]. In [85], necessary and sufficient stability conditions are given for a directed communication architecture with homogeneous¹ delay, but the study assumes that there is a self-delay on each agent’s own state feedback signal. However, this assumption is restrictive when the value of the time delay is unknown. In [68], sufficient stability conditions are given for directed architectures with homogeneous delay and without self-delay, but the results depend on the restrictive assumption that the degree matrix is a scalar multiple of the identity matrix. In [51], sufficient stability conditions are given for heterogeneous delays, but the results are only given for undirected architectures. Two other studies consider higher-order agent dynamics [44, 52], in which double integrators are a special case, but these results do not readily provide explicit conditions on the control gains that guarantee stability. Moreover, the result in [44] provides only sufficient conditions, and the results [52] are restricted to directed graphs. Necessary and sufficient stability conditions have not yet been determined for directed architectures with homogeneous delay without self-delay. This chapter addresses this gap and develops these conditions by obtaining a new synchronization result. We then apply this result to the rigid body attitude synchronization problem.

¹The term homogeneous means that all time delays are assumed to have the same value.

In the rigid body attitude synchronization problem, communication time delays have not yet been considered. This chapter applies the synchronization result described above to the rigid body attitude synchronization problem. Our application of the synchronization result is nontrivial because the agent dynamics are nonlinear and the presence of communication time delays. It is assumed that the communicated state feedback signals have homogeneous time delay, but that each agent's own state information is instantaneously available, i.e. there is no self-delay. This allows feedback linearization of a modified Rodrigues parameter (MRP) representation of each agent's attitude kinematics [66]. Accordingly, the control effort for each agent is split into two parts. One term linearizes the dynamics, and the second term achieves consensus using a standard consensus protocol. Global exponential convergence of the rigid body attitudes to a synchronized attitude is shown whenever the control gains and time delay satisfy a necessary and sufficient stability condition. Delay-independent results are obtained for a range of control gains. These results hold for any directed communication graph with a spanning tree, which is the most general directed communication architecture required to achieve consensus. Leader-follower and undirected architectures are special cases. Tracking of a prescribed desired leader trajectory can be achieved for leader-follower architectures provided all the follower agents have feedforward information of the leader's desired trajectory.

Section 7.2 overviews spectral graph theory. Section 7.3 presents a new second-order consensus theory result with time delays. Section 7.4 reviews a

method for feedback linearization of an MRP representation of the attitude dynamics. Section 7.5 then applies the second-order consensus result to the feedback linearized rigid body attitude dynamics to solve the attitude synchronization problem. Section 7.6 illustrates the theory via simulations. Section 7.7 gives concluding remarks.

7.2 Problem Statement and Graph Theory Preliminaries

7.2.1 Rigid Body Attitude Synchronization

The rigid body attitude synchronization problem is to design torque control laws in a feedback fashion to asymptotically synchronize the attitude orientation of a team of rigid bodies. Suppose there are N rigid bodies. The rotational kinematics and dynamics of the i th agent can be expressed using the Modified Rodrigues Parameters (MRP) attitude representation as

$$\dot{\sigma}_i(t) = \frac{1}{4}B(\sigma_i(t))\omega_i(t) \quad (7.1)$$

$$J_i\dot{\omega}_i(t) = -\omega_i(t)^\times J_i\omega_i(t) + u_i(t) \quad (7.2)$$

where $\sigma_i(t) \in \mathbb{R}^3$ is the MRP vector, $\omega_i(t) \in \mathbb{R}^3$ is the angular velocity vector in a body fixed reference frame, $J_i = J_i^T \in \mathbb{R}^{3 \times 3}$ is the i th agent's inertia matrix, and $u_i(t) \in \mathbb{R}^3$ is the torque control input. For any $a, b \in \mathbb{R}^3$, the skew symmetric matrix operator a^\times represents the cross product between a and b with $a^\times b = a \times b$, and

$$B(\sigma_i) = [(1 - \sigma_i^T \sigma_i)I_3 + 2\sigma_i^\times + 2\sigma_i\sigma_i^T] \quad (7.3)$$

Shuster gives a comprehensive survey of attitude representations and their associated kinematics and dynamics in [69]. Our objective is to design the torque control laws $u_i(t)$ for each agent such that the attitudes of each rigid body synchronize to the same inertial orientation and the formation comes to rest asymptotically, i.e.

$$\lim_{t \rightarrow \infty} \sigma_i(t) = \lim_{t \rightarrow \infty} \sigma_j(t) \quad \forall i, j, \quad \lim_{t \rightarrow \infty} \omega_i(t) = 0 \quad \forall i \quad (7.4)$$

7.2.2 Spectral Graph Theory Preliminaries

This section reviews spectral graph theory concepts related to consensus theory. To achieve the synchronization objective, each agent may receive, via communication, certain local state information from other agents. The communication architecture is modeled as a directed graph $G = (V, E)$, where V is a set of vertices $V = \{1, 2, \dots, N\}$ representing the agents and a set of edges $E \subseteq V \times V$ representing information flow amongst the agents. If agent j receives state information from agent i , then there is a directed edge $(j, i) \in E$ from vertex i to vertex j . The *in degree* of vertex i , denoted $d(i)$, is the number of incoming edges to which it is incident. The *weighted adjacency matrix* of a graph G , denoted $A = [a_{ij}]$, is an $N \times N$ matrix with diagonal entries $a_{ii} = 0$ and positive off-diagonal entries $a_{ij} > 0$ if $(j, i) \in E$. The *weighted Laplacian matrix* of a graph G , denoted $L = [l_{ij}]$, is an $N \times N$ matrix with diagonal entries $l_{ii} = \sum_i a_{ij}$ and off-diagonal entries $l_{ij} = -a_{ij}$.

¹For undirected graphs $a_{ij} = a_{ji}$ which means that A is symmetric. For directed graphs A is not necessarily symmetric.

It will be advantageous to utilize a particular weighted adjacency matrix, which we denote \bar{A} , which has off-diagonal entries that sum to unity: $\sum_i \bar{a}_{ij} = 1$.² The Laplacian corresponding to this weighted adjacency matrix is denoted \bar{L} .

For an undirected graph, it is somewhat obvious that the graph necessarily must be connected to achieve synchronization. For directed graphs, however, there are multiple notions of connectivity: weak connectivity, in which the underlying undirected graph is connected; strong connectivity, in which there is a directed path between every pair of vertices; and containing a spanning tree, in which there is at least one vertex from which there is a directed path to every other vertex. It is less obvious which of these directed notions is necessary to achieve synchronization. It turns out that a directed graph that contain a spanning tree is necessary, and sufficient depending on the agent dynamics³. We therefore focus on directed graphs with a spanning tree in this chapter. Clearly, every strongly connected graph contains a directed spanning tree (indeed, every vertex is a root for some spanning tree), but a graph does not need to be strongly connected to contain a directed spanning tree.

It is useful to distinguish two types of directed graphs with a spanning

²One way to achieve this particular weighting is to set $\bar{a}_{ij} = 1/d(i)$ if $(j, i) \in E$ and $d(i)$ is non-zero.

³Having a directed spanning tree is necessary and sufficient to achieve synchronization for single integrator agents with a standard consensus control law [60].

tree. A *leader-follower*⁴ graph is one that contains a spanning tree with a *single* root. This root corresponds to the leader, which transmits its own state information, but does not receive state information from other agents, and is therefore free to move independently. A *leaderless* graph is one that contains a spanning tree but has *multiple roots*.

The advantage of working with the particular weighted adjacency and Laplacian matrices \bar{A} and \bar{L} is that their eigenvalues are related by a spectral shift, which we now demonstrate.

For leaderless graphs, $\sum_{j=1}^N \bar{a}_{ij} = d(i) \frac{1}{d(i)} = 1$, for $i = 1, \dots, N$ and the weighted Laplacian is given by

$$\bar{L} = I_N - \bar{A} \quad (7.5)$$

Thus, $\lambda_i(\bar{L}) = 1 - \lambda_i(\bar{A})$ where $\lambda_i(M)$ denotes the i th eigenvalues of a square matrix M .

For leader-follower graphs, we denote the 1st agent as the leader without loss of generality. We have $\sum_{j=1}^N \bar{a}_{1j} = 0$ and $\sum_{j=1}^N \bar{a}_{ij} = 1$, for $i = 2, \dots, N$. In this case, \bar{A} has the form

$$\bar{A} = \begin{bmatrix} 0 & \dots & 0 \\ \nu & & \tilde{A} \end{bmatrix} \quad (7.6)$$

where $\nu \in \mathbb{R}^{(n-1) \times 1}$ and $\tilde{A} \in \mathbb{R}^{(n-1) \times (n-1)}$ and \bar{L} is given by

$$\bar{L} = \begin{bmatrix} 0 & \dots & 0 \\ 0 & I_{N-1} & \end{bmatrix} - \begin{bmatrix} 0 & \dots & 0 \\ \nu & & \tilde{A} \end{bmatrix}. \quad (7.7)$$

⁴The leader-follower graphs discussed in this chapter are not related to the leader-follower type graphs associated with persistent formations as discussed in Chapters 2-4.

Here, all eigenvalues of \bar{L} and \bar{A} except one are related by a spectral shift: $\lambda_1(\bar{L}) = \lambda_1(\bar{A}) = 0$ and $\lambda_i(\bar{L}) = 1 - \lambda_i(\bar{A})$ for $i = 2, \dots, N$.

We can now use the two results on the spectrum of the weighted Laplacian matrix to parameterize the spectrum of the weighted adjacency matrix. We first recall the following result from [61].

Theorem 7.2.1. *The weighted Laplacian matrix L of a directed graph G has a simple eigenvalue at zero iff G contains a directed spanning tree.*

Consequently, (7.5) implies that \bar{A} has a simple eigenvalue at 1 for leaderless graphs, and does not have an eigenvalue at 1 for leader-follower graphs. In acyclic leader-follower graphs, \bar{A} has all eigenvalues at 0 [23].

Further, we recall the Gershgorin circle theorem [25, 26], first stated in 1931.

Theorem 7.2.2 (Gershgorin Circle Theorem). *For any square matrix $M \in \mathbb{R}^{n \times n}$,*

$$\lambda_i(M) \subseteq \bigcup_{i=1}^n D_i \tag{7.8}$$

where $D_i \doteq \{z \in \mathbb{C} : |z - M_{ii}| \leq \sum_{j \neq i}^n |M_{ij}|\}$.

Applying Theorem 7.2.2 to the weighted adjacency matrix, we can conclude that the eigenvalues of \bar{A} all lie inside a unit circle in the complex plane centered at the origin. Accordingly, we can parameterize the spectrum of \bar{A}

as follows. For leaderless graphs, we have

$$\begin{aligned}\lambda_1(\bar{A}) &= 1, & \lambda_i(\bar{A}) &= \rho_i e^{j\theta_i}, & i &= 2, \dots, N \\ \rho_i &\in [-1, 1], & \theta_i &\in [0, \pi] \\ \lambda_i(\bar{A}) &\neq 1 & \forall i &\neq 1\end{aligned}\tag{7.9}$$

For cyclic leader-follower graphs, we have

$$\begin{aligned}\lambda_1(\bar{A}) &= 0, & \lambda_i(\bar{A}) &= \rho_i e^{j\theta_i}, & i &= 2, \dots, N \\ \rho_i &\in [-1, 1], & \theta_i &\in [0, \pi] \\ \lambda_i(\bar{A}) &\neq 1 & \forall i\end{aligned}\tag{7.10}$$

The next section discusses the design of the control law for consensus of *double integrator* agents. In our framework, there is no self-delay, i.e. each agent has instantaneous access to its own state for feedback purposes. There is a homogenous unknown delay in all communicated position state signals. We do not require the communication of rate information. To solve the rigid body attitude synchronization problem, part of the external torque control input for each agent will be used to linearize governing nonlinear attitude dynamics (7.1-7.2), using the development in [66]. After linearization, each agent's dynamics will have the form of three double integrators, decoupled from each other and with connections to corresponding double integrators of the neighbor agents. The remainder of the control effort will be employed in order to drive the linearized dynamics formation to consensus.

7.3 Consensus of Second-Order Systems with Communication Time Delays

In this section, we derive a consensus result for a team of double integrators with an directed communication architecture and a constant homogeneous time delay, but without self-delay. Let $x_i \in \mathbb{R}$ be a scalar state value associated with vertex i governed by the double integrator dynamics

$$\ddot{x}_i(t) = u_i(t) \quad (7.11)$$

where $u_i(t)$ is a control input to be specified. The pair (G, x) with $x = [x_1, x_2, \dots, x_N]^T$ denotes a *formation* with communication architecture G . We say the formation *achieves consensus*⁵ if

$$\lim_{t \rightarrow \infty} x_i(t) = \lim_{t \rightarrow \infty} x_j(t) \quad \forall i, j \in V \quad \text{and} \quad \lim_{t \rightarrow \infty} \dot{x}_i(t) = 0.$$

For leaderless formations, consider the following control input for subsystem i :

$$u_i(t) = \alpha \sum_{j=1}^N \bar{a}_{ij} (x_j(t - \tau) - x_i(t)) - \beta \dot{x}_i(t) \quad (7.12)$$

where $\sum_i^N \bar{a}_{ij} = 1 \quad \forall i$, $\alpha > 0$ is a position gain, $\beta > 0$ is a velocity gain, and $\tau > 0$ is a constant, unknown time delay. For leader-follower formations, we can *prescribe* a desired consensus position x_c to the leader and design the

⁵Our objective in this chapter is to obtain position consensus and drive the velocities to zero. By contrast, other work, e.g. [52, 85], design the control laws to obtain consensus for both positions and velocities (and higher order derivatives in [52]).

control law for the leader and the agents $i = 2, \dots, N$ to respectively be

$$u_1(t) = -\alpha(x_1(t) - x_c) - \beta\dot{x}_1(t) \quad (7.13)$$

$$u_i(t) = \alpha \sum_{j=1}^N \bar{a}_{ij}(x_j(t - \tau) - x_i(t)) - \beta\dot{x}_i(t) \quad (7.14)$$

We state a delay-independent result for the two cases of graph architecture.

7.3.1 Delay-independent stability

Theorem 7.3.1. *Let G be directed graph with a directed spanning tree associated with formation (G, x) . The formation agents have double integrator dynamics in (7.11) with control laws in (7.12) or (7.13-7.14) for leaderless or leader-follower formations, respectively. The formation achieves a consensus with exponential convergence $\forall \tau > 0$ if and only if*

- $\beta^2 \geq 2\alpha$ if G is cyclic
- $\alpha > 0$ and $\beta > 0$ if G is acyclic

Proof. The closed-loop dynamics for leaderless formations are given by

$$\ddot{x}_i(t) = \alpha \sum_{j=1}^N \bar{a}_{ij}(x_j(t - \tau) - x_i(t)) - \beta\dot{x}_i(t) \quad (7.15)$$

For leader-follower formations, defining $e_i(t) = x_i(t) - x_c$, $i = 1, \dots, N$ and $e(t) = [e_1(t) \ e_2(t) \ \dots \ e_N(t)]^T$, the closed-loop dynamics are given by

$$\ddot{e}_1(t) = -\alpha e_1(t) - \beta\dot{e}_1(t) \quad (7.16)$$

$$\ddot{e}_i(t) = \alpha \sum_{j=1}^N \bar{a}_{ij}(e_j(t - \tau) - e_i(t)) - \beta\dot{e}_i(t), \quad i = 2, \dots, N \quad (7.17)$$

In both cases, the state-space equations have the form

$$\dot{X}(t) = A_0 X(t) + A_1 X(t - \tau) \quad (7.18)$$

with $X(t) = [x(t)^T, \dot{x}(t)^T]^T$ for leaderless and $X(t) = [e(t)^T, \dot{e}(t)^T]^T$ for leader-follower, where

$$A_0 = \begin{bmatrix} 0_N & I_N \\ -\alpha I_N & -\beta I_N \end{bmatrix}; \quad A_1 = \begin{bmatrix} 0_N & 0_N \\ \alpha \bar{A} & 0_N \end{bmatrix}$$

where 0_N and I_N are the $N \times N$ zero and identity matrices, respectively. The characteristic equation for the formation can be written as

$$\begin{aligned} \det(sI_{2N} - A_0 - e^{-s\tau} A_1) &= \det \begin{bmatrix} sI_N & -I_N \\ \alpha(I_N - e^{-s\tau} \bar{A}) & (s + \beta)I_N \end{bmatrix} \\ &= \det[s^2 I_N + \beta s I_N + \alpha(I_N - e^{-s\tau} \bar{A})] \quad (7.19) \\ &= \prod_{i=1}^N [s^2 + \beta s + \alpha(1 - e^{-s\tau} \lambda_i(\bar{A}))] = 0 \end{aligned}$$

Note that the justification of going from the second to third line in (7.19) depends crucially on the spectral shift relationship between the particular weighted adjacency and Laplacian matrices. Recall from the Gershgorin circle theorem that we can parameterize the eigenvalues of \bar{A} as $\lambda_i(\bar{A}) = \rho_i e^{j\theta_i}$, $i = 1, \dots, N$ with $\rho_i \in [-1, 1]$, $\theta_i \in [0, \pi)$. The multiplicative term in the characteristic equation for a specified $\lambda_i(\bar{A})$ is

$$s^2 + \beta s + \alpha(1 - e^{-s\tau} \lambda_i(\bar{A})) = 0 \quad (7.20)$$

We first consider the leaderless case. The closed-loop system (7.18) is stable if and only if the roots of (7.19) all have negative real parts. Our

analysis focuses on proving this for all $\lambda_i(A)$ which lie in the closed disc of radius 1 centered at the origin in the complex plane. For $\lambda_1(\bar{A}) = 1$, we have

$$s^2 + \beta s + \alpha(1 - e^{-s\tau}) = 0 \quad (7.21)$$

Clearly, $s = 0$ is a root of (7.21) $\forall \alpha, \beta, \tau > 0$. Moreover if we differentiate the left hand side expression of (7.21) and evaluate at $s = 0$, we get $\beta + \alpha\tau$, which is positive $\forall \alpha, \beta, \tau > 0$. Hence, $s = 0$ is a simple root. It is also easy to observe that any $s \in \mathbb{R}$ such that $s > 0$ is not a root of (7.21) because each term on the left hand side would be positive. Thus, the roots of (7.21) can only be in the right half plane if there is a $j\omega$ axis crossing in the complex plane for some α, β, τ . For this situation, let $s = j\omega$ and use (7.21) to obtain

$$(j\omega)^2 + j\beta\omega + \alpha(1 - e^{-j\omega\tau}) = 0 \quad (7.22)$$

Separating the real and imaginary parts and some algebra yields the following quadratic equation in ω^2

$$\omega^2[\omega^2 + (\beta^2 - 2\alpha)] = 0 \quad (7.23)$$

$\omega = 0$ corresponds to the root at the origin. It is clear that there are no real roots if and only if $\beta^2 \geq 2\alpha$. In summary, for $\lambda_i(\bar{A}) = 1$, we have shown $\forall \tau > 0$, that the characteristic equation has a simple root at $s = 0$ and has no roots with positive real parts if and only if $\beta^2 > 2\alpha$. For the rest of the eigenvalues, we have

$$s^2 + \beta s + \alpha(1 - \rho_i e^{-s\tau} e^{j\theta_i}) = 0 \quad (7.24)$$

Consider $s = 0$ in the above expression. Separating the real and imaginary parts in (7.24) leads to $\sin(\theta_i) = 0$ and $\cos(\theta_i) = \rho_i$. There is no $\theta_i \in (0, \pi)$ which satisfies these expressions, which leads to the fact that $s = 0$ is not a root. Consider $s \in \mathbb{R}^+$. The imaginary part of the characteristic equation in (7.24) yields $\sin(\theta_i) = 0$, which means that $\theta_i = \pi$. Hence, there can be no characteristic roots $s \in \mathbb{R}^+$ for (7.24) $\forall \alpha, \beta > 0$. It now remains to ensure that $s = j\omega$ is not a characteristic root. Separating the real and imaginary parts of the characteristic equation (7.24) leads to the following quadratic expression for ω^2

$$\omega^4 + (\beta^2 - 2\alpha)\omega^2 + \alpha^2(1 - \rho_i^2) = 0 \quad (7.25)$$

Since $\rho_i \leq 1 \forall i$, then $\beta^2 \geq 2\alpha$ is necessary and sufficient to ensure that there are no real and positive roots for ω^2 .

We now focus on cyclic leader-follower formations. In this case, the eigenvalues of \bar{A} are characterized by (7.10). The characteristic equation term corresponding to $\lambda_i = 0$ is

$$s^2 + \beta s + \alpha = 0 \quad (7.26)$$

which is stable $\forall \tau > 0, \forall \alpha, \beta > 0$. Since there is no eigenvalue at 1, the closed loop characteristic equation has no roots at the origin. For the rest of the eigenvalues, the same analysis as above leads to $\beta^2 \geq 2\alpha$ as a necessary and sufficient condition to ensure that there is no imaginary axis crossing of the characteristic roots.

Finally, for acyclic leader-follower graphs, $\lambda_i(\bar{A}) = 0 \forall i$ and hence the closed loop characteristic equation (7.19) becomes

$$(s^2 + \beta s + \alpha)^N = 0 \tag{7.27}$$

which has stable roots $\forall \alpha, \beta > 0$, i.e. delay-independent stability is obtained for all positive gain values.

□

In the stability proof, we use the position consensus x_c for analysis purposes only. In leader-follower formations, the consensus value is prescribed by the leader. For a leaderless formation, the analysis shows that a consensus position exists, but we have not yet determined what value it takes. An expression for the consensus position is derived analytically in the next section.

7.3.2 Characterization of the Consensus Position

As shown in the previous section, the consensus position in leader-follower formations is directly controlled by the leader. In leaderless formations, the consensus position is determined by the initial conditions, control gains, and communication time delay. In this section, we derive an expression for the consensus position for leaderless formations in terms of the initial conditions, control gains, and communication time delay. We assume that the initial state conditions $x(-\tau) = x_\tau = [x_{1\tau}, x_{2\tau}, \dots, x_{n\tau}]^T$ and $\dot{x}(-\tau) = \dot{x}_\tau = [\dot{x}_{1\tau}, \dot{x}_{2\tau}, \dots, \dot{x}_{n\tau}]^T$ are given and the state trajectories $x_i(t)$

during $-\tau < t < 0$ are specified. The communicated signals are received at $t = 0$.

For leaderless formations, the weighted adjacency matrix \bar{A} has a simple eigenvalue at unity and the remaining eigenvalues are contained in the unit disk. Then the adjacency matrix can be expressed as

$$\bar{A} = QJ_{\bar{A}}Q^{-1} \quad (7.28)$$

where Q is a matrix whose columns are the eigenvalues of \bar{A} and $J_{\bar{A}}$ is the Jordan block of \bar{A} with the structure

$$J_{\bar{A}} = \begin{bmatrix} \bar{J}_{\bar{A}} & 0 \\ 0 & 1 \end{bmatrix}. \quad (7.29)$$

Consider the coordinate transformation $z(t) = Q^{-1}x(t)$. Then we have

$$\begin{aligned} \ddot{z}(t) &= Q^{-1}\ddot{x}(t) \\ &= -\beta\dot{z}(t) - \alpha z(t) + J_{\bar{A}}z(t - \tau) \end{aligned} \quad (7.30)$$

Now define $z(t) = [z_1^T(t), z_2(t)]^T$, where $z_1 \in \mathbb{R}^{n-1}$ and $z_2 \in \mathbb{R}$. Then we have

$$\ddot{z}_1(t) = \beta\dot{z}_1(t) - \alpha z_1(t) + \alpha\bar{J}_{\bar{A}}z_1(t - \tau) \quad (7.31)$$

$$\ddot{z}_2(t) = \beta\dot{z}_2(t) - \alpha z_2(t) + \alpha z_2(t - \tau) \quad (7.32)$$

Based on the analysis in the previous section, the control gains can be chosen such that the characteristic equation of Equation (7.31) has roots in the open left half-plane $\forall \tau > 0$; thus, $z_1 \rightarrow 0$ exponentially. Therefore, the consensus

position is determined by the steady-state value of $z_2(t)$. Taking the Laplace transform of Eq. (7.32) and solving for $z_2(s)$ yields

$$z_2(s) = \frac{(s + \beta)z_{20} + \dot{z}_{20} + \alpha \int_{-\tau}^0 z_2(\sigma) e^{-(\sigma+\tau)s} d\sigma}{s^2 + \beta s + \alpha(1 - e^{-s\tau})} \quad (7.33)$$

From the final value theorem, we evaluate the following limit to obtain the steady-state value of z_2

$$z_c = \lim_{t \rightarrow \infty} z_2(t) = \lim_{s \rightarrow 0} s z_2(s) = \frac{\beta}{\beta + \alpha\tau} z_{20} + \frac{1}{\beta + \alpha\tau} \dot{z}_{20} + \frac{\alpha}{\beta + \alpha\tau} \int_{-\tau}^0 z_2(\sigma) d\sigma \quad (7.34)$$

In the original coordinates, we have

$$x_c = \lim_{t \rightarrow \infty} x(t) = Q \lim_{t \rightarrow \infty} z(t) = Q \begin{bmatrix} 0 \\ z_c \end{bmatrix} = z_c \mathbf{1} \quad (7.35)$$

where $\mathbf{1} = [1, \dots, 1]^T \in \mathbb{R}^N$ is the eigenvector corresponding to the simple eigenvalue of \bar{A} at unity. Thus,

$$x_c = z_c \mathbf{1} \quad (7.36)$$

i.e. all of the position coordinates converge to z_c as $t \rightarrow \infty$. Since $z(t) = Q^{-1}x(t)$, then

$$z_2(t) = q_n^T x(t) \quad (7.37)$$

where q_n^T is the last row of Q^{-1} . Therefore, $z_{20} = q_n^T x_0$ and $\dot{z}_{20} = q_n^T \dot{x}_0$, and the consensus position is then given by

$$z_c = \frac{\beta}{\beta + \alpha\tau} q_n^T x_0 + \frac{1}{\beta + \alpha\tau} q_n^T \dot{x}_0 + \frac{\alpha}{\beta + \alpha\tau} \int_{-\tau}^0 q_n^T x(\sigma) d\sigma \quad (7.38)$$

It remains to specify the dynamics of each system over the time interval $-\tau < t < 0$ during which no communicated signals are available due to the time delay. This will allow us to explicitly evaluate the final term of Eq. (7.38) and evaluate the state values at $t = 0$. Assume that $x_i(-\tau) = [x_{i\tau}, \dot{x}_{i\tau}]^T$ is given, and let us suppose that each agent performs the feedback linearization scheme detailed in the next section, and the remainder of the control effort, denoted by $v_i(t)$, is simply a linear feedback of its own instantaneous position and velocity states:

$$v_i(t) = -\alpha x_i(t) - \beta \dot{x}_i(t) \quad -\tau < t < 0 \quad (7.39)$$

Then each agent has the following trajectory over $-\tau < t < 0$

$$x_i(t) = \frac{\lambda_2 x_{i\tau} - \dot{x}_{i\tau}}{\lambda_2 - \lambda_1} e^{\lambda_1(t+\tau)} + \frac{\dot{x}_{i\tau} - \lambda_1 x_{i\tau}}{\lambda_2 - \lambda_1} e^{\lambda_2(t+\tau)} \quad (7.40)$$

where

$$\gamma_{1,2} = \frac{1}{2}(-\beta \pm \sqrt{\beta^2 - 4\alpha}). \quad (7.41)$$

Integrating over $-\tau < t < 0$ yields

$$\int_{-\tau}^0 x_i(\sigma) d\sigma = \frac{\gamma_2 x_{i\tau} - \dot{x}_{i\tau}}{\gamma_1(\gamma_2 - \gamma_1)} (e^{\gamma_1\tau} - 1) + \frac{\dot{x}_{i\tau} - \gamma_1 x_{i\tau}}{\gamma_2(\gamma_2 - \gamma_1)} (e^{\gamma_2\tau} - 1). \quad (7.42)$$

Finally, the state values at $t = 0$ are given by

$$x_i(0) = x_{i0} = \frac{\gamma_2 x_{i\tau} - \dot{x}_{i\tau}}{\gamma_2 - \gamma_1} e^{\gamma_1\tau} + \frac{\dot{x}_{i\tau} - \gamma_1 x_{i\tau}}{\gamma_2 - \gamma_1} e^{\gamma_2\tau} \quad (7.43)$$

$$\dot{x}_i(0) = \dot{x}_{i0} = \gamma_1 \frac{\gamma_2 x_{i\tau} - \dot{x}_{i\tau}}{\gamma_2 - \gamma_1} e^{\gamma_1\tau} + \gamma_2 \frac{\dot{x}_{i\tau} - \gamma_1 x_{i\tau}}{\gamma_2 - \gamma_1} e^{\gamma_2\tau}. \quad (7.44)$$

7.4 Feedback linearization and linear closed loop dynamics

In this section, we employ feedback linearization following the development in [66] in order to express the attitude dynamics equations as a system of interconnected double integrators with time-delay. We desire to obtain the following closed-loop linear dynamics

$$\ddot{\sigma}_i(t) = v_i(t) \quad (7.45)$$

where $v_i(t) = \alpha \sum_{j=1}^{|N_i|} \frac{1}{d_i} (\sigma_j(t - \tau) - \sigma_i(t)) - \beta \dot{\sigma}_i(t)$ as dictated by (7.12) is the control effort that achieves consensus for the linearized dynamics via Theorem 7.3.1. The actual nonlinear MRP dynamics are given by differentiating (7.1)

$$\ddot{\sigma}_i = \frac{1}{4} B(\sigma_i) [-J_i^{-1} \omega_i^\times J_i \omega_i + u_i] + \frac{1}{4} \dot{B}(\sigma_i) \omega_i \quad (7.46)$$

Setting (7.45) equal to (7.46), the linearizing torque control input for the i th agent can be extracted as

$$u_i = \omega_i^\times J_i \omega_i + J_i (\omega_i \omega_i^T - \frac{1}{2} \omega_i^T \omega_i I_3) \sigma_i + \frac{4}{(1 + \sigma_i^T \sigma_i)^2} J_i B^T(\sigma_i) v_i \quad (7.47)$$

This extraction depends on the following expression for the inverse of $B(\sigma_i)$, which is always valid as long as σ_i remains bounded.

Remark 7.4.1. The control law (7.47) consists of two parts. The first set of terms ensures feedback linearization of the attitude dynamics. The last term in (7.47) is designed using consensus theory for double integrator agents with communication delay from the previous section.

7.5 Simulations

This section presents simulations that illustrate the results from the previous sections. We examine an eight-agent formation for two cases: (1) a leaderless communication architecture shown in Figure 1, and (2) a leader-follower communication architecture shown in Figure 2. The inertia matrix

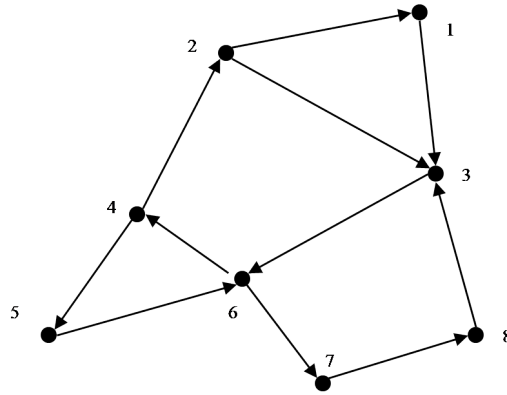


Figure 7.1: Leaderless directed communication architecture.

for all the agents is given by

$$J = \begin{bmatrix} 20 & 2 & 3 \\ 2 & 19 & 2 \\ 3 & 2 & 25 \end{bmatrix}.$$

For both cases, the initial conditions for each of the eight agents are given by Table 7.1.

For the leader-follower case, we demonstrate the delay-independent stability result. The control gains are $\alpha = 1$ and $\beta = 2$, which is in the

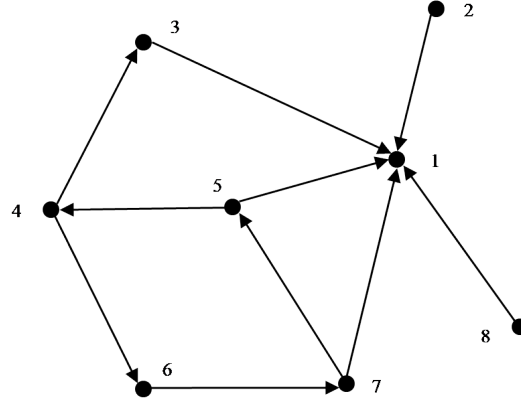


Figure 7.2: Leader-follower directed communication architecture. Agent 1 is the leader.

Table 7.1: Initial conditions for agents

Agent	$\sigma(-\tau)$	$\omega(-\tau)$
1	$[-0.1, -0.2, 0.3]^T$	$[0.01, -0.01, -0.02]^T$
2	$[0.1, 0.2, -0.3]^T$	$[-0.01, 0.01, 0.02]^T$
3	$[0.3, 0.1, -0.1]^T$	$[0.02, -0.03, -0.01]^T$
4	$[-0.3, -0.1, 0.1]^T$	$[-0.02, 0.03, 0.01]^T$
5	$[-0.2, 0.3, -0.2]^T$	$[0.01, -0.02, -0.03]^T$
6	$[0.1, 0.4, -0.3]^T$	$[0.03, -0.05, -0.04]^T$
7	$[0, 0, -0.1]^T$	$[0, 0, 0]^T$
8	$[0, 0, 0]^T$	$[0, -0.01, 0]^T$

delay-independent range $\beta^2 > 2\alpha$. The prescribed consensus attitude is $\sigma_c = [-0.1, 0, 0.2]^T$. For a communication delay of 6.91, Figure 5 shows the time evolution of the composite MRP and angular velocity errors defined by

$$e_\sigma = \sum_i \|\sigma_i - \sigma_c\|, \quad e_\omega = \sum_i \|\omega_i\|.$$

The formation achieves consensus.

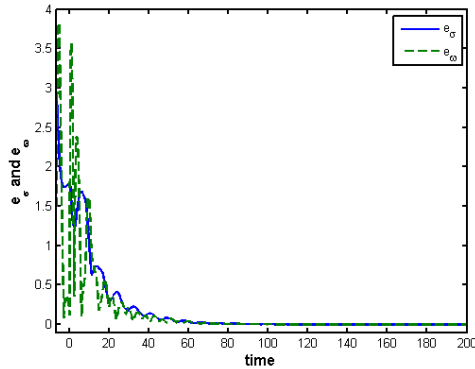


Figure 7.3: Leader-follower directed communication architecture, $\alpha = 1$, $\beta = 2$, $\tau = 6.91$.

For the leaderless case, we demonstrate that consensus can still be achieved if $\beta^2 < 2\alpha$. However, there is a critical time-delay above which consensus will not be achieved; a corresponding delay-dependent stability result is given in [17]. The control gains are $\alpha = 1$ and $\beta = 1.2$, which is not in the delay-independent range $\beta^2 \geq 2\alpha$. The corresponding critical time-delay is $\tau_c = 6.9060$ [17]. For a communication delay of 4, Figure 3 shows the time evolution of the composite MRP and angular velocity errors where here the consensus MRP is $\sigma_c = [0.0121, 0.0165, -0.0318]^T$ from (7.38). Since the communication delay is less than the critical delay, the formation achieves consensus. For a communication delay of 6.91, Figure 4 shows the time evolution of the composite MRP and angular velocity errors. Instability is evident as the communication delay is greater than the critical delay.

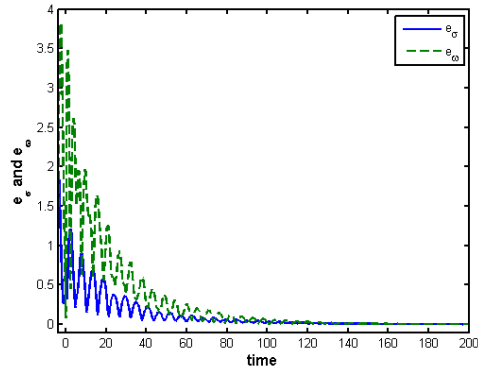


Figure 7.4: Leaderless directed communication architecture, $\alpha = 1$, $\beta = 1.2$, $\tau = 4$.

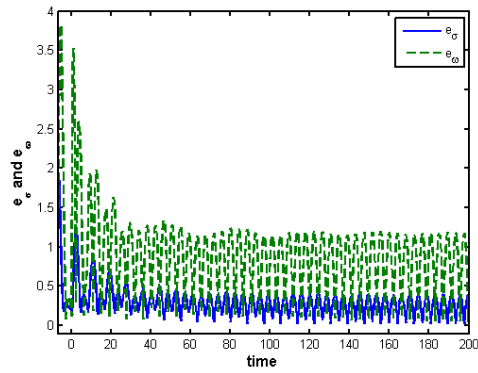


Figure 7.5: Leaderless directed communication architecture, $\alpha = 1$, $\beta = 1.2$, $\tau = 6.91$.

7.6 Conclusions

This chapter has applied a new synchronization result for double integrator agent dynamics with communication time delays to the rigid body attitude synchronization problem. Instantaneous availability of each agent's own state allowed feedback linearization of each agent's dynamics. The result holds for any directed communication graph with a spanning tree. We obtained a necessary and sufficient delay-independent condition that is independent of the structure of the graph. Sufficiently large velocity gain ensures stability. The assumption of homogeneous delay is of course restrictive; there may be different delays associated with different communicated states. However, the homogeneous delay formulation allowed us to obtain the simple necessary and sufficient stability condition.

The next chapter summarizes the work in this dissertation and discusses future research directions.

Chapter 8

Conclusion

8.1 Summary

This dissertation has solved mathematical variations on three problems for autonomous vehicle formations: formation shape control, robust information architecture design, and rigid body attitude synchronization. Chapter 3 demonstrated how *instances* of persistent information architectures, which are related to *rigid graph theory*, could inform the control law design in a coordinated standoff tracking problem. The analysis featured nonlinear, non-holonomic agent models, kinematic constraints, and adaptive control, and the persistent graph properties allowed the cooperative formation objectives to be achieved. Chapter 4 solved a formation shape problem for a *class* of persistent information architectures, completing the stabilizability characterization for minimally persistent formations. Chapter 5 turned to the global stability analysis of a four-agent formation and showed that a class of rectangular incorrect equilibrium shapes, which was thought to be attractive, is in fact an unstable saddle. It also showed how to compute a desired equilibrium shape from a supposed incorrect equilibrium shape and emphasized several open problems for the general case. Chapter 6 illustrated two methods to allow robustness to the loss of an agent from the formation. One method repaired

the information architecture by adding new links in the event of agent loss to *recover* properties that are required for formation shape control and localization. The other built robustness into the information architecture a priori so that these properties were *preserved*. Chapter 7 solved a rigid body attitude synchronization problem with communication time delays. The solution utilized *spectral graph theory* and gave simple and precise delay-independent conditions for asymptotic stability of the in terms of the control gains.

8.2 Future Research Directions for Control of Autonomous Vehicle Formations

There remain many research challenges to be addressed in the control of autonomous vehicle formations, and there are many active efforts in several research communities to address these challenges. This section describes some potential future research directions arising from the work in this dissertation.

8.2.1 Formation Shape Control

The analysis and results in Chapter 3 were restricted to wind and target motion with unknown, but *constant* velocity. A similar adaptive control approach could be used to accommodate *time-varying* wind and target motion.

Chapter 4 demonstrated the local stabilizability of directed minimally persistent leader-remote-follower and coleader formations in the plane. However, while the choice of stabilizing gains does not depend on the position of the entire formation, it does depend on the orientation of the entire formation.

In other words, the stability properties of the control law are translation, but not rotation invariant. One could investigate whether or not it is possible to constrain the gain matrices in order to obtain rotational invariance. Preliminary calculations suggest that this will not always be possible. Additionally, non-minimally persistent formations will eventually be of interest because it may be desirable to control more than the minimum number of distances for formation shape maintenance in order to obtain a level of robustness. A significant future research goal would be to prove local stabilizability for any persistent formation.

The most significant open problem in the global stability analysis of an undirected four-agent formation in which every interagent distance is actively controlled is to show whether or not there can ever exist an incorrect, locally attractive equilibrium shape. Further open problems include calculating incorrect equilibrium shapes, or at least counting the number possible, given an arbitrary desired shape. The ultimate goal is to characterize global stability of an n -agent formation, for both undirected and directed information architectures. The four-agent undirected problem will be an important special case for the general theory.

There are several broad future research directions for both directed and undirected rigidity-based formation shape control. The first is the use of more general models for agent dynamics. The current literature has only considered single integrators to obtain stability results for classes of rigid or persistent

formations¹. While these have been a reasonable starting point in the initial stages of theoretical development, this agent model needs to be generalized to more accurately describe vehicle physics.² A good starting point for generalized models might be undirected, rigid formations with double integrator agent models. Other models might include n -integrators, linear systems, unicycles, under-actuated rigid bodies (these can model helicopters or vertical-takeoff-and-landing aircraft), or fully-actuated rigid bodies. Of course, many other linear or nonlinear models could be investigated depending on the specific application. Also, the translational models could be allowed to evolve in three dimensional space. However, obtaining complete results for rigidity-based formation shape control would depend on finding a three-dimensional analog to Laman’s theorem for graph rigidity in two dimensions, which unfortunately remains a significant and elusive unsolved problem in rigid graph theory.

A second broad future research direction is utilizing different types of *measurements*. Typically, it is assumed that certain relative positions measure-

¹The coordinated standoff tracking problem in this dissertation used a more general unicycle model, which is nonlinear and non-holonomic, but assumed a particular instance of a persistent formation and also required a circular orbit around the target. Similarly, other areas in the literature, e.g. in robotics, may use more general models for agent dynamics, but the analyses are always for particular instances of rigid or persistent formations rather than for classes of formations, as considered in this dissertation.

²In contrast, consensus-based formation shape control results have been obtained for general linear agent models [23], which include single and double integrators as special cases, and unicycle models. This difference can be attributed to the facts that rigidity-based distance control is inherently nonlinear in the position states whereas consensus-based relative position control is linear. While rigidity-based control is relatively under-developed at present, it has the advantage of permitting the agents to operate with arbitrary local coordinate bases.

ments are available. Relative position measurements involve both a distance and a bearing. We have already noted how the solution approach changes drastically based on whether or not each agent has knowledge of a global coordinate system. One might consider how the strategy would change if instead the measurements were only interagent distances or bearings, or some combination thereof. Bearing-based formation shape control has been studied very recently for a three-agent formation in [8], in which global stability of the desired shape (with a scaling ambiguity) is demonstrated. It is not yet clear how to extend this approach to more than three agents. Some combination of distance and bearing control may allow an arbitrary shape to be obtained with fewer measurements and may be instrumental in achieving global stability results. Also, noisy and indirect measurements (e.g. estimating an interagent distance based on the strength of a received signal) will be an important consideration in implementations.

Another area where rigidity-based formation shape control currently lags behind consensus-based control is in analyzing time-varying information architectures. In a time-varying information architectures, the neighbors of each agent are permitted to change with time. This is useful, for example, when agents have limited sensing or communication ranges. It would be interesting to study analogous problems in rigidity-based formations.

Finally, rigidity-based formation shape control algorithms should be implemented on an experimental testbed using wheeled robots, UAVs, or autonomous underwater vehicles to identify specific aspects of the current theory

that are most in need of generalization.

8.2.2 Robust Information Architecture Design

Chapter 6 elucidated a fundamental, yet subtle, difference between minimal rigidity and minimal 2-vertex rigidity. In particular, there are two different ways one can define minimal 2-vertex-rigidity, which are equivalent for minimal rigidity. This difference currently prevents a complete characterization for (non-minimal) 2-vertex-rigidity. It also therefore prevents a complete characterization of (non-minimal) 2-vertex-global rigidity. A complete characterization of 2-vertex-rigidity could take the form of either Laman-like necessary and sufficient conditions on a graph or Henneberg-like operations that would provably allow one to construct *all* 2-vertex-rigid graphs. Such a result will of course be fundamental for characterizing *k-vertex-rigidity* and *k-vertex-global-rigidity* for $k > 2$, which would allow robustness to loss of more than one agent.

One could also consider how the strategy might change if the failure just involved a single sensor, actuator, or communication link. For example, if the failure just involved a single sensor, then the effected agent could potentially accommodate the failure by communicating with nearby agents and leveraging their sensing and communication capabilities. Finally, these ideas could be extended to formations in three dimensions. However, this again would depend on finding a three-dimensional analog to Laman's theorem for graph rigidity in two dimensions.

8.2.3 Rigid Body Attitude Synchronization

The simple conditions on the control gains that yielded delay-independent stability in the rigid body attitude synchronization problem relied on an assumption of homogeneous delay, i.e. that delays were assumed to be the same value for all communicated signals. In general, these delays may have different values and so one future research problem is to consider heterogeneous delays, though obtaining simple and precise stability conditions may be difficult in this case. There are several optimization problems that could be formulated. One could begin with a directed graph with a spanning tree and add a given number of edges to the graph so that the convergence rate is maximized. One could also consider choosing the adjacency matrix and control gains to maximize the convergence rate or minimize the control energy. Finally, the feedback linearization of the modified Rodrigues parameter attitude representation depended on instantaneous availability of each agent's own state and on exact knowledge of inertia parameters. One could consider the nonlinear consensus problem that results from relaxing either of these two requirements.

8.3 Conclusion

Broadly, this dissertation is about the relationship between information architectures and stability in autonomous vehicle formations. Autonomous vehicle formations can be thought of as complex networks of dynamical systems, in which many subsystems and controllers interact dynamically through information exchange. Crucially, the controllers each have access to limited

and different information about the state of the whole system, and the challenge of cooperatively meeting common stability and performance objectives is highly non-trivial. This type of analysis represents a new trend in the field of control theory as control theorists attempt to apply their ideas and techniques to ever larger, more complex systems and relate the discrete graphical structure of such systems to continuous stability and performance properties. Exciting new application areas include autonomous vehicle formations, regional/national power grids, systems biology, the Internet, national/global economies, and urban traffic networks. These systems feature immense and stunning complexity, challenging our ability to understand and control them. Much interesting and important research lies ahead.

Bibliography

- [1] B.D.O. Anderson, C. Yu, S. Dasgupta, and A. Stephen Morse. Control of a three-coleader formation in the plane. *Systems & Control Letters*, 56(9-10):573–578, 2007.
- [2] B.D.O. Anderson, C. Yu, B. Fidan, and J.M. Hendrickx. Rigid graph control architectures for autonomous formations. *IEEE Control Systems Magazine*, 28(6):48–63, 2008.
- [3] L. Asimow and B. Roth. The rigidity of graphs. *Transactions of the American Mathematical Society*, pages 279–289, 1978.
- [4] L. Asimow and B. Roth. The rigidity of graphs II. *SIAM Journal of Applied Mathematics*, 68:171–190, 1979.
- [5] J. Aspnes, T. Eren, D.K. Goldenberg, A.S. Morse, W. Whiteley, Y.R. Yang, B.D.O. Anderson, and P.N. Belhumeur. A theory of network localization. *IEEE Transactions on Mobile Computing*, 5(12):1663–1678, 2006.
- [6] B. Aulbach. *Continuous and discrete dynamics near manifolds of equilibria*. Springer-Verlag New York, 1984.

- [7] J. Baillieul and A. Suri. Information patterns and hedging Brockett's theorem in controlling vehicle formations. In *Proceedings of the 42nd IEEE Conference on Decision and Control*, pages 556–563, 2003.
- [8] M. Basiri, A.N. Bishop, and P. Jensfelt. Distributed control of triangular formations with angle-only constraints. *Systems & Control Letters*, 59(2):147–154, 2010.
- [9] L. Berenhtein, L. Chavez, and W. Whiteley. Inductive constructions for 2-rigidity: bases and circuits via tree partitions. Technical report, York University, Toronto, 2002.
- [10] A.R. Berg and T. Jordán. A proof of Connelly's conjecture on 3-connected circuits of the rigidity matroid. *Journal of Combinatorial Theory, Series B*, 88(1):77–97, 2003.
- [11] L.M. Blumenthal. Theory and applications of distance geometry. *Bulletin of the American Mathematical Society*, 2(9904):272–274, 1954.
- [12] M. Cao, B.D.O Anderson, A.S Morse, and C. Yu. Control of acyclic formations of mobile autonomous agents. In *Proceedings of the 47th IEEE Conference on Decision and Control, Cancun, Mexico*, pages 1187–1192, 2008.
- [13] M. Cao, AS Morse, C. Yu, BDO Anderson, and S. Dasgupta. Controlling a triangular formation of mobile autonomous agents. In *Proceedings of*

- the 46th IEEE Conference on Decision and Control*, pages 3603–3608, 2007.
- [14] M. Cao, C. Yu, A.S. Morse, B.D.O. Anderson, and S. Dasgupta. Generalized controller for directed triangle formations. In *Proceedings of the 2008 IFAC World Congress, Seoul, Korea*, pages 6590–6595, 2008.
- [15] J. Carr. *Applications of Centre Manifold Theory*. Springer, 1981.
- [16] A.L. Cauchy. Recherches sur les Polyèdres-Premier Mémoire. *Journal de l'école polytechnique*, 9:68–86, 1813.
- [17] A. Chunodkar, T.H. Summers, and M.R. Akella. Rigid body attitude synchronization with unknown communication time delays. *submitted to Systems & Control Letters*, 2010.
- [18] Moore D., Leonard J., Rus D., and Teller S. Robust distributed network localization with noisy range measurements. In *Proceedings of the 2nd International Conference on Embedded Networked Sensor Systems*, pages 50–61, 2004.
- [19] F. Dorfler. Geometric analysis of the formation problem for autonomous robots. Master's thesis, University of Toronto & University of Stuttgart, 2008.
- [20] T. Eren, B.D.O. Anderson, A.S. Morse, W. Whiteley, and P.N. Belhumeur. Operations on rigid formations of autonomous agents. *Communications in Information and Systems*, 3(4):223–258, 2004.

- [21] T. Eren, P.N. Belhumeur, B.D.O. Anderson, and A.S. Morse. A framework for maintaining formations based on rigidity. In *Proceedings of the 15th IFAC World Congress, Barcelona, Spain*, pages 2752–2757, 2002.
- [22] L. Euler. *Opera Postuma I.* pages 494–496, 1862.
- [23] J.A. Fax and R.M. Murray. Information flow and cooperative control of vehicle formations. *IEEE Transactions on Automatic Control*, 49(9):1465–1476, 2004.
- [24] E.W. Frew, D.A. Lawrence, and S. Morris. Cooperative standoff tracking of moving targets using Lyapunov guidance vector fields. *AIAA Journal of Guidance, Control, and Dynamics*, 31(2):290–306, 2008.
- [25] S. Gerschgorin. Über die abgrenzung der eigenwerte einer matrix. *Izv. Akad. Nauk SSSR Ser. Mat.*, 7:749–754, 1931.
- [26] G.H. Golub and C.F. Van Loan. *Matrix Computations.* Johns Hopkins University Press, Baltimore, 1996.
- [27] J.E. Graver, B. Servatius, and H. Servatius. *Combinatorial Rigidity.* American Mathematical Society, 1993.
- [28] S.R. Griffiths. Vector field approach for curved path following for miniature aerial vehicles. In *Proceedings of the AIAA Guidance, Navigation, and Control Conference*, volume 61, pages 63–64, 2006.

- [29] J.L. Gross and J. Yellen. *Graph Theory And Its Applications*. Chapman & Hall/CRC, 2006.
- [30] B. Hendrickson. Conditions for unique graph realizations. *SIAM Journal on Computing*, 21(1):65–84, 1992.
- [31] J.M. Hendrickx. *Graphs and networks for the analysis of autonomous agent systems*. PhD thesis, Universite Catholique de Louvain, 2008.
- [32] J.M. Hendrickx, B.D.O. Anderson, and V.D. Blondel. Rigidity and persistence of directed graphs. In *44th IEEE Conference on Decision and Control and European Control Conference*, pages 2176–2181, 2005.
- [33] J.M. Hendrickx, B.D.O. Anderson, J.C. Delvenne, and V.D. Blondel. Directed graphs for the analysis of rigidity and persistence in autonomous agent systems. *International Journal of Robust and Nonlinear Control*, 17(10-11):960–981, 2007.
- [34] L. Henneberg. *Die Graphische Statik der Starren Systeme*. BG Teubner, 1911.
- [35] B. Jackson and T. Jordán. Connected rigidity matroids and unique realizations of graphs. *Journal of Combinatorial Theory, Series B*, 94(1):1–29, 2005.
- [36] D.J. Jacobs, AJ Rader, L.A. Kuhn, and MF Thorpe. Protein flexibility predictions using graph theory. *Proteins: Structure, Function, and Bioinformatics*, 44(2):150–165, 2001.

- [37] D. Kingston and R. Beard. UAV Splay State Configuration for Moving Targets in Wind. *Lecture Notes in Control and Information Sciences*, pages 109–128, 2007.
- [38] L. Krick, M.E. Broucke, and B.A. Francis. Stabilization of infinitesimally rigid formations of multi-robot networks. *International Journal of Control*, 82(3):423–439, 2009.
- [39] Kaltenegger L. and Fridlund M. The Darwin mission: Search for extra-solar planets. *Advances in Space Research*, 36(6):1114–1122, 2005.
- [40] G. Laman. On graphs and rigidity of plane skeletal structures. *Journal of Engineering Mathematics*, 4(4):331–340, 1970.
- [41] J.P. LaSalle. *The stability of dynamical systems*. Society for Industrial and Applied Mathematics, 1976.
- [42] P.R. Lawson, O.P. Lay, K.J. Johnston, and C.A. Eds. Beichman. Terrestrial Planet Finder Interferometer Science Working Group Report. Technical Report JPL Publication 07-1, Jet Propulsion Laboratory, California Institute of Technology, 2007.
- [43] J.R. Lawton and R.W. Beard. Synchronized multiple spacecraft rotations. *Automatica*, 38(8):1359–1364, 2002.
- [44] D. Lee and M.W. Spong. Agreement with non-uniform information delays. In *Proceedings of the American Control Conference, Minnesota, USA*, pages 756–761, 2006.

- [45] D. Lee and MW Spong. Stable flocking of multiple inertial agents on balanced graphs. *IEEE Transactions on Automatic Control*, 52(8):1469–1475, 2007.
- [46] Z. Lin, M. Broucke, and B. Francis. Local Control Strategies for Groups of Mobile Autonomous Agents. *IEEE Transactions on Automatic Control*, 49(4):622–629, 2004.
- [47] I.G. Malkin. *Theory of stability of motion*. United States Atomic Energy Commission, 1952.
- [48] J.A. Marshall, M.E. Broucke, and B.A. Francis. Formations of vehicles in cyclic pursuit. *IEEE Transactions on Automatic Control*, 49(11):1963–1974, 2004.
- [49] J.A. Marshall, M.E. Broucke, and B.A. Francis. Pursuit formations of unicycles. *Automatica*, 42(1):3–12, 2006.
- [50] S. Martínez and F. Bullo. Optimal Sensor Placement and Motion Coordination for Target Tracking. *Automatica*, 42(4):661–668, 2006.
- [51] U. Munz, A. Papachristodoulou, and F. Allgower. Delay-Dependent Rendezvous and Flocking of Large Scale Multi-Agent Systems with Communication Delays. In *47th IEEE Conference on Decision and Control, Cancun, Mexico*, pages 2038–2043, 2008.
- [52] U. Munz, A. Papachristodoulou, and F. Allgower. Generalized Nyquist Consensus Condition for High-Order Linear Multi-Agent Systems with

- Communication Delays. In *48th IEEE Conference on Decision and Control, Shanghai, P.R. China*, pages 3709–3714, 2009.
- [53] R. Olfati-Saber. Flocking for multi-agent dynamic systems: Algorithms and theory. *IEEE Transactions on Automatic Control*, 51(3):401–420, 2006.
- [54] R. Olfati-Saber, J.A. Fax, and R.M. Murray. Consensus and cooperation in networked multi-agent systems. *Proceedings of the IEEE*, 95(1):215–233, 2007.
- [55] R. Olfati-Saber and R.M. Murray. Graph Rigidity and Distributed Formation Stabilization of Multi-Vehicle Systems. *Proceedings of the 41st IEEE Conference on Decision and Control*, 3, 2002.
- [56] N.B. Priyantha, H. Balakrishnan, E. Demaine, and S. Teller. Anchor-free distributed localization in sensor networks. In *Proceedings of the 1st International Conference on Embedded Networked Sensor Systems*, pages 340–341, 2003.
- [57] W. Ren. Distributed attitude alignment in spacecraft formation flying. *International journal of adaptive control and signal processing*, 21(2-3):95–113, 2007.
- [58] W. Ren. On consensus algorithms for double-integrator dynamics. *IEEE Transactions on Automatic Control*, 53(6):1503–1509, 2008.

- [59] W. Ren and R.W. Beard. Consensus seeking in multiagent systems under dynamically changing interaction topologies. *IEEE Transactions on Automatic Control*, (5):655–661, 2005.
- [60] W. Ren, R.W. Beard, and E.M. Atkins. Information consensus in multi-vehicle cooperative control. *IEEE Control Systems Magazine*, 27(2):71–82, 2007.
- [61] W. Ren, R.W. Beard, and T.W. McLain. Coordination variables and consensus building in multiple vehicle systems. In *Lecture Notes in Control and Information Sciences*, volume 309, pages 439–442. Springer Berlin/Heidelberg, 2004.
- [62] A. Sard. The measure of the critical values of differentiable maps. *Bulletin of the American Mathematical Society*, 48:883–890, 1942.
- [63] A. Sarlette, R. Sepulchre, and N.E. Leonard. Autonomous rigid body attitude synchronization. *Automatica*, 45(2):572–577, 2009.
- [64] S. Sastry. *Nonlinear Systems: Analysis, Stability, and Control*. Springer, 1999.
- [65] K. Savla, F. Bullo, and E. Frazzoli. On traveling salesperson problems for Dubins vehicle: stochastic and dynamic environments. In *Proceedings of the 44th IEEE Conference on Decision and Control*, pages 4530–4535, 2005.

- [66] H. Schaub, M.R. Akella, and J.L. Junkins. Adaptive control of nonlinear attitude motions realizing linear closed loop dynamics. *Journal of Guidance, Control, and Dynamics*, 24(1):95–100, 2001.
- [67] B. Servatius. Birigidity in the Plane. *SIAM Journal on Discrete Mathematics*, 2(4):582–599, 1989.
- [68] A. Seuret, D. Dimarogonas, and K. Johansson. Consensus of double integrator multi-agents under communication delay. In *8th IFAC Workshop on Time Delay Systems, Sinala, Romania*, pages 3709–3714, 2009.
- [69] M.D. Shuster. Survey of attitude representations. *Journal of the Astronautical Sciences*, 41:439–517, 1993.
- [70] R.S. Smith and F.Y. Hadaegh. Control of Deep-Space Formation-Flying Spacecraft: Relative Sensing and Switched Information. *AIAA Journal of Guidance, Control, and Dynamics*, 28(1):106–114, 2005.
- [71] H.G. Tanner, A. Jadbabaie, and G.J. Pappas. Stable flocking of mobile agents, part I: Fixed topology. In *Proceedings of the 42nd IEEE Conference on Decision and Control*, 2003.
- [72] H.G. Tanner, A. Jadbabaie, and G.J. Pappas. Stable flocking of mobile agents part II: Dynamic topology. In *Proceedings of the 42nd IEEE Conference on Decision and Control*, pages 2016–2021, 2003.
- [73] T. Tay and W. Whiteley. Generating Isostatic Frameworks. *Structural Topology*, 11:21–69, 1985.

- [74] T. Ten Brummelaar, M. Creech-Eakman, and J. Monnier. Probing stars with optical and near-IR interferometry. *Physics Today*, 62(6):28, 2009.
- [75] MF Thorpe and PM Duxbury. *Rigidity theory and applications*. Kluwer Academic/Plenum Publishers New York, 1999.
- [76] N. Trawny, X.S. Zhou, K.X. Zhou, and S.I. Roumeliotis. 3D relative pose estimation from distance-only measurements. In *IEEE International Conference on Intelligent Robots and Systems*, pages 1071–1078, 2007.
- [77] PKC Wang, FY Hadaegh, and K. Lau. Synchronized formation rotation and attitude control of multiple free-flying spacecraft. *Journal of Guidance Control and Dynamics*, 22:28–35, 1999.
- [78] W. Whiteley. Infinitesimally Rigid Polyhedra. I. Statics of Frameworks. *Transactions of the American Mathematical Society*, 285(2):431–465, 1984.
- [79] S. Wiggins. *Introduction to Applied Nonlinear Dynamical Systems and Chaos*. Springer, 2003.
- [80] G. Xie and L. Wang. Consensus control for a class of networks of dynamic agents. *International Journal of Robust and Nonlinear Control*, 17(10):941–959, 2007.
- [81] C. Yu. *Formation control based on graph rigidity theory*. PhD thesis, Australian National University, 2007.

- [82] C. Yu and B.D.O. Anderson. Development of Redundant Rigidity Theory for Formation Control. *International Journal of Robust and Nonlinear Control*, 19(13):1427–1446, 2009.
- [83] C. Yu, B.D.O. Anderson, S. Dasgupta, and B. Fidan. Control of minimally persistent formations in the plane. *SIAM Journal on Control and Optimization*, 48(1):206–233, 2009.
- [84] C. Yu, J.M. Hendrickx, B. Fidan, B.D.O. Anderson, and V.D. Blondel. Three and higher dimensional autonomous formations: Rigidity, persistence and structural persistence. *Automatica*, 43(3):387–402, 2007.
- [85] W. Yu, G. Chen, and M. Cao. On second-order consensus in multi-agent dynamical systems with directed topologies and time delays. In *48th IEEE Conference on Decision and Control, Shanghai, P.R. China*, pages 3709–3714, 2009.

Vita

Tyler Holt Summers was born in Albuquerque, New Mexico, the son of Dr. Randall M. Summers and Candice H. Summers. He received the Bachelor of Science degree in Mechanical Engineering from Texas Christian University in December 2004 and the Master of Science degree in Aerospace Engineering from the University of Texas at Austin in May 2007. He was a Fulbright Scholar at the Australian National University in Canberra, Australia from September 2007 to November 2008. He has held various summer internships at Sandia National Laboratories in Albuquerque, NM and Air Force Research Laboratories in Dayton, OH.

Permanent address: 1501 Barton Springs Rd #231
Austin, Texas 78704

This dissertation was typeset with L^AT_EX[†] by the author.

[†]L^AT_EX is a document preparation system developed by Leslie Lamport as a special version of Donald Knuth's T_EX Program.